A MODEL OF THE NEURONAL ENCODING MECHANISM

A MODEL OF THE NEURONAL ENCODING MECHANISM

FOR STUDYING NEURAL SYSTEMS

by

Vincent Varano

M.Eng.Thesis   August 1973

A MODEL OF THE NEURONAL ENCODING MECHANISM

FOR STUDYING NEURAL SYSTEMS

by

Vincent Varano, B.Eng. (Hons. Elect., McGill U.)

A thesis submitted to the Faculty of
Graduate Studies and Research
in partial fulfillment of the requirements
for the degree of
Master of Engineering

Department of Electrical Engineering
McGill University
Montreal, Canada
August, 1973

ABSTRACT

The present work deals with the mechanism with which a neuron encodes current produced by an input stimulus into an output series of spikes(pulses). We have formulated a lumped model of the encoding mechanism by considering the experimentally observed properties of the neuronal membrane. The model consists of a forward path and two negative feedback paths. In the forward path, there is the well-known R-C model in series with a block which emits a spike whenever the membrane potential exceeds a threshold level. The two feedback paths model two processes present in the membrane: the increase in the potassium conductance triggered by the emitted spikes and the increased activity of the electrogenic sodium pump. The model has been studied by simulation on the digital computer and analyzed mathematically. The results show that many of the observed properties of the encoding mechanism are due to either the potassium conductance process or the electrogenic sodium pump process.

In addition to increasing our understanding of the encoding mechanism of the individual neuron, the model can be used for studying neural systems because of the following features: (i) The parameters of the model are expressed as a function of the "size" of the neuron since neurons in some neural systems are of various sizes, (ii) Only the properties which are significant in the encoding are incorporated in the model and as a result, a neural system can be represented realistically by many neurons and the cost of simulations remains acceptable, (iii) The model appears to be applicable to various types of neurons such as the cat motoneuron and the crayfish stretch receptor neuron.

SOMMAIRE

Le présent travail porte sur le mécanisme par lequel un neurone convertit un stimulus d'entré en une série de potentiels d'actions (impulsions) à la sortie. Nous avons formulé un modèle global du mécanisme de codage du stimulus en tenant compte des propriétés observées expérimentalement des membranes de neurones. Le modèle consiste d'une branche de transmission directe et de deux boucles de rétroaction. Dans la branche directe se trouve le modèle R-C bien connu en série avec un bloc émettant une impulsion lorsque le potentiel membranaire dépasse un seuil donné. Les deux boucles de rétroaction représentent deux processus présent dans la membrane: l'augmentation de la conductance du potassium déclenchée par les impulsions émises et l'augmentation de l'activité de la pompe électrogénique du sodium. Le modèle a été étudié par simulation sur ordinateur digital et par analyse mathématique. Les résultats démontrent que plusieurs des propriétés observées du mécanisme de codage sont dûs au processus responsable de la conductance du potassium ou de la pompe électrogénique du sodium.

En plus d'accroître notre connaissance du mécanisme de codage du neurone, le modèle peut-être utilisé pour l'étude des systèmes neuraux à cause des propriétés suivantes: (i) Les paramètres du modèle sont exprimés en fonction des dimensions du neurone étant donné que ceux-ci peuvent varier à l'intérieur de certains systèmes, (ii) Seulement les propriétés qui sont importantes dans le processus de codage du signal d'entré sont incluses dans le modèle, ce qui fait qu'un système neural peut-être représenté d'une façon réaliste par plusieurs neurones avec un coût de simulation demeurant acceptable, (iii) Le modèle paraît appliquable à différents types de neurones tels les motoneurones du chat et les récepteurs d'extension des écrevisses.

ACKNOWLEDGEMENTS

TABLE OF CONTENTS

ABRIDGED LIST OF SYMBOLS

MN   Motoneuron

AHP   after-hyperpolarization

AP   action potential which includes the spike and the AHP

i stimulating current

I intensity of a stimulating current step

g_{Na} sodium conductance

g_K potassium conductance

E_K potassium equilibrium potential

Δi_K increase in the potassium current given by,
$$\Delta i_K = \Delta g_K (e_m + E_K)$$

e_m membrane potential

Δe_m change in the membrane potential, $\Delta e_m = e_m + E_{r0}$; $\Delta e_m < 0$ is a hyperpolarization, $\Delta e_m > 0$ is a depolarization

g_{Kb} potassium conductance when no spikes are emitted

Δg_K temporary increase in the potassium conductance that produces the AHP

R lumped resistance of the neuron

C   lumped capacitance of the neuron

E_r magnitude of the equilibrium or resting potential

K_m $1/C$

A_m $A_m = 1/T_m = 1/RC$

T_m time constant of the membrane $T_m = 1/A_m = RC$

TH   threshold voltage

I_{th} threshold current

d   diameter of the neuron

AHP_d duration of the after-hyperpolarization

T_K time constant of the decay of Δg_K

A_K $A_K = 1/T_K$

ΔG_{KO} value of Δg_K immediately after a spike

f_m minimum firing frequency

f_i instantaneous firing frequency

t_i emission time of the i th spike

E_Z $E_Z = TH + E_K - E_r$

f_{SK} adapted firing frequency in the basic model

S_d alope of the f_{SK} – I curve

V_a conduction velocity of the axon

T_P time constant in the transfer function representing the electrogenic Na pump process

A_P $A_P = 1/T_P$

K_P gain in the transfer function representing the electrogenic Na pump process

i_P inhibitory current generated by the electrogenic Na pump process

i_{PS} steady-state value of i_P

f_{SP} adapted firing frequency in the general model

CHAPTER I

INTRODUCTION

1.1   Motivation and objective

In the nervous system there are many subsystems which perform specific functions.   As an example, a subsystem (or simply, a system) of about three hundred motoneurons operate more or less in parallel to control the contraction of the cat gastrocnemius muscle.

In order to investigate how the neurons function together as a system, it is necessary to observe and analyze their simultaneous activities.   We could attempt to study experimentally the responses of as many neurons as possible, but it is difficult to record simultaneously from more than several interacting neurons and very difficult to resolve their individual activities.   Alternatively, we may approach the problem by a simulation study of a model of the system together with experimental observations from one neuron during the operation of the system.   An initial model can be developed by integrating available information on the operation of the individual neuron and on the interconnections of the neurons.   It can then be improved continually by using the experimental data in conjunction with results from the simulation study of the model.   An adequate model should then explain how the neurons operate as a system and predict possible functional properties which in turn may clarify the experimental observations from the individual neuron in the system.   Using this approach we have begun to investigate the functional significance of

the Renshaw cell feedback in the spinal motoneuron pool(56).

In order to model a neural system, we require a model of the individual neuron in the system. We have not found in the literature a physiologically meaningful model suitable for this purpose. In the present thesis, we shall develop a model of the neuronal encoding mechanism which can be extended, as we shall do for the motoneuron, to give a complete neuron model (see Figure 1-1). By "neuronal encoding mechanism" we refer to the mechanism with which a neuron encodes current produced by an input stimulus, such as excitatory spikes (pulses) from other neurons, into an output series of spikes. Reported experimental observations, cited in the thesis, indicate that the main properties of the operation of certain neurons can be attributed to the encoding mechanism.

Although a model can be formulated by only considering the observed input-output relations and the subthreshold changes of the membrane potential without regard to the processes present in the neuronal membrane, it is desirable to make the model more physiologically meaningful by considering these processes. Extensive experimental tests on the motoneuron and the crayfish stretch receptor neuron indicate that changes in a potassium conductance process and in an electrogenic sodium pump process due to the occurrence of spikes play an important role in regulating the output spike frequency (12, 22, 34, 45). However, we have not found a mathematical model nor any verbal description that would reveal how both of these processes are involved simultaneously in the encoding mechanism. The model of the encoding mechanism that we shall formulate and analyse will include both of these processes. The applicability of the model to various types of neurons, including the motoneuron and the crayfish stretch

receptor neuron, shall be discussed.

The model must also meet the following requirements in order that it can be useful for studying neural systems:

(i) The parameters of the model must be expressed as a function of the size of the neuron. Neurons in some neural systems such as the spinal motoneuron pool are of various sizes. The size affects both the operation of the neuron and the system. For example, motoneurons in a spinal motoneuron pool are recruited into action in order of increasing size (55).

(ii) The model must be "simple". By "simple" we mean that the model incorporates only those properties which are significant in the encoding. For example, it is not necessary that the model reproduces the shape of the spike in the action potential but, on the other hand, it is essential that the model emits the spikes at the correct times. This requirement is necessary because the cost of simulations of a model of a system is proportional to the complexity of the neuron model and the number of neurons in the model. Thus, in order that the system can be represented realistically by many neurons and its simulations be economically acceptable, the neuron model must be simple.

1.2 Previous work

An extensive review of neural modelling prior to 1966 has been reported by Harmon and Lewis (1). In the following, we review again some of the relevant models, as well as others which have been reported more recently. First we describe each model and then, in the last para-

graph, we discuss the general limitations of these models.

(a) The cornerstone of neural modelling has been the Hodgkin-Huxley model for a patch of membrane of the squid axon (2). The model describes the underlying changes that occur in the membrane during one action potential. The properties of other neuronal membranes have been generally discussed in terms of this model. We will review this model in detail in Chapter II.

(b) Lewis (3, 4) constructed an electronic analogue of an extended version of the Hodgkin-Huxley model and he explored various modes of operation, including its subthreshold behaviour. One finding was that, under certain conditions, there can be spontaneous subthreshold oscillations of the membrane potential and these oscillations can lead to the emission of a series of action potentials. Synaptic conductance changes were included and the analogue was used to explore simple neuro-electric interactions between spatially distributed regions of a single neuron, and neuroelectric activities in very small groups of neurons.

(c) Harmon (1, 53) designed an electronic model which accounted for spatial and temporal summation, absolute and relative refractoriness, and graded inhibition. This model had three primitive input-output properties: a single input spike elicited a single spike; a step input produced a train of spikes; and spatial or temporal summation of the effect of subthreshold input spikes elicited a spike. By appending circuits to this primitive model, a variety of other properties could be produced such as, accommodation, adaptation, self-sustained discharge, and post-spike hyperpolarization. The model was used to study neural systems in the retina and cochlea, and to investigate the possible neurological origin

of flicker- fusion phenomena.

(d) Hiltz (6) proposed a model with a transfer function in a forward path that transformed input potentials into an equivalent transmembrane potential. This transmembrane potential was applied to a feedback path with a transfer function (which accounted for accommodation) in series with a comparator and a single shot multivibrator whose output was summed with the input potentials. The model was implemented with electronic circuits, and it reproduced the following properties: the subthreshold step response, the strength-latency curve, accommodation of the threshold to ramp inputs with low rate of rise, refractoriness after a spike, the after-hyperpolarization, repetitive firing, and adaptation of firing frequency.

(e) Roberge (5) proposed a description of the neuronal membrane at the ionic level and then he modelled the motoneuron by fitting relations between the observed subthreshold step response, the excitatory postsynaptic potential, and the action potential. The model was implemented with electronic circuits and it was used to study the motoneuron–Renshaw cell system.

(f) Pavlidis (51) proposed a model with a forward path and a negative feedback path. The forward path was designated a Σ-pulse frequency modulator and it consisted of a leaky integrator to model the membrane dynamics in series with a spike emitter. The output of the integrator was reset to zero whenever a spike was emitted. The negative feedback path was included in order to account for relative refractoriness and the time constants in both paths were taken to be equal. The model

was used to study possible neural nets such as an oscillating neural net.

(g) Perkel [from (1)] proposed a model in which the membrane potential was hyperpolarized after a spike but it returned towards an input level. If the threshold was set below the input level, a spike was emitted whenever the membrane potential reached the threshold. If the threshold was set above the input level, no spikes were emitted. For each presynaptic input, a potential was instantaneously added to the membrane potential and the membrane potential then returned from this new value towards the input level with the same rate constant as that of the decline of the polarization after a spike. Simulations of the model predicted accurately how a regular inhibitory synaptic input affects the output firing frequency in Aplysia pacemaker cells and in the crayfish stretch receptors.

(h) Jenik and Kupfmuller (1, 52) designed an electronic analog to simulate a simplified form of the Hodgkin-Huxley model. They included synaptically induced currents and the parameters were chosen to simulate mammalian motoneurons. The model exhibited an EPSP, IPSP and action potential similar to those observed in motoneurons. The model was used to investigate the processing of input spike trains. One finding was that when two noncoherent, periodic, spike trains were simultaneously applied to the model, the average output firing frequency was proportional to the product of the two input frequencies.

(i) French and Stein (54) designed a model which was implemented with integrated circuits. A leaky integrator summed the inputs from a number of sources over a period determined by its time constant T_1 . The integrated subthreshold voltage was continually compared to a

threshold voltage, and when this was exceeded, a pulse was generated at the output. The subthreshold voltage was fed forward to increase the threshold level with a time constant T_2 , so that the analog showed accommodation. Each output pulse reset the integrator and also incremented the threshold voltage by a fixed amount which decayed with the time constant T_2 . If T_2 was short compared to the normal intervals between pulses, it produced relative refractoriness. However if T_2 was long compared to the intervals between pulses, the increments in threshold accumulated and produced an adaptation of the firing frequency. The model showed that noise disrupted the phase-locked patterns produced by sinusoidal stimuli and the average response became a smooth sinusoidal function in the presence of added noise.

(j) Connor and Stevens (28) analyzed the behaviour of the molluscan soma mambrane in terms of three conductance mechanisms. Two conductances corresponded to the sodium and potassium conductances in the analysis by Hodgkin and Huxley and exhibited qualitatively similar behaviour. The tnird conductance was also a potassium conductance but it had no counterpart in the Hodgkin-Huxley model. Its time constants were intermediate between those for the other two conductances. This third conductance tended to dominate the behaviour in the interval between spikes.

(k) Pertile and Harth (7) proposed a model in which the membrane potential was a linear superposition of voltages from different sources: the resting potential, the post-spike hyperpolarization, and the input voltage. Two distinct processes contributed to the post-

spike hyperpolarization. Each of these processes independently added an increment to the membrane potential. These increments had fixed values at the end of the absolute refractory period and decayed/exponentially, each with a different time constant. The nature of the two processes was not specified but rather, two processes were postulated because a single process could not account for adaptation. The parameters were found by fitting the solution of the model equations to certain experimental data. The model had adaptation of firing frequency and post-stimulus inhibition.

(1) Kernell (8, 9) modelled the motoneuron and investigated a few properties of the model. In the first paper (8), he proposed a mathematical expression which related firing frequency to the input current. The expression was based on the behaviour of the increase in the potassium conductance after a spike. If did not include summation of the increases after many spikes. The model could apparently account for the experimentally observed primary and secondary ranges of firing. In his second paper (9), he presented a compartmental model in which each compartment was modelled with a circuit containing: the conventional resistance-capacitance model of the membrane, a branch to account for the increase in the potassium conductance after a spike, and two branches to account for excitatory and inhibitory synaptic conductance changes. The model was used to investigate how the firing frequency is affected by synapses and by post-spike conductance increases in the dendrites or soma.

(m) Sokolove (10) proposed a model in which the effective input was equal to the stimulating current minus a postulated inhibitory

current produced by the electrogenic sodium pump. This inhibitory current was incremented by each spike with an amount that decayed exponentially with a time constant that was long compared to the interspike intervals. The effective input was applied to an ideal integrator and a spike was emitted whenever the output of the integrator reached a threshold value. The spikes reset the output of the integrator to zero. The integration was arbitrarily stopped during the time that the effective input was negative. The model reproduced the following properties observed for the crayfish stretch receptor neuron: the gradual adaptation of the firing frequency, the final phase of the hyperpolarization after a tetanic train of spikes, and the two segments in the curve relating the posttrain interval to the number of spikes in the train.

Some of these previous models (c, d, e, f, g, i, k) were developed by considering the subthreshold changes of the membrane potential and input-output relations. However, the processes present in the neuronal membrane that are significantly involved in the encoding mechanism were not considered. The other models (b, h, j, l, m) were developed by considering to some extent these processes. However, these models do not provide a complete understanding of the encoding mechanism in the sense that these models include only one of the two processes which will be considered in this thesis. We shall compare in detail our model with these latter models in Chapter VIII. The Hodgkin-Huxley model considered the processes underlying the generation of one action potential while we are interested in how an input is encoded into a series of action potentials. In essence, we have to modify the Hodgkin-Huxley model. Thus, we begin our work by reviewing this model and then we

develop our model in the context of this model.   Finally, none of these
models has its parameters expressed as a function of the size of the
neuron.

1.3   Outline of the thesis

The block diagram of the model of the neuronal encoding
mechanism proposed in this thesis is shown in Figure 1-1.
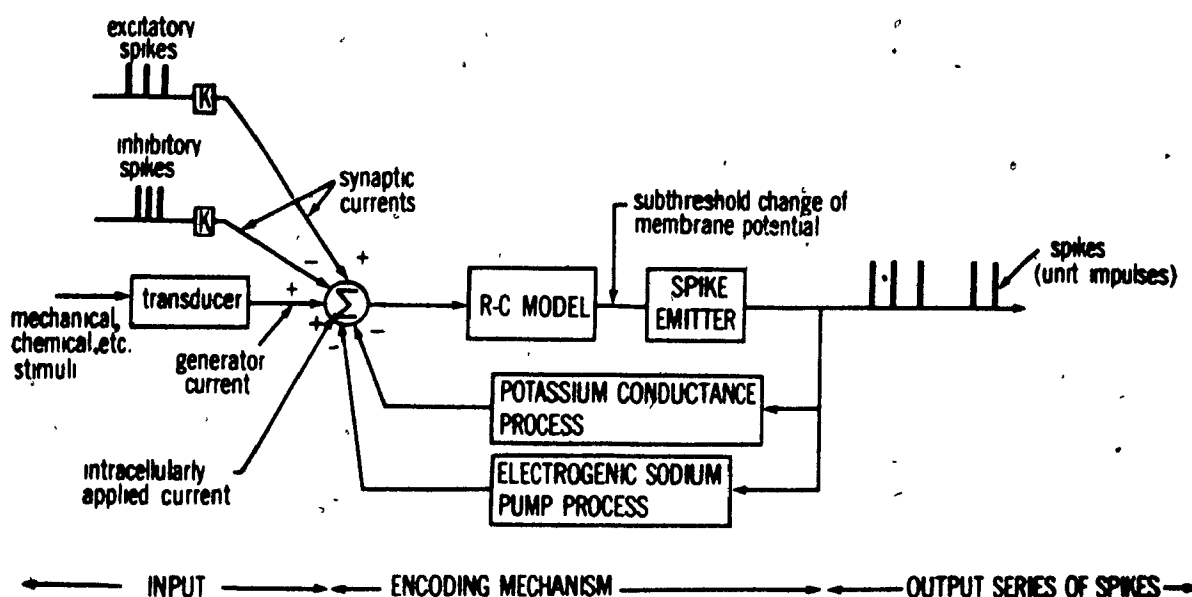
FIGURE 1-1   BLOCK DIAGRAM OF THE NEURON MODEL PROPOSED IN THIS THESIS.
THE ENCODING MECHANISM IS DEVELOPED IN DETAIL.

The model will be formulated and then analyzed mathematically and by
simulations in two stages.   Firstly, in Chapter II, we describe the
relevant electrophysiological properties of the neuronal membrane.   In

Chapters III - VI, the forward path and the inner feedback path are formulated and analyzed. These paths include the well-known R-C model, a spike emitter, and a potassium conductance process activated by the emitted spikes. The presence of this process is based on experimental results reported for the motoneuron. The combination of these paths is called the basic model. Secondly, in Chapter VII, the outer feedback path is added to the basic model in order to include the electrogenic sodium pump process activated by the emitted spikes. The presence of this process is based on experimental results reported for the crayfish stretch receptor neuron. The entire model is called the general model and it is analyzed by extending the analysis of the basic model. Finally, in Chapter VIII, various aspects of the general model are discussed, our model is compared to some previous models, and areas for further research are suggested.

CHAPTER II

RELEVANT ELECTROPHYSIOLOGICAL PROPERTIES OF THE NEURONAL MEMBRANE

In this Chapter, we provide some essential background information

for the presentation of our model of the neuronal encoding mechanism (2,

11a, 11b, 12).

2.1   Excitability property

The membrane of excitable cells separates two electrolytic

solutions with very different compositions. Two layers of charges exist

immediately across the membrane, negative on the inside, positive on the

outside.   These two layers constitute a charged capacitor which exhibits

a transmembrane potential difference, known simply as the membrane poten-

tial e_m.· If a stimulating current, i, is passed through the membrane

from inside to the outside, the membrane will be depolarized, that is,

there is a change in the membrane potential $\Delta e_m > 0$.   Suppose that at

time t = 0 a quantity of charge is transferred to the membrane capacitor

by applying a very brief pulse of current so that the membrane is de-

polarized by an amount Δe_m (t ≈0).   Then, depending on whether Δe_m (t ≈0)

is greater than or less than a threshold voltage, the time courses of the

membrane potential will be dramatically different as illustrated in Figure

2-1   (The values are for the squid axon).   If Δe_m (t ≈0) is less than

the threshold voltage, the response is subthreshold and Δe_m (t) will decay

to zero with an "exponential" time course lasting several msec (curve (a)).

On the other hand, if Δe_m (t ≈0) is greater than or equal to the threshold

voltage, then as shown by curve (b), Δe_m (t) will rise to about 100 mv and return to zero in about 1 msec, undershoot below zero (the resting potential) and gradually return to zero in several milliseconds. This latter response is called the action potential (AP). The 100 mv pulse of 1 msec duration in the AP is called a spike or a pulse.

2.2 The Hodgkin-Huxley model

The underlying changes in the membrane that govern these responses were clarified by A. L. Hodgkin and A. F. Huxley for the squid axon in 1952. A modified version of the model that they proposed (2) is shown in Figure 2-2. We have explicitly shown the two branches containing the Na and K pumps which they lumped in the branch containing g_L [13] because recent experimental evidence shows that these pumps are involved in the encoding mechanism. This model is strictly valid for a patch of membrane of the squid axon but the properties of other neuronal membranes have been generally discussed in terms of this model.

According to this model, the membrane is permeable to Na, K, and other ions which are referred to as leakage ions L. The movement of these ions across the membrane is assumed to satisfy Ohm's law,

$$i_j = g_j (E_j + e_m) \qquad (2-1)$$

where subscript j represents Na, K, or L.

i_j is the current per unit area carried by ion j

g_j is the conductance of the membrane per unit area for ion j

E_j is the equilibrium potential for ion j.
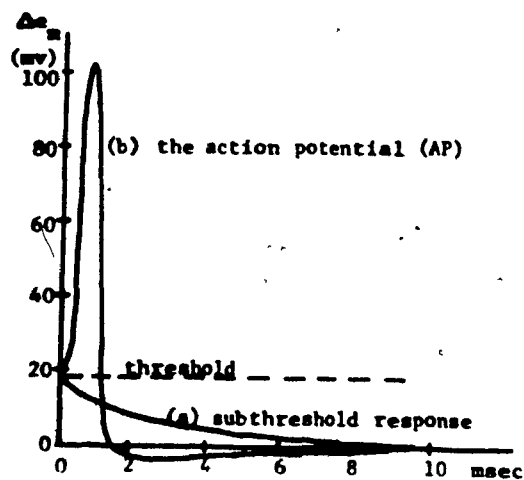
FIGURE 2-1   ILLUSTRATION OF THE EXCITABILITY
PROPERTY OF THE MEMBRANE
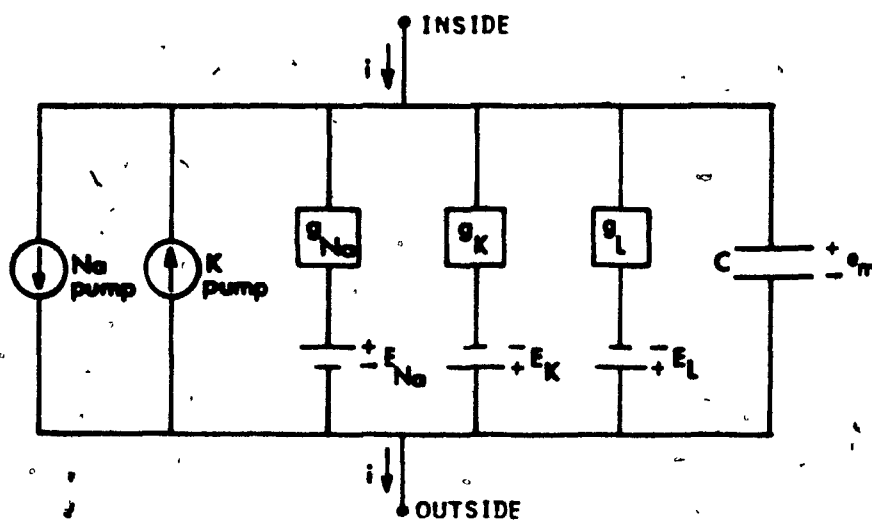
FIGURE 2-2   MODEL OF A PATCH OF NEURONAL MEMBRANE (2)

At the resting potential, Na ions move into the cell and K ions move out of the cell under the influence of the forces $(E_j + e_m)$. It is generally accepted that the concentration differences are maintained in a steady state by a Na pump and a K pump which actively transport an equal quantity of the ions in the opposite direction.

Using the voltage-clamp method (step changes in the membrane potential) Hodgkin and Huxley found that g_{Na} and g_K were time-variant and voltage-dependent as shown in Figure 2-3 whereas g_L was constant. In all curves for g_{Na}, there is a rapid increase followed by a gradual decline even though the voltage step was maintained. For g_K, there is a somewhat exponential growth towards a steady-state value. These experimental results were formulated into an empirical set of equations. The solution of these equations predicted quite accurately the observed behaviour of the squid axon. A calculated AP with the underlying changes in g_{Na} and g_K is shown in Figure 2-4.

FIGURE 2-3 (a) BEHAVIOUR OF g_{Na} DURING STEP CHANGES Δe_m (2)

FIGURE 2-3(b)   BEHAVIOUR OF g_K DURING
STEP CHANGES Δe_m (2)
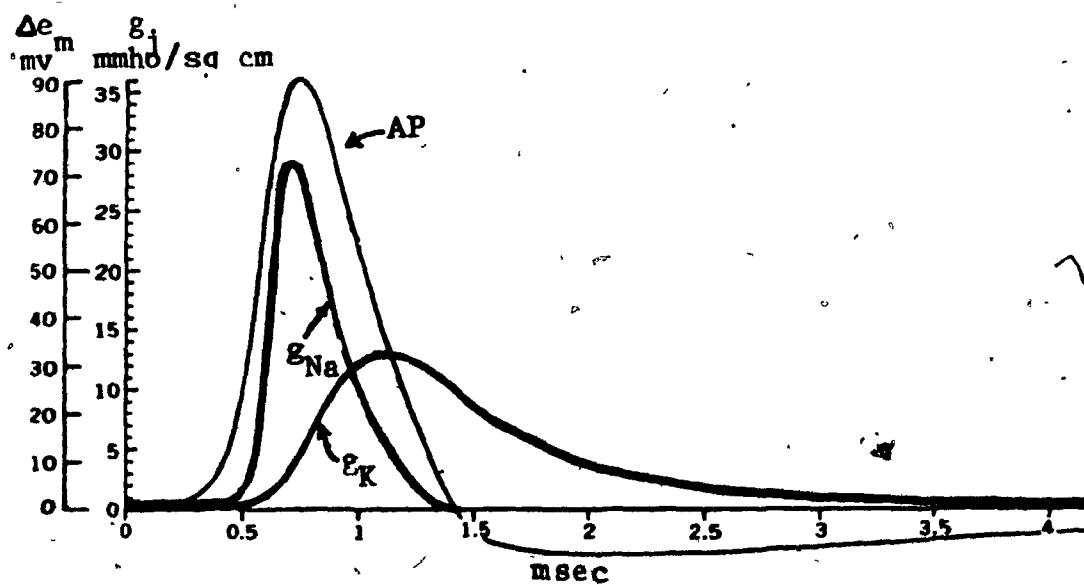
FIGURE 2-4   THE AP AND THE UNDERLYING CHANGES IN g_{Na} AND g_K (2)

According to the Hodgkin-Huxley model, the threshold phenomenon and the AP are the result of the antagonistic action of the Na current which tends to depolarize the membrane and the K current which tends to hyperpolarize the membrane. When the membrane is initially depolarized by a brief pu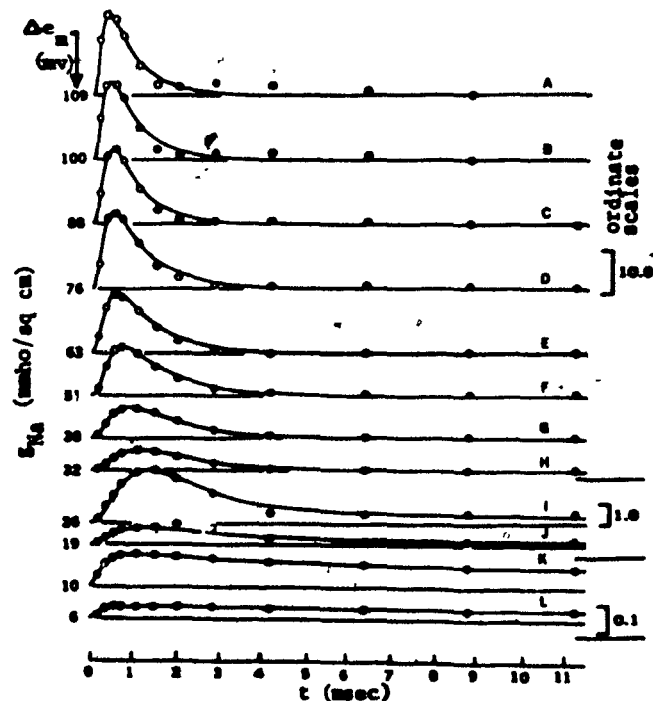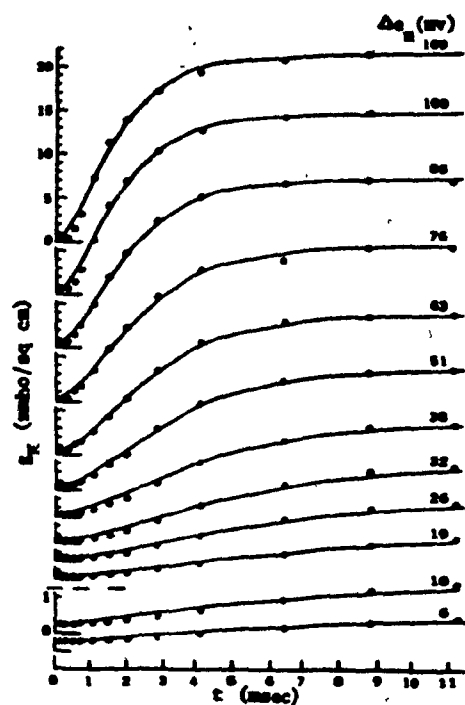lse of current, g_{Na} and g_K increase. Consequently, both the Na current and the K current increase. However, most of the brief transient increase in g_{Na} occurs before the lag increase in g_K. Thus an unbalance arises between the Na current and the K current. This unbalance is directly proportional to the magnitude of the initial depolarization. At a definite threshold level, which is not evident from the characteristics in Figure 2-3, this unbalance is sufficiently large for the AP to be generated. The larger Na current depolarizes the membrane which in turn increases g_{Na} and further increases the Na current. The membrane becomes rapidly depolarized along the rising portion of the AP. However, increases in g_{Na} are not sustained. Meanwhile, g_K increases since it follows changes in the membrane potential with a time lag. The K current overtakes the Na current and the membrane potential returns to zero. But after the 1 msec spike, g_K slowly returns to its value at the resting potential and the K current produces the after-hyperpolarization (AHP).

2.3 Illustrating certain properties with simple transfer functions

In order to establish a sufficiently large unbalance between the Na current and the K current which results in an AP, at least three factors need to be considered:

(1) the rate at which the membrane is depolarized by the external

stimulus

(ii) the state of the Na conductance process

(iii) the state of the K conductance process

We shall illustrate these factors with the simple transfer functions shown in Figure 2-5. The experimentally observed increases in g_{Na} and g_K from their resting values when voltage steps in the membrane potential are applied were shown in Figure 2-3. These changes can be considered to be originating from unknown systems whose unit-step responses are known and they are the simple exponential curves shown in Figure 2-5(b). The transfer functions for such systems are shown in (c).

If the membrane is depolarized slowly in the manner of a ramp function shown in (d) for example, then the outputs of the transfer functions for this ramp input are shown in (e). It is evident that Δg_{Na} is never substantially greater than Δg_K as it is the case in (b) for a step depolarization. Consequently, if the membrane is depolarized slowly, the AP may not be initiated even though the stimulus may rise gradually to an intensity many times greater than that at which a square pulse is effective. This property has been observed experimentally for nerve fibers (14).

The states of the Na and the K conductance processes are different before and after the spike in the AP even though the membrane potential is close to the resting level at both times. First, let us consider the Na process. During voltage steps, g_{Na} rapidly increases and then gradually declines or, as termed by Hodgkin and Huxley, g_{Na} is inactivated. If the inactivation is considered to be the result of negative forces "setting in", it would be of interest to know how quickly these forces are removed when the membrane potential is returned to the resting
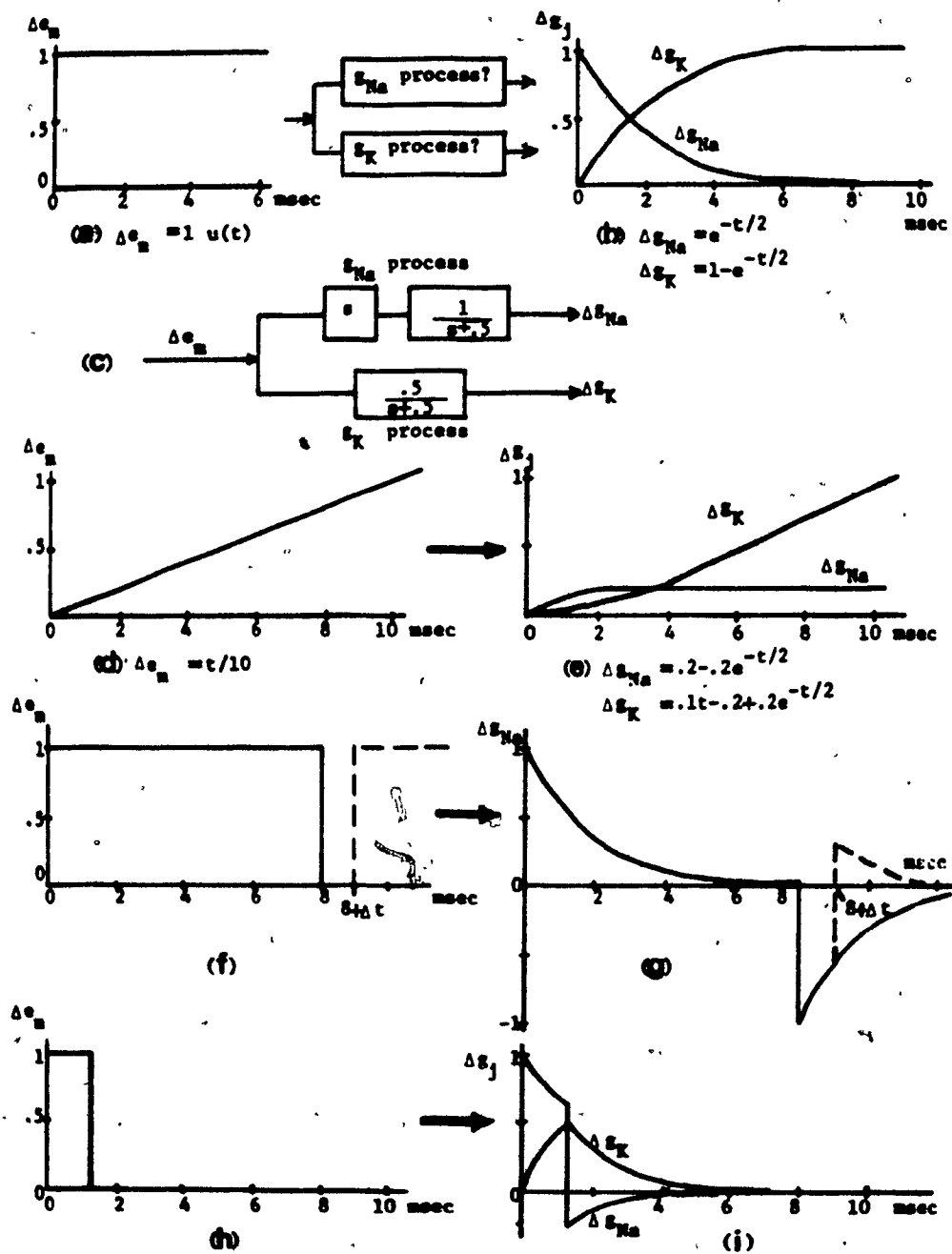
FIGURE 2-5 ILLUSTRATING WITH SIMPLE TRANSFER FUNCTIONS
THE PROPERTIES OF THE g_{Na} AND g_K PROCESSES

level.   In the case shown in (f) and (g), a unit voltage step is applied

at t = 0 and it is returned to resting potential when Δg_{Na} is approximately

zero at t = 8 msec.   It is of interest to know what is the peak of Δg_{Na}

when the unit step is re-applied at t = 8 + Δt.   Hodgkin and Huxley pre-

sented experimental evidence (15) which showed that the peak of Δg_{Na} at

t = 8 + Δt is less than the peak of Δg_{Na} at t = 0.   It was found that

the g_{Na} process returns to normal after the membrane potential is returned

to the resting level with a time constant equal to the time constant of

the decline of Δg_{Na} when the voltage step is applied at t = 0.   In the

illustration, the curves in (g) are the outputs of the transfer function

of the g_{Na} process for the inputs shown in (f).   There is a gradual re-

covery of the peak Δg_{Na} at t = 8 + Δt just as experimentally observed.

However, in the illustration Δg_{Na} attains negative values which would

mean that g_{Na} becomes negative because the resting value is a small

positive number compared to the large negative Δg_{Na}.   In reality, the

conductance for Na ions can only have a minimum of zero.   The transformation,

though, serves its purpose to illustrate the after-effect caused by the

inactivation of g_{Na}.

In Figure 2-5(h), a spike has been idealized as a rectangular

pulse and the outputs of the transfer functions for such an input are

shown in (i).   After a spike, there remains a temporary inactivation of

g_{Na} which means that then it is more difficult to establish an increase

in the Na current.   Moreover, there is a temporary increase Δg_K which

means that then there is an additional potassium current to be overcomed

by the Na current. As a result, after a spike, it is temporarily more dif-

ficult to establish the unbalance between the Na and the K currents.

During this period, known as the relative refractory period, the magnitude of a current pulse necessary to trigger a second spike is larger than the magnitude necessary to trigger a first spike.

CHAPTER III

MODELLING A POTASSIUM CONDUCTANCE PROCESS AND

OTHER PROPERTIES OF THE MOTONEURON - BASIC MODEL

3.1   Introduction (12, 16)

We begin to model the neuronal encoding mechanism by consider-
ing a particular type of neuron, the motoneuron in the spinal cord of the
cat, which has been studied experimentally in considerable detail. The
main morphological features of the motoneuron(MN) are illustrated in Figure
3-1. An extensive dendritic tree radiates from the soma. The initial
segment of the axon has a diameter which is significantly smaller than the
diameter of the axon itself. Thousands of excitatory and inhibitory fibers
converge on the MN with synapses on the dendrites and the soma.

Each spike converging on the MN causes a brief pulse of current
to flow across the membrane, and this current in turn produces a positive
(for an excitatory spike)or negative (for an inhibitory spike) transient
pertubation of the membrane potential called a miniature postsynaptic
potential (mPSP).   The spatial summation of the mPSPs due to spikes con-
verging along parallel fibers, and the temporal summation of the mPSPs
due to consecutive spikes converging along an individual fiber produce
an effective change of the membrane potential at the initial segment of
the axon.   Whenever this change of the membrane potential reaches a
threshold value, a spike is generated which propagates along the axon
and also invades the soma and dendrites.
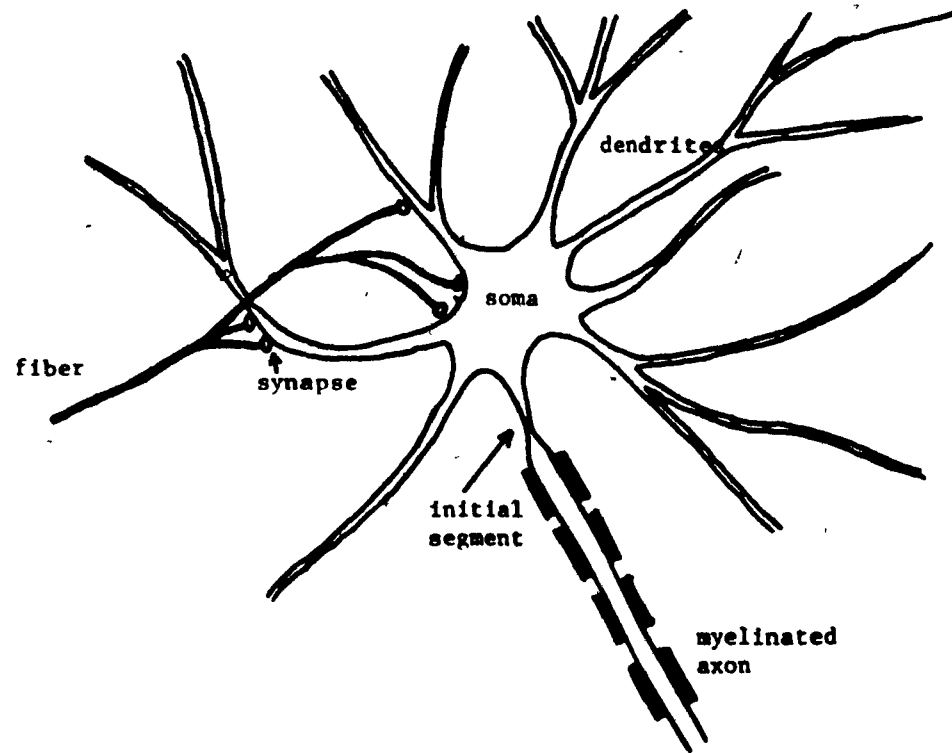
FIGURE 3-1 MORPHOLOGY OF THE MOTONEURON

A fundamental problem is: How does the MN encode the numerous input spike trains into the output spike train ? The output spike train can be recorded along the axon or with a microelectrode inserted into the MN, but it is difficult to control and quantitate the input spike trains. As an alternative approach, the MN is stimulated by a controlled current passed through the microelectrode. By studying how this current is en-

coded into the output spike train, the resulting information can be used to investigate how the input spike trains are encoded.

A single action potential (AP) observed for the MN has a spike and a prolonged after-hyperpolarization (AHP). Reported experimental observations which will be described during the development of our model in this and subsequent chapters, show that the AHP is of primary importance in the encoding mechanism. Since the AHP of the MN lasts much longer than the AHP of the squid axon, at least the parameters of the Hodgkin-Huxley model for the squid axon would have to be modified in order that this model could reproduce the AHP of the MN. In this chapter, we develop a model, in the context of the Hodgkin-Huxley model, which will reproduce the AHP of the MN. Since it is believed that the AHP is caused by a prolonged increase in a potassium conductance, we will be modelling mainly a potassium conductance process. We will refer to the resultant model as the basic model. The spike will not be reproduced because it is generally agreed that the shape of the spike carries no information in the encoding. Furthermore, a model which could reproduce the spike would be unnecessarily complex for studying neural systems.

3.2   Modelling the spike emission

When a MN is depolarized by applying current with a micro-electrode, a spike is generated if the change of the membrane exceeds a threshold voltage (TH) (17, 18). For a motoneuron with a resting potential of -70 mv, TH is about 15 mv [in (17) TH = 14 mv for a MN with a resting potential of -69 mv, in (18) TH = 10 mv for a MN already de-

polarized with a resting potential of -64 mv]. It is generally accepted that the spike originates at the initial segment of the axon and then it propagates out along the axon and back towards the soma and dendrites (12). The threshold of 15 mv is the equivalent threshold of the initial segment as it appears from the soma. The threshold for MNs is not significantly dependent on the rate at which the MN is depolarized (19), unlike for nerve fibers (see section 2.3).

In our model, the emission of spikes will be performed by the block shown in Figure 3-2. The input to the block is the change of the membrane potential at the soma, $\Delta e_m(t)$, given by,

$$\Delta e_m(t) = e_m(t) + E_r \qquad (3-1)$$

where, $e_m(t)$ is the membrane potential at the soma

and E_r is the magnitude of the resting potential

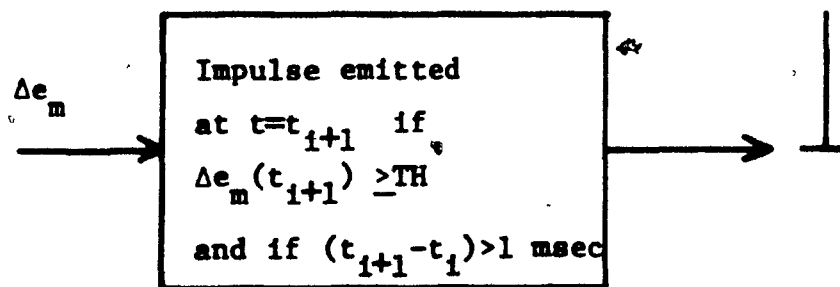The output of the block are unit impulses that represent spikes emitted

FIGURE 3-2 SPIKE EMITTER

at times t_i, $i = 1, 2, 3 \ldots \ldots$ An impulse is emitted whenever the criterion given in the block is satisfied. The first condition satisfies the threshold phenomenon. The period between two spikes $(t_{i+1}-t_i)$ must satisfy the second condition because of the absolute refractoriness during a spike. Incorporation of the relative refractoriness will be described in the next two sections.

3.3 Modelling mainly the potassium conductance process which produces the after-hyperpolarization

The basic features of an action potential observed at the soma of a MN are shown in Figure 3-3. The parameter values shown are those of a large MN with a "diameter" of 79 μm (12, 40, and see Chapter VI). The action potential has a 1 msec spike and a prolonged period of hyperpolarization called the after-hyperpolarization (AHP). The AHP reaches a maximum magnitude (AHP_m) of 5 mv at t = 10 msec and gradually declines towards the resting potential. Near its termination, the AHP reverses into a small after-depolarization. The duration of the AHP which is denoted AHP_d is 45 msec.

In order to develop a model which will reproduce the AHP of the MN, we begin with the Hodgkin-Huxley (H-H) model because the H-H model reproduces the AHP of the squid axon. The H-H model is for a patch of membrane of the squid axon, whereas the MN is a complex structure. Nevertheless, the MN could be represented with a large number of circuits of the type shown in Figure 2-2 (H-H model) in parallel. Each section of the model would represent a portion of the MN. However, we shall use the circuit in Figure 2-2 as a lumped model of the entire MN for two
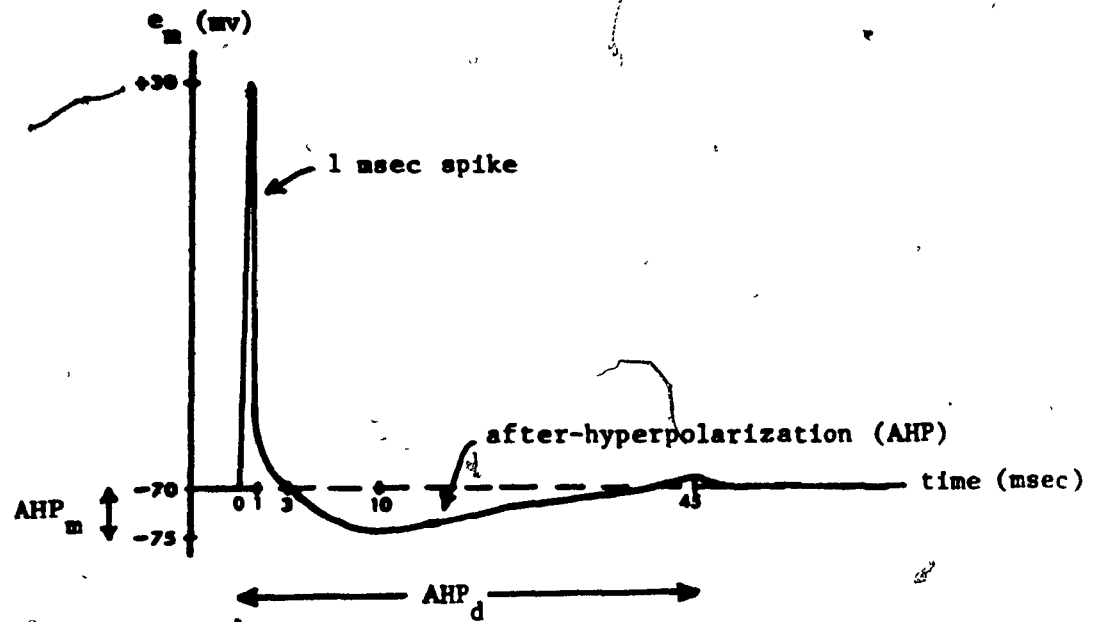
FIGURE 3-3 THE ACTION POTENTIAL OF THE MOTONEURON

reasons. Firstly, the properties of the various portions of the MN are presently not well understood. Secondly, a model with many sections would be too complex for initial studies of neural systems. The elements in the circuit now represent the effective load presented to the input current source (the microelectrode in the soma).

According to the H-H model described in Chapter II, the AHP of the squid axon is due to a temporary increase of the potassium conductance of the membrane. Experimental results (8, 12, 18, 21, 22) indicate that the AHP of the MN is also due to a temporary increase of the potassium conductance triggered by the spike. Thus, the potassium conductance g_K is given by $g_K = g_{Kb} + \Delta g_K$, where, Δg_K is the temporary increase of g_K triggered by the spike, and g_{Kb} describes the behaviour of g_K when no spikes are emitted. Hence, the potassium conductance branch in Figure 2-2 can be subdivided into two parallel branches as shown in Figure 3-4(a). The current pumps have been removed for the present development but they will be considered in Chapter VII. Now, by using this new representation,

the circuit in Figure 2-2 can be simplified into the circuit shown in Figure 3-4(b). The branches containing g_{Na}, g_{Kb}, and g_L have been lumped into the branch with constant resistance R in series with a constant voltage source E_r which is equal to the resting potential. The circuit in Figure 3-4(b) has also been used by Kernell (9) as we described in Section 1.2. If the Δg_K branch is removed, we are left with the well-known R-C model of the passive membrane which has been used, for example, to investigate various effects of the dendritic tree and to derive the strength-duration relation (20, 11b).

The latter simplification is contrary to the Hodgkin-Huxley model which states that g_{Na} and g_{Kb} are time-varying voltage-dependent conductances. However, the H-H model is based on experimental data for the squid axon and, while it may be qualitatively applicable to any neuronal membrane, the values of the parameters for different membranes should be different. For the MN, there exists no quantitative analysis of g_{Na} and g_{Kb}. During the spike these conductances certainly vary considerably, but we are mainly interested in their subthreshold behaviour. An indication of their combined subthreshold effect can be found by stimulating the MN with steps of current and then observing the subthreshold change of the membrane potential. The subthreshold step response reaches a maximum at about 15 msec after the onset of the current step and thereafter it declines gradually within 100 msec to a steady level that is about 70% of the maximum value (23). The over-shoot of this observed response cannot be reproduced by the R-C circuit of Figure 3-4(b) ($\Delta g_K = 0$ before a spike). However, as shown later, a model based on this circuit reproduces several properties observed when the MN emits spikes. Although a 2nd order transfer function could be

fitted to the subthreshold step response(5), such a transfer function may not be valid when spikes are emitted because the spikes change the behaviour of g_{Na} by inactivation so that the combined effect would be modified. Furthermore, an advantage of the R-C circuit is that it is based on a physiological substratum.

The behaviour of Δg_K has been inferred (8, 22) from measurements of the change of the input resistance R of the MN at various times after a spike. The increase Δg_K decays from an initial value ΔG_{KO} immediately after the spike to zero approximately exponentially with a time constant T_K , that is,

$$\Delta g_K(t) = \Delta G_{KO}\, e^{-t/T_K} \qquad (3-2)$$

Thus, $\Delta g_K(t)$ declines to about 5% of its initial value in three time constants T_K . The resultant AHP declines concurrently so that the duration of the AHP, AHP_d , is approximately given by,

$$AHP_d = 3\, T_K \qquad (3-3)$$

The complete basic model is shown in Figure 3-5. The forward path includes the transfer function $K_m/(s + A_m)$ for the R-C branches of the circuit in Figure 3-4(b), and the spike emitter in Figure 3-2. The feedback path corresponds to the Δg_K branch of the circuit in Figure 3-4(b). The increase and subsequent exponential decay of Δg_K triggered by a spike is the impulse response of the block $G_{KO}/(s + A_K)$.

A simulation of the basic model reproduces the after-hyperpolarization as shown in Figure 3-6. The parameters of the model were those of a large MN and were chosen according to experimental observations:

"diameter" of 79 μm $\Big\}$ (see Chapter VI)

$R = .75\ M\Omega$
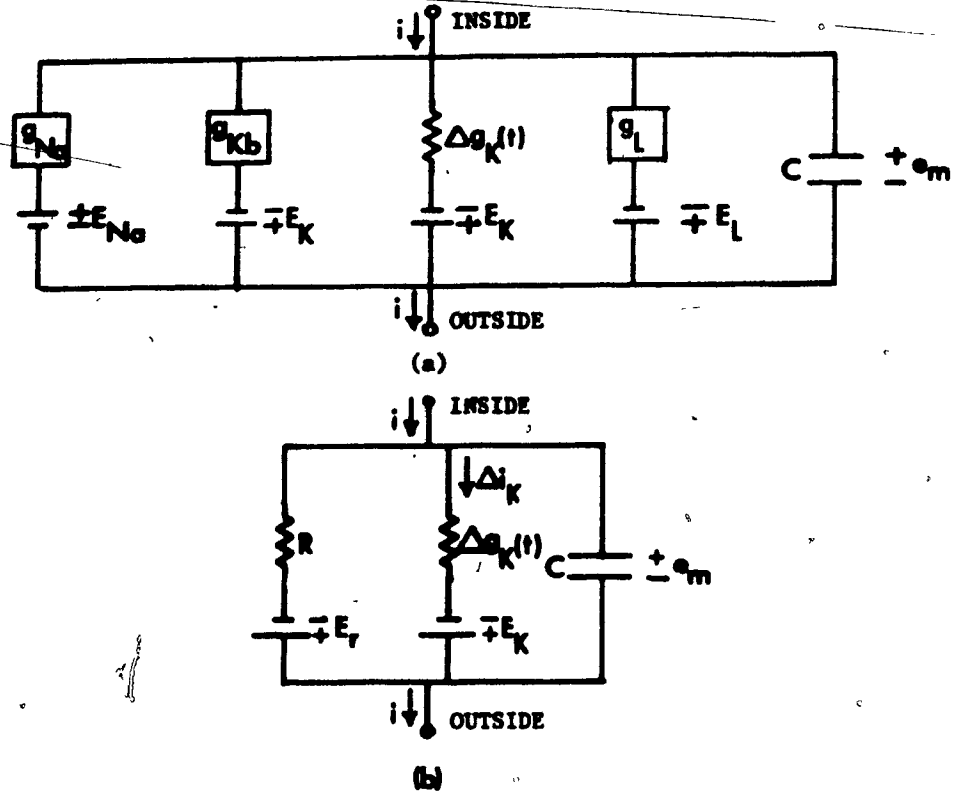
FIGURE 3-4   SIMPLIFICATION OF THE CIRCUIT IN FIGURE 2-2 FOR SUBTHRESHOLD
             OPERATION - CIRCUIT IN (b) IS NOW CONSIDERED AS A LUMPED MODEL

$K_m = 1/C$

$A_m = 1/RC \equiv 1/T_m$

$A_K = 1/T_K$

$\Delta e_m = e_m + E_r$
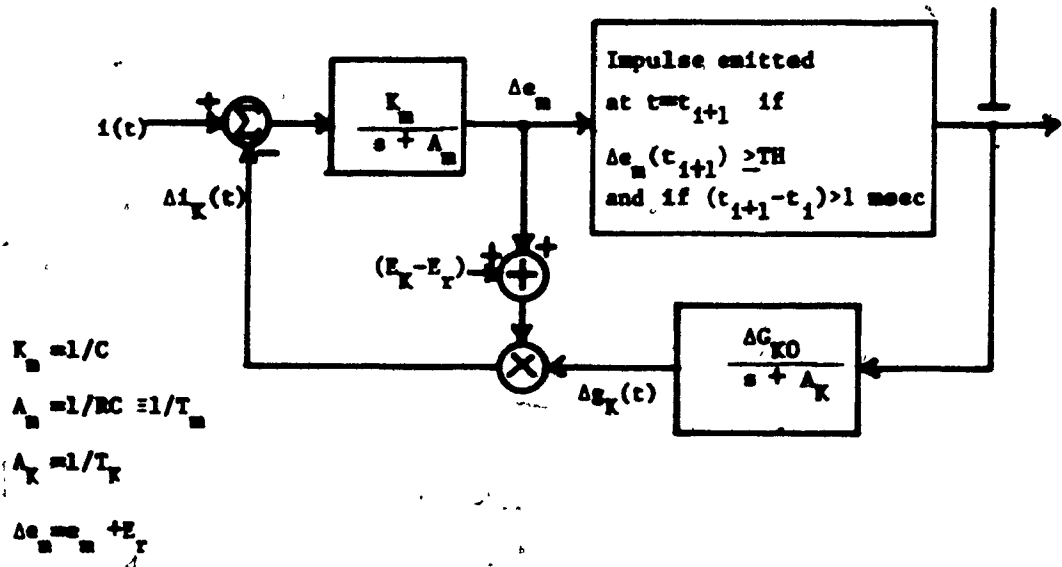
FIGURE 3-5   BASIC MODEL - A COMBINATION OF THE SPIKE EMITTER IN FIGURE 3-2,
             THE CIRCUIT IN FIGURE 3-4(b), AND EQUATION (3-2)

$$T_K = 14.2 \text{ msec} \qquad \text{(see Chapter VI)}$$

$$TH = 15 \text{ mv} \qquad \text{(see Section 3.2)}$$

$$T_m = 5 \text{ msec} \qquad (24)$$

$$\dot{E}_K = 90 \text{ mv} \qquad (12)$$

$$E_r = 70 \text{ mv} \qquad (12)$$

ΔG_{KO} was chosen equal to .68/R in order that the resultant maximum mag-nitude of the AHP be equal to the observed 5 mv. However, the observed percentage change of the MN conductance immediately after a spike with
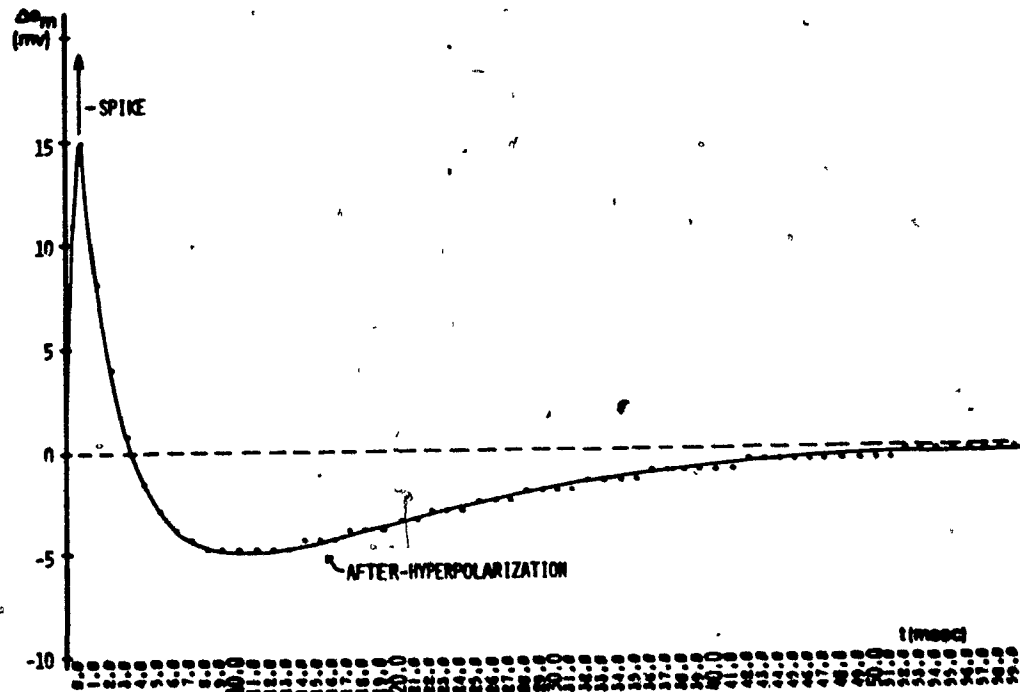
FIGURE 3-6   THE AFTER-HYPERPOLARIZATION IN SIMULATION OF THE BASIC MODEL

respect to the conductance before a spike is also about 70% (22). All simulations in the thesis were done on the digital computer by using Euler's method of solving a first-order differential equation and a time increment of 0.25 msec. A spike (drawn) has been elicited by applying a pulse of current until Δe_m reaches TH and then Δe_m returns to zero autonomously due to the negative feedback current $\Delta i_K(t)$. Similar to the experimental observation, the AHP of the model reaches a maximum magnitude of 5mv at 11msec and thereafter it declines to approximately zero in about 45msec. It should be pointed out, however, that the AHP of the MN ends abruptly with a hump of after-depolarization at about 45 msec whereas the AHP of the model decays asymptotically.

3.4   Refractory periods

In this section we show that the basic model incorporates the absolute and relative refractoriness. The refractoriness of the basic model at various times after a spike is shown in Figure 3-7(b) with published experimental data shown in Figure 3-7(a) (25). A measure of refractoriness is the relative stimulus strength I_2/I_1, where I_1 and I_2 are the minimum intensities of current pulses that are necessary to trigger the first and second spikes respectively. The abscissa is the time interval between the two stimulating pulses. It is shown mathematically in the Appendix that I_2/I_1 for the basic model is given by,

$$\frac{I_2}{I_1} = \infty \qquad\qquad t < 1 \text{ msec}$$

$$\doteq \frac{15 - \Delta e_m(t)}{15} \qquad t \geq 1 \text{ msec} \qquad\qquad (A-5)$$

where, $\Delta e_m(t)$ is the change in the membrane potential in mv after a spike. This change is shown in Figure 3-6 and it includes mostly the AHP.
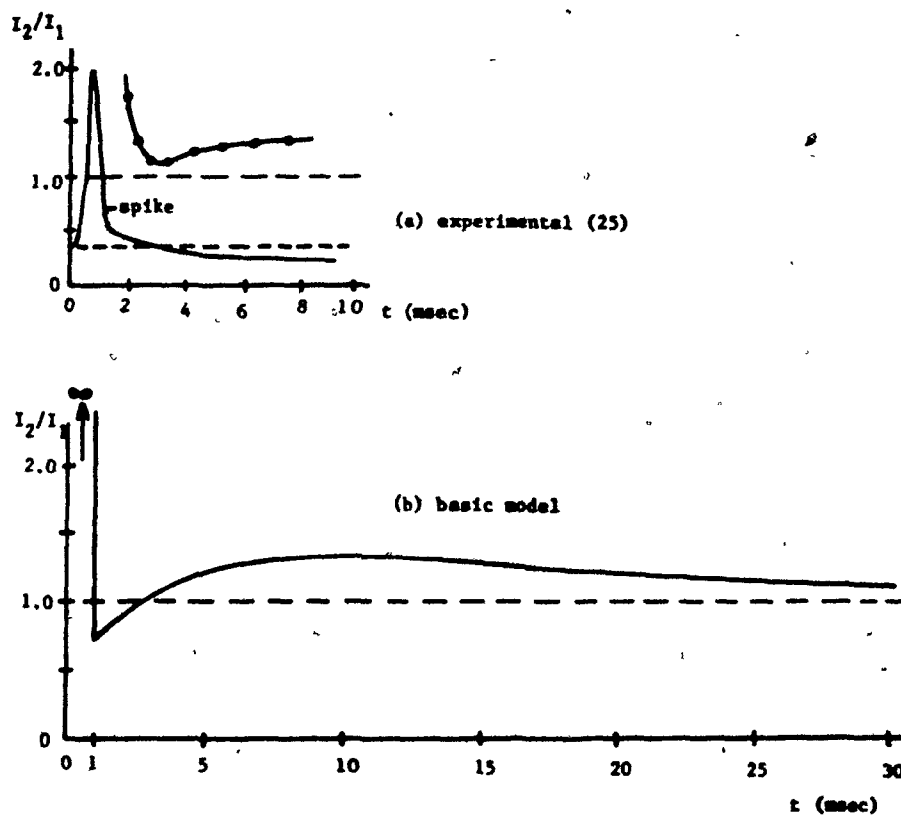

FIGURE 3-7 REFRACTORINESS AFTER A SPIKE

During the first spike, it is not possible experimentally to trigger a second spike and this period is known as the absolute refractory period. In the model, the spike is represented by the ideal unit impulse and the absolute refractory period is satisfied with the condition $(t_{i+1} - t_i) \geq 1$ msec. After the spike, during the so-called relative refractory period, a second spike can be elicited both experimentally and in the model only if I_2/I_1 is greater than or equal to the values given by the curves. For intervals from 4 to 8 msec, the experimental and theoretical values agree, so that during this period the relative refractoriness is accounted for by the fact that the membrane potential is hyperpolarized by the AHP. Experimental values for intervals greater than 8 msec have not been reported. However, we can expect that they also agree with the theoretical values for the following reason. The magnitude of the monosynaptic reflex discharge of a MN pool stimulated by a pulse applied to the dorsal root is directly proportional to the number of MNs which emit a spike (11e). For each MN which emits a spike, there is a temporary refractoriness. As a result, some of these MNs cannot emit a second spike if a second consecutive pulse is applied to the dorsal root. Thus, the magnitude of a second consecutive discharge of the pool would be less than the magnitude of a first discharge as ex- perimentally observed (26). Furthermore, the discharge is reduced by an amount which is directly proportional to the magnitude of the AHP (26). Consequently, the relative refractoriness of a MN is directly proportional to the magnitude of the AHP. Finally, for intervals from 1 to 4 msec, the theoretical and experimental values do not agree. This disagreement is not significant because, for normal conditions, the inter-spike inter-

val is usually greater than 4 msec (i.e. firing frequency less than 250 pulses per second) and, at the time of emission of any spike, the refractoriness from a previous spike is accounted for by the model.

3.5   Comparison with the aid of the model between the potassium conductance which produces the after-hyperpolarization for the motoneuron and the one for the squid axon

The AHP observed for a MN lasts much longer than the AHP observed for the squid axon.   It is revealing to compare the underlying increase Δg_K for the MN and the squid axon.   From Figure 2-4, we note that g_K for the squid axon increases from a resting value less than 1 mmho/ sq. cm to a maximum of 10 mmho/sq. cm immediately after a spike.   This is an increase of more than 1000 percent.   The value of g_K for the MN before a spike has been emitted may be assumed to be at least 50% of the MN conductance 1/R (16).   Therefore, for the MN, the percentage increase in g_K is only equal to ($\Delta G_{KO}/g_{Kb}$) x 100 = [(.68/R)/(.5/R)] x 100 = 136% which is substantially less than the 1000% for the squid axon.   Furthermore, the increase $\Delta g_K(t)$ for the squid axon is over in 3 msec while $\Delta g_K(t)$ for the MN is much more prolonged because it declines exponentially with a time constant of 14 msec.

Such substantial differences in the magnitude as well as in the time course of $\Delta g_K(t)$ for the squid axon and the MN suggests the possibility that two different mechanisms might be involved.   The Hodgkin-Huxley model states that for the squid axon the declining portion of the

spike is caused by the increase in the potassium conductance. Since the percentage increase of the potassium conductance for the MN is much less than for the squid axon, we should investigate whether or not the increase Δg_K for the MN is sufficiently large in order to cause the spike to decline in less than 1 msec as experimentally observed. We can investigate this theoretically by using the circuit in Figure 3-4(b). Although the circuit is applicable only to subthreshold operation, it can also serve our present purpose for the following reason:

Let us consider as the initial time the instant when the spike is at its peak so that, the initial condition of the voltage across the capacitor is about +10 mv. We are interested in determining the time that it takes for the voltage to be reduced to the threshold potential of -55 mv, because it has been observed experimentally (12) that the spike declines in less than 1 msec up to about this point, and thereafter it continues as a declining depolarization for several milliseconds before crossing over to become the AHP. The voltage is partially reduced by the increase in the potassium current through the Δg_K branch in the circuit in Figure 3-4(b). The current through the branch containing R also reduces the voltage across the capacitor. Since this branch lumps the g_{Na}, g_{Kb}, and g_L branches and since g_{Na} increases considerably during the spike, then R is not constant during the decline of the spike. However, the increase in g_{Na} produces a current that depolarizes the capacitor (increases its voltage). Thus, in fact, the total current through g_{Na}, g_{Kb}, and g_L does not reduce the voltage as quickly as the current through the fixed resistance R. Consequently, the time that it takes for the spike to decline, which will be calculated with this simplified circuit, is an underestimate.

The differential equation for the circuit in Figure 3-4(b) is

$$C \frac{de_m}{dt} + (e_m + E_K) \Delta g_K(t) + \frac{(e_m + E_r)}{R} = 0 \qquad (3\text{-}4)$$

Substituting in (3-4),

$$\Delta e_m = e_m + E_r \;,\; T_m = RC, \; E_K - E_r = 20 \text{ mv} \quad (12)$$

Also, although during the decline of the spike $\Delta g_K(t)$ varies (see Figure 2-4), we set it equal to its average value which is approximately equal to ΔG_{KO}, the value of Δg_K at the end of the spike. We get,

$$\frac{T_m}{\Delta G_{KO}R+1} \frac{d \Delta e_m}{dt} + \Delta e_m = \frac{-20 \,\Delta G_{KO}R}{\Delta G_{KO}R+1} \qquad (3\text{-}5)$$

The solution of equation (3-5) with the initial condition equal to the spike height, that is, $\Delta e_m(t{=}0) = e_m(t{=}0) + E_r = 10 + 70 = 80$ mv is

$$\Delta e_m = 80 \, e^{-t/(T_m/ \Delta G_{KO}R+1)} - \left(1 - e^{-t/(T_m/\Delta G_{KO}R+1)}\right) \frac{20\Delta G_{KO}R}{\Delta G_{KO}R+1}$$

$$(3\text{-}6)$$

The time that it takes for the spike to decline to $\Delta e_m = -55 + 70 = 15$ mv is found by solving equation (3-6) for t,

$$t = \frac{T_m}{\Delta G_{KO}R+1} \ln \left(\frac{80(\Delta G_{KO}R+1) + 20 \,\Delta G_{KO}R}{15(\Delta G_{KO}R+1) + 20 \,\Delta G_{KO}R} \right) \qquad (3\text{-}7)$$

Substituting in (3-7), $T_m = 5$ msec and $\Delta G_{KO}R = .68$ (see Section 3.3) we get $t = 3.7$ msec which is significantly larger than the experimental value of less than 1 msec. Thus, it appears that the prolonged increase $\Delta g_K(t)$ which produces the AHP for the MN is not sufficiently large in order to cause the spike to decline in less than 1 msec. There should be an ad-

ditional brief increase during the spike. If we substitute $\Delta G_{KO} = 5/R$ in equation (3-6) we find that, theoretically, the spike would decline in 0.93 msec. This represents an increase of 1000% in the potassium conductance and it is the same value as for the squid axon. Thus, theoretically it appears that, for the MN, in addition to the prolonged increase Δg_K which produces the after-hyperpolarization, there may be a brief transient increase of g_K similar to that for the squid axon. The basic model includes the component of g_K which produces the AHP, whereas the other component is not included because the model does not have to reproduce the shape of the spike.

This theoretical conclusion agrees with the experimental observation (27) that for some MNs there is a distinct rapid repolarization at the end of the spike and the AHP occurs, thereafter. More interestingly, this conclusion is also supported by the experimental results and conclusions of Connor and Stevens for the molluscan soma membrane (28). They concluded that, in addition to possessing conductances analogous to the g_{Na} and g_K of the Hodgkin-Huxley model, the soma of that neuron also has an operationally distinct potassium conductance mechanism which tends to dominate the neuron's behaviour in the interval between spikes.

It is also possible that the time constant of the g_K dynamics in the Hodgkin-Huxley model may be inversely related to the dimensions of the structure of the particular portion of the neuron. This possibility is suggested by two experimental observations. The duration of the AHP is inversely related to the size of the MN (see Chapter VI) so that T_K is inversely related to the size of the cell. If the same correlation exists for the different parts of the cell, then, T_K for the membrane of the dendrites would be larger than T_K for the membrane of the soma since

the cross-sectional diameter of dendrites is much smaller than that of the soma. As a result, the long AHP observed in the MN would be due to a prolonged Δg_K in the dendrites. Also, according to the analysis above, the spike in the dendrites would decline much slower than the spike in the soma because the prolonged Δg_K that produces the AHP is not a large increase. It has been observed experimentally (12) that there is such a difference in the time course of the spike as observed in the soma and dendrite.

3.6 Summary

In this chapter, we have developed a basic model of the encoding mechanism of the motoneuron in the context of the Hodgkin-Huxley model. It consists of a forward path and a negative feedback path. The forward path includes the transfer function for the R-C model of the membrane and a spike emitter which emits a unit impulse whenever the change in the membrane potential exceeds a threshold value. The negative feedback path accounts for the inhibitory current produced by the prolonged increase in a potassium conductance triggered by the emitted spike. We have made two major simplifications in modelling: (i) the motoneuron is represented by a lumped model, and (ii) the time-varying voltage-dependent conductances are replaced by a fixed resistance for subthreshold operation. The model reproduces the experimentally-observed after-hyperpolarization and the significant portion of the relative refractory period, although it does not reproduce the overshoot in the subthreshold step response. The

theoretical analysis based on the model and published experimental observations indicate that the potassium conductance process which causes the long after-hyperpolarization for the motoneuron may be different from the potassium conductance process which causes the decline of the spike in the Hodgkin-Huxley model.

In the next chapter, we shall compare other properties of the model with those of the motoneuron.

CHAPTER IV

RESPONSE OF THE BASIC MODEL TO STIMULATION BY

STEPS, RAMPS, AND SINUSOIDS OF CURRENT

In the previous chapter, a brief pulse was applied to the basic
model and a single spike was emitted.   In this chapter, step, ramp, and
sinusoidal waveforms are applied to the basic model and a series of spikes
are emitted.   All simulation results presented in this chapter are for a
large MN with a "diameter" of 79 μm whose parameters have been specified
in Section 3.3.   The simulation results for MNs of different size will
be presented in Chapter VI.

4.1   Response to stimulation by steps of current

4.1.1 Threshold current and minimum firing frequency

When a MN is stimulated with a step of current through a micro-
electrode, there is a threshold intensity above which the MN fires (emits
a spike) repetitively [29].   A typical recording of the trajectory of the
membrane potential during repetitive firing is shown in Figure 4-1(a).
The basic model also fires repetitively for an input step above the
threshold current I_{th} given by

$$I_{th} = \frac{THA_m}{K_m} = \frac{TH}{R} \qquad\qquad (4-1)$$

where, TH is the threshold voltage (see Figure 3-5)

and   R is the resistance of the MN (see Figure 3-4(b)).

The responses of the basic model for input steps just below and above I_{th}
are shown in Figure 4-1(b) and (c) respectively.   There is either
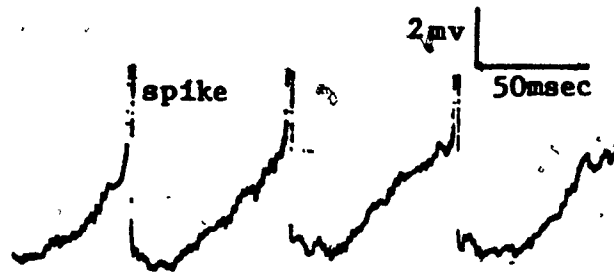
repetitive firing or no firing at all.

FIGURE 4-1(a)   EXPERIMENTALLY OBSERVED TRAJECTORY OF THE MEMBRANE
POTENTIAL DURING REPETITIVE FIRING (31)

However, for the real MN, with input current steps less than the
threshold current but greater than the so-called rheobase current, the MN
can emit only a few spikes after the onset of the step.   The threshold .
current is on the average 1.5 times the rheobase current (29).

The operation of the encoding mechanism in the basic model is
illustrated in Figure 4-1(c).   Curve S represents the depolarization due
to the input current i(t).   Curve A represents the after-hyperpolarization
(AHP) due to the negative feedback current Δi_K.   Since the change in the
membrane potential, Δe_m, is the output of a linear transfer function
(see Figure 3-5), curve • which represents Δe_m is the difference between
curve S and curve A.   The second and subsequent spikes are emitted when-
ever the AHP has decayed sufficiently to allow Δe_m to reach the threshold
voltage.

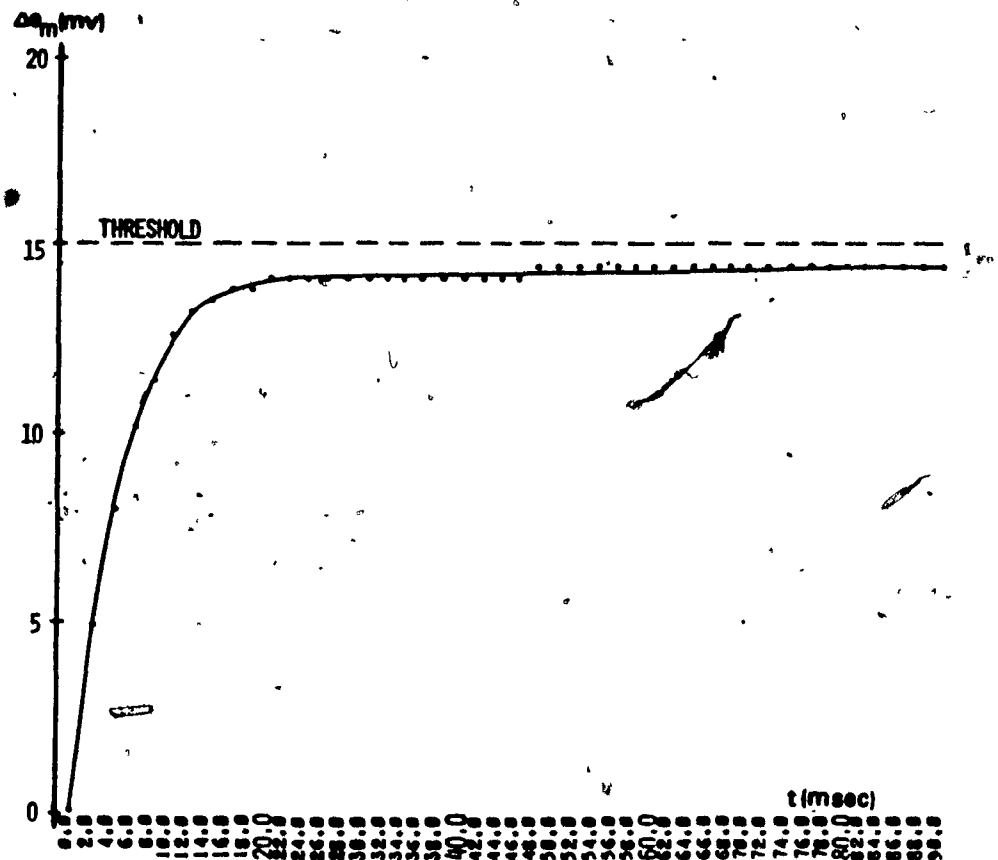During repetitive firing in Figure 4-1(c), the maximum magnitude

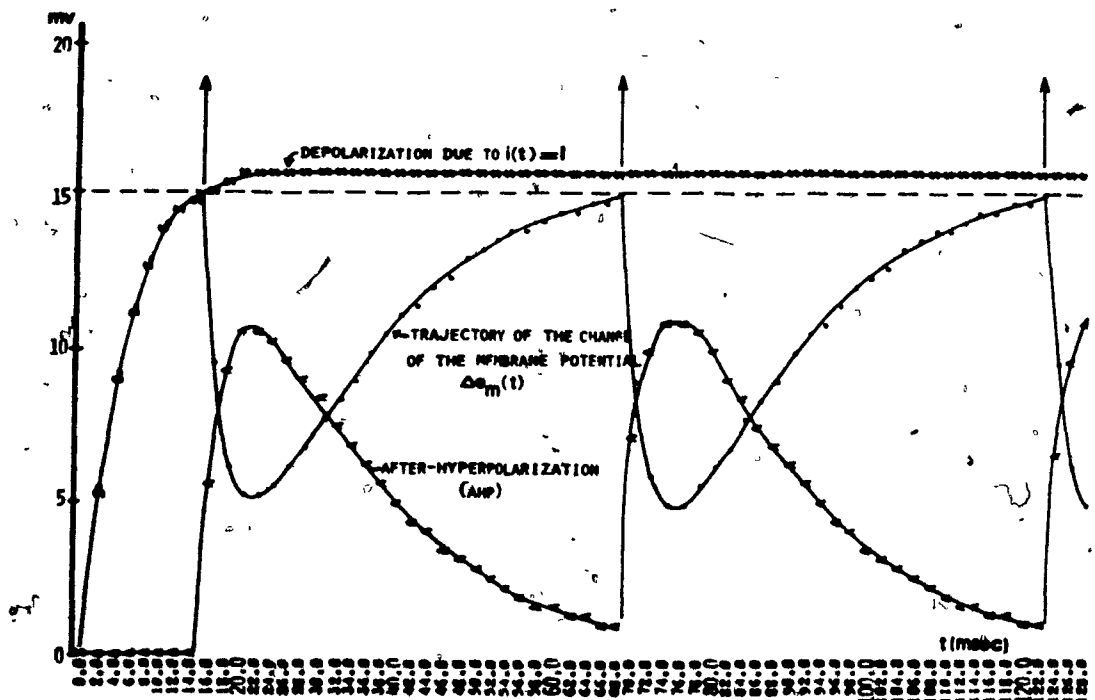FIGURE 4-1 (b)   SUBTHRESHOLD STEP RESPONSE OF THE BASIC MODEL

FIGURE 4-1 (c)   REPETITIVE FIRING OF THE BASIC MODEL FOR A STEP INPUT
JUST ABOVE THE THRESHOLD CURRENT

of the AHP is about 10 mv, whereas after the single spike in Figure 3-6 it was only 5 mv. This apparent contradiction can be explained as follows (18):

From the basic model in Figure 3-5,

$$\Delta i_K(t) = \Delta g_K(t) \left[\Delta e_m(t) + (E_K - E_r) \right] \qquad (4-2)$$

As shown in Figure 4-1(c), $\Delta e_m(t)$ varies from 5 to 15 mv during the AHP. Substituting these values and $E_K - E_r = 20$ mv (12) into (4-2), we find that $\Delta i_K(t)$ is between $25\Delta g_K(t)$ and $35\Delta g_K(t)$. By similar analysis for the single spike in Figure 3-6, $\Delta i_K(t)$ is between $15\Delta g_K(t)$ and $20\Delta g_K(t)$. Since $\Delta g_K(t)$ is the same for both cases (at the same time after the first spike), $\Delta i_K(t)$ and the resultant AHP during repetitive firing are about two times their values for the single spike case. This effect has been observed experimentally (18, 31).

When repetitive firing is established in a MN by applying a step of current just above the threshold current, the MN fires with a definite minimum firing frequency (also known as pulse or spike frequency) (30). For example, a large MN either fires with a firing frequency greater than about 20 pulses per second (pps) or it does not fire repetitively at all (see Chapter VI). The minimum firing frequency f_m is equal to the inverse of the duration of the after-hyperpolarization (AHP_d) (30), that is,

$$f_m = \frac{1000}{AHP_d} \qquad (4-3)$$

where, AHP_d is in msec and f_m is in pulses per second (pps).

This property is possibly due to the fact that the AHP ends with a hump

of after-depolarization which causes Δe_m to abruptly cross the threshold
voltage (30). In the model, the firing frequency approaches zero when
the depolarization due to I minus the threshold voltage is infinitesmally
small because $\Delta g_K(t)$ decays to zero exponentially. However, as it will
be evident in section 4.1.3, the range of the input I for which the firing
frequency is less than f_m is quite small so that this discrepancy in the
behaviour of the model is not significant.

4.1.2 Summation of the potassium conductance process and adaptation of
firing frequency

During repetitive firing in the basic model, the output $\Delta g_K(t)$
of the transfer function $\Delta G_{KO}/(s+A_K)$ exhibits a temporal summation of
the form,

$$\Delta g_K(t) = \sum_{j=0}^{\infty} \Delta G_{KO}\, e^{-(t-t_{i-j})/T_K}, \quad t \geq t_i \qquad (4\text{-}4)$$

where, t_{i-j}, $j = 0, 1, 2 \ldots\ldots$ are the times of occurrence of spikes
prior to time t. It has been shown experimentally that a summation of
the potassium conductance process does in fact occur. Baldissera and
Gustafsson (22) observed that the percentage increase of the MN conduc-
tance, which is believed to be due to Δg_K, after two immediately con-
secutive spikes was twice as large as the increase after only one spike.
This observation also indicates that Δg_K summates linearly as in the
model. On the other hand, Ito and Oshima (21) observed that the resultant
AHP summates nonlinearly as shown in Figure 4-2 curves (a) - (d). The
AHP after two spikes in (b) is larger than the AHP after a single spike
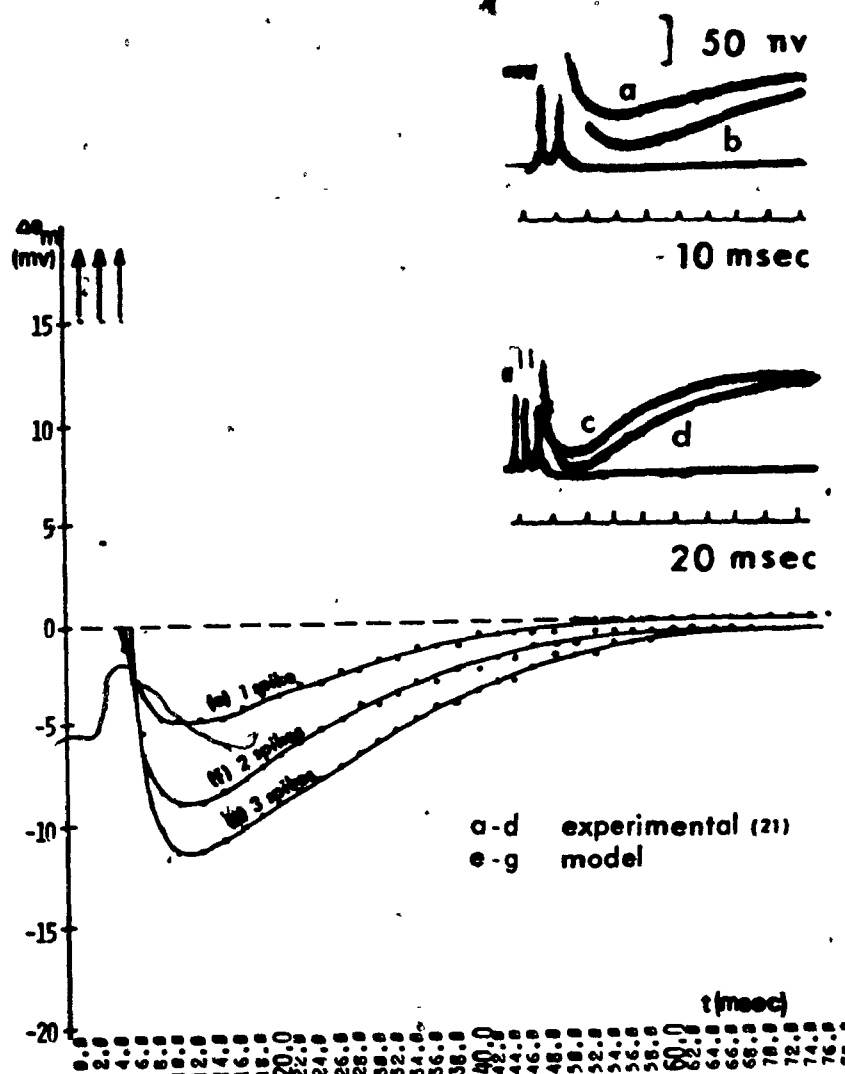
FIGURE 4-2 SUMMATION OF THE AFTER-HYPERPOLARIZATION

in (a). The AHP after three spikes in (d) is not much larger than the

AHP after two spikes in (c). Although Δg_K summates linearly, a non-

linear summation of the AHP is also observed in the simulation results of

the model as shown in Figure 4-2 curves (e) - (g). This effect is clari-

fied by considering the following hypothetical case which is amenable to

a mathematical analysis:

In the basic model, let $i(t) = 0$ and $\Delta g_K(t) =$ constant X

Then, Δe_m is constant and it is found from,

$$\Delta e_m = -\frac{K_m}{A_m} \Delta i_K \tag{4-5}$$

and, $$\Delta i_K = X \left[\Delta e_m + (E_K - E_r) \right] \tag{4-6}$$

Substituting (4-6) into (4-5) and solving for Δe_m,

$$\Delta e_m = \frac{-\frac{K_m}{A_m} X(E_K - E_r)}{1 + \frac{K_m}{A_m} X} \tag{4-7}$$

The plot for (4-7) with $(E_K - E_r) = 20$ mv as in the simulation in shown in Figure 4-3.

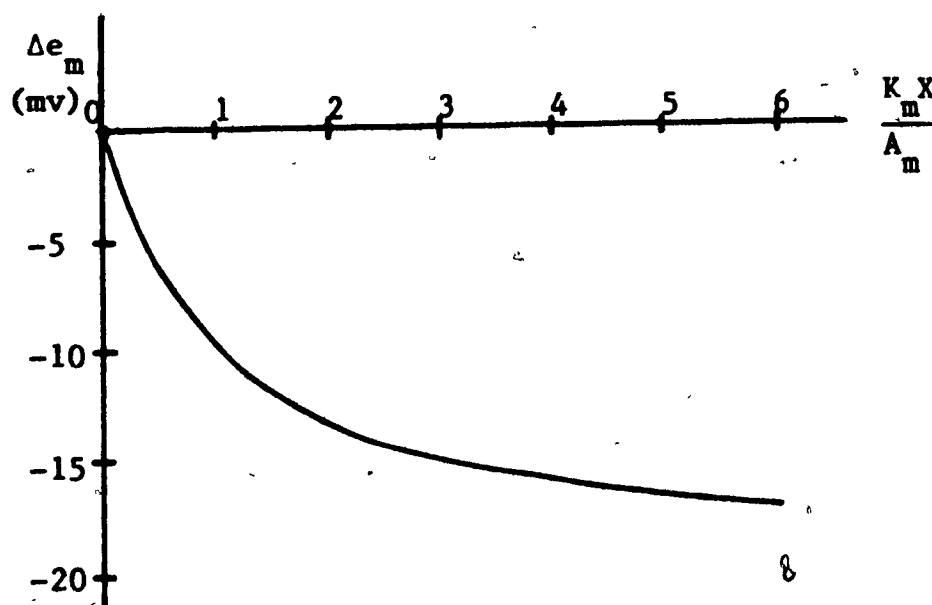

FIGURE 4-3   PLOT OF EQUATION (4-7) WITH $(E_K-E_r) = 20$ mv

It is evident that Δe_m is not linearly dependent on X (K_m/A_m is a constant). The nonlinearity is pronounced for $\Delta e_m < -10$ mv and Δe_m is limited at

-20 mv.   Likewise, for the actual case in Figure 4-2, the nonlinearity is clearly evident at about -10 mv.

Based on some experimental results, several workers (22, 29, 32) have suggested that summation of the potassium conductance process produces an adaptation of the firing frequency.   Figure 4-4(a) shows the firing of a MN at the onset of two stimulating current steps of different magnitude (32).   It is evident that in both cases the instantaneous firing frequency for the first interval, that is, the inverse of the first interval, is larger than the adapted (steady state) firing frequency.   The same effect is observed in the simulations with the basic model shown in Figure 4-4 (b) and (c).   The AHP clearly summates and, as a result, the adapted firing frequency is less than the instantaneous firing frequency for the first two intervals.   In Figure 4-4(c), the instantaneous firing frequency for the first interval is 1000 pps while, in reality, initial firing frequencies are generally only a few hundred pulses per second (33). This discrepancy arises because the model does not correctly account for the relative refractoriness from 1 to 4 msec after a spike (see section 3.4).

In addition to the adaptation of the firing frequency within a few initial intervals, Kernell (29) observed in some MNs a late phase of adaptation which was evident gradually over a time span of several seconds. However, the degree of this late phase of adaptation was small compared to the marked initial adaptation.   We shall neglect it for the present discussion, but we shall propose a general model in Chapter VII which will include a late phase of adaptation due to the electrogenic sodium pump process.

FIGURE 4-4(a)   EXPERIMENTALLY OBSERVED FIRING OF A MN FOR
TWO DIFFERENT STEP INPUTS (32)
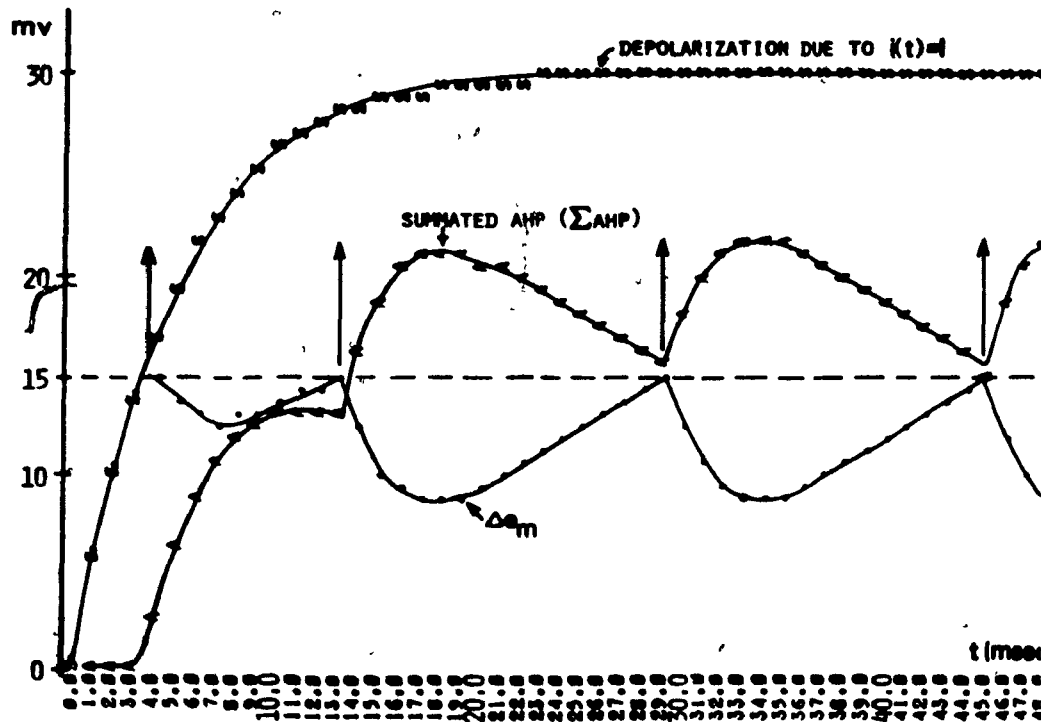
FIGURE 4-4(b)   REPETITIVE FIRING OF THE BASIC MODEL FOR A STEP INPUT $I=2I_{th}$
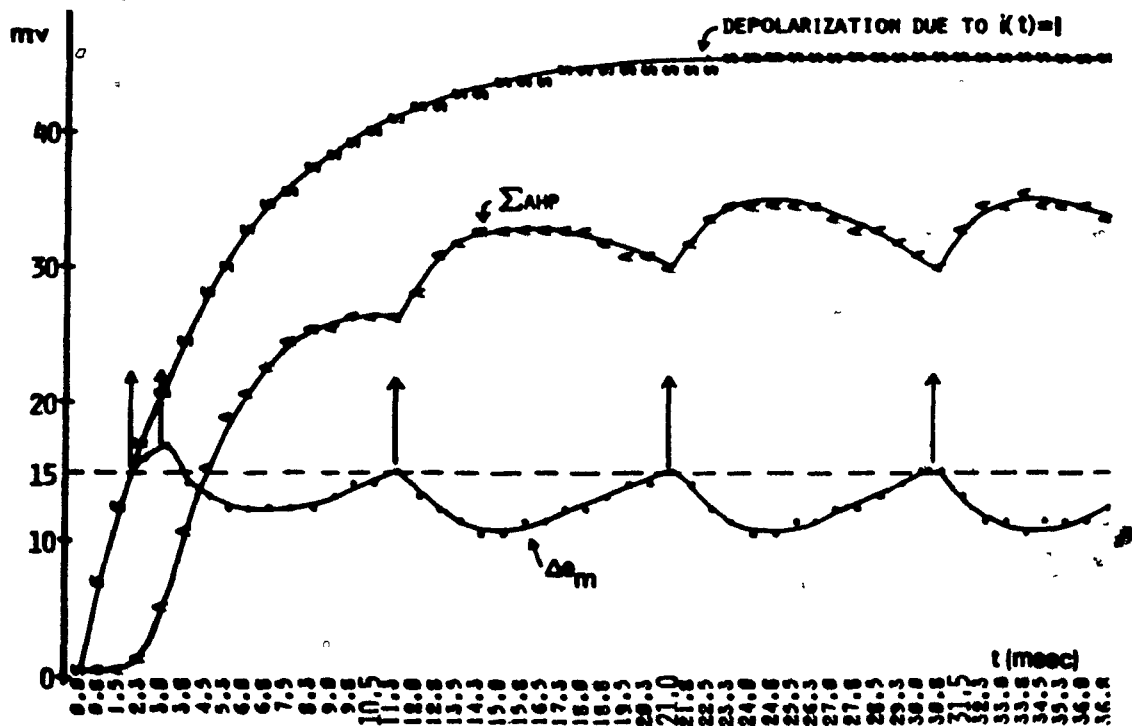
FIGURE 4-4(c)   REPETITIVE FIRING OF THE BASIC MODEL FOR A STEP INPUT $I=3I_{th}$

4.1.3 Relationship between adapted firing frequency versus intensity

of the current step

A plot of the adapted firing frequency f_{SK} versus the intensity
of the step of stimulating current is shown in Figure 4-5: curve (a) is
for the model while curve (b) is from the experimental data obtained by
Kernell (33).   We can reasonably compare the experimental data with the
simulation results because the minimum firing frequency, f_m, and the
threshold current I_{th}, for the real MN indicate that this particular MN
has a size which is similar to the model MN, as we shall explain in
Chapter VI.

FIGURE 4-5   ADAPTED FIRING FREQUENCY f_{SK} VERSUS THE INTENSITY
OF THE STIMULATING STEP I

The experimental curve can be approximated by two straight-line segments which were denoted by Kernell as follows:, the primary range for input currents from the threshold current to about 2.5 times the threshold current (i.e. from 20 nA to 50 nA in this case); the secondary range for input currents above 50 nA. The curve for the model is mostly a single straight line whose equation is
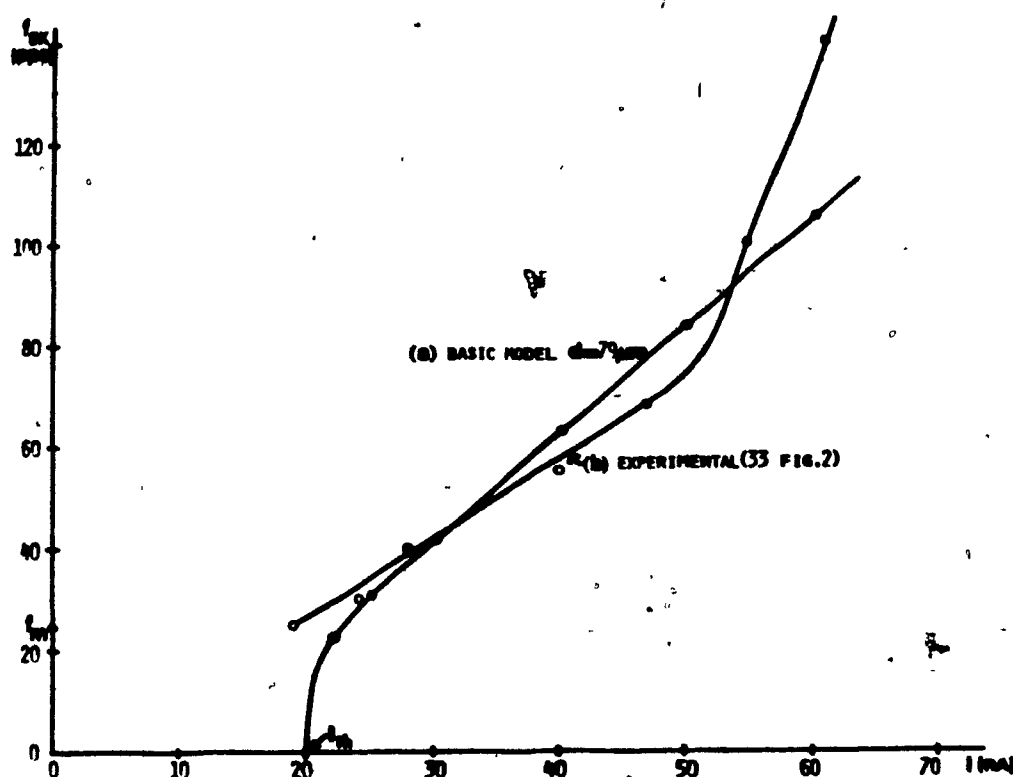
$$f_{SK} = 2(I - 20) + 20 \qquad I > 20 \text{ nA}$$
$$= 0 \qquad\qquad I \leq 20 \text{ nA} \qquad (4-8)$$

where, f_{SK} is in pps and I is in nA.

There is adequate agreement in the primary range between the experimental values of f_{SK} and those predicted by the model. We note that the model fires with a frequency much less than the actual minimum frequency only for inputs in a small range from 20 nA to 22 nA so that, in view of the entire range of operation, the fact that the model does not have a definite minimum firing frequency is not significant. Unlike the experimental curve, the curve for the model does not have a secondary range of firing. It is not known what causes the relatively larger increase of the firing frequency in the secondary range. In fact, in 50% of the MNs tested by Kernell, firing stopped altogether instead of firing in the secondary range. The maximum firing frequency within the primary range can cause the motor unit to develop 85% of its maximum tetanic tension (34), so that it is likely that under normal conditions the MN operates within the primary range.

4.2 Response to stimulation by ramps of current

Frank and Fuortes (19) stimulated MNs with ramps of current of different slopes. Their observations for one MN are reproduced in the insets of Figure 4-6 (a) - (c). The linearly-rising curve is the stimulating current and the other curve is the trajectory of the membrane potential. The spikes were not recorded because the sweep was too slow. The responses of the basic model to the same inputs are also shown in Figure 4-6 (a) - (c). It is clearly evident that the model and the real MN operate very similarly for these ramp inputs.
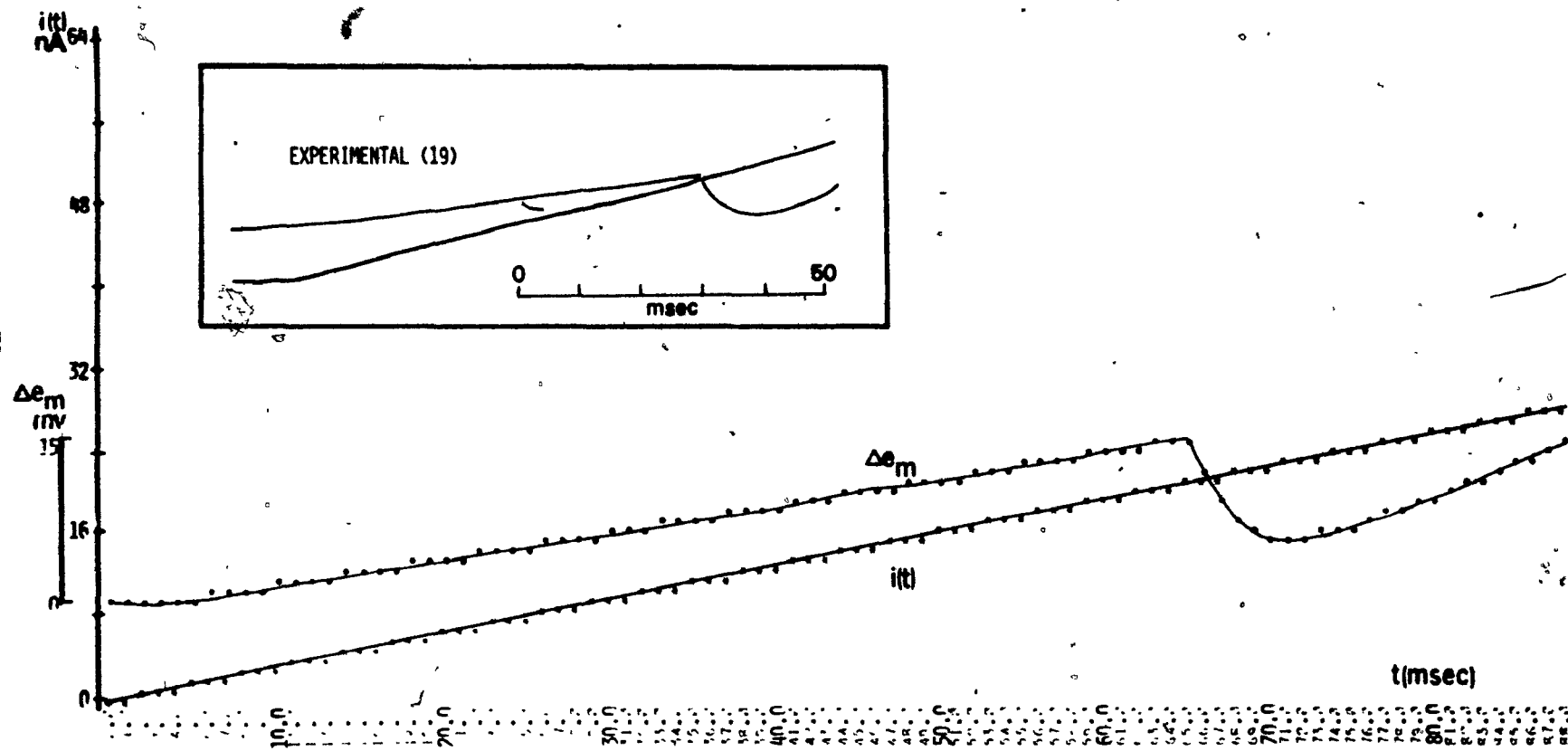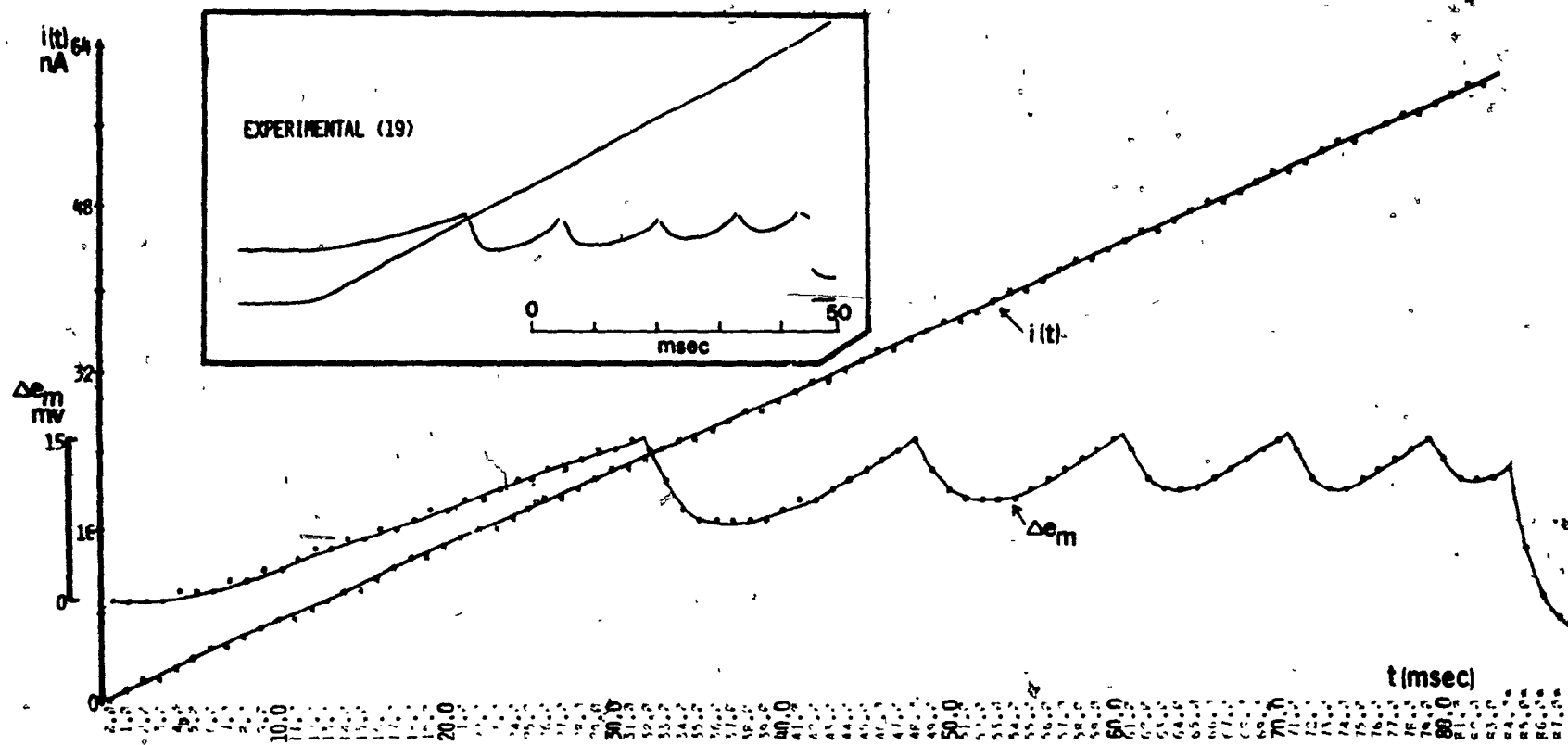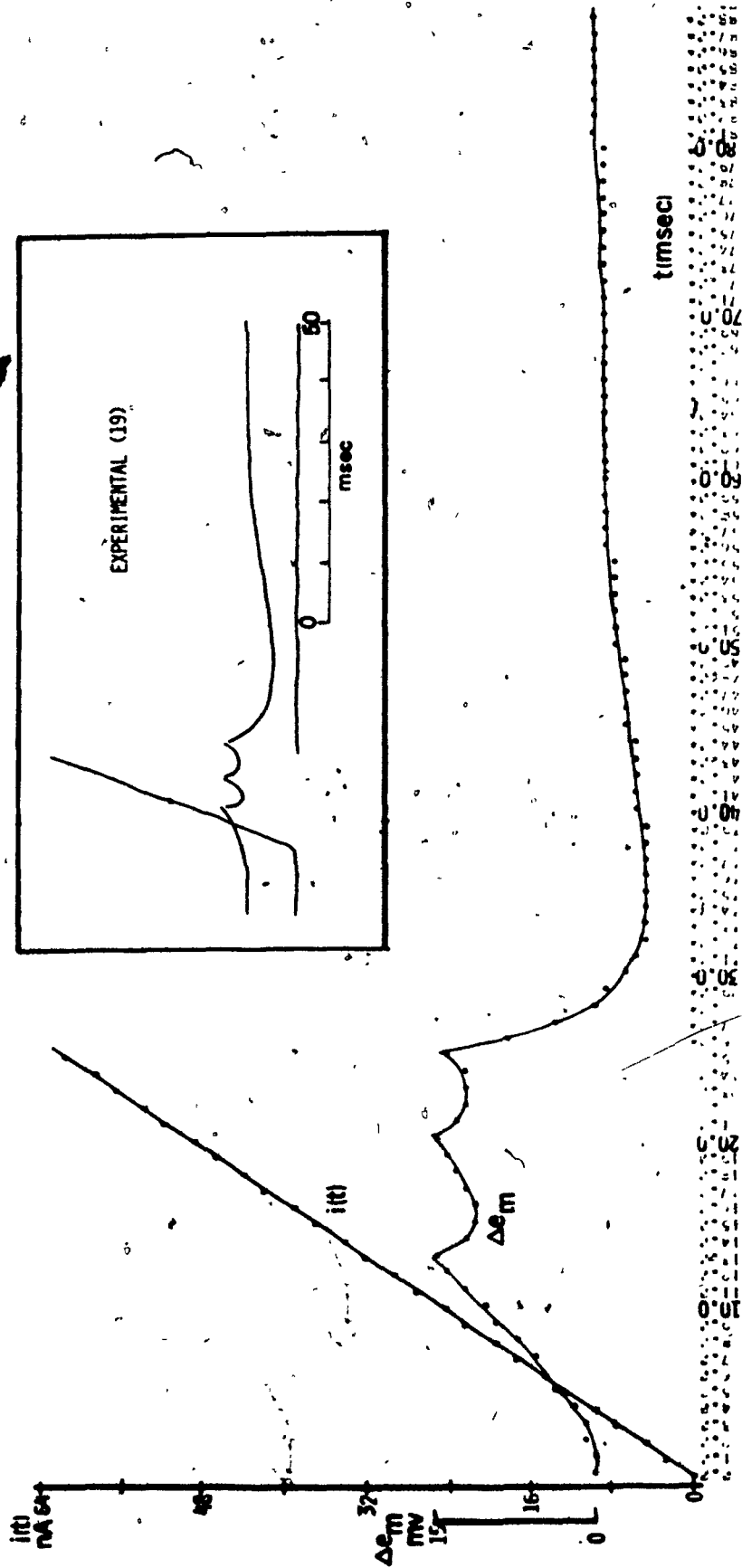
FIGURE 4-6(a)   RESPONSE TO RAMP INPUT i=.33t

FIGURE 4-6(b)   RESPONSE TO RAMP INPUT i=.75t

54

EXPERIMENTAL (19)

FIGURE 4-6(c) RESPONSE TO RAMP INPUT $i=2.5t$

4.3   Response to stimulation by sinusoids of current

We shall first investigate how the basic model responds to
sinusoidal inputs of different amplitudes but of one particular frequency
(2 Hz).   The simulation results are shown in Figure 4-7 (a) - (d) for
four different inputs.   The lower printout, denoted by *, shows the in-
put i(t) and the dashed line is the level of the threshold current.   The
top printout shows the instantaneous firing frequency $f(t_i)$ which is de-
fined as the inverse of the interval between the spike emission times
t_{i-1} and t_i.   The time of occurrence of the first spike after t = 0 is
indicated by ⊞ while the other spike occurrence times are indicated by
+.   Because of the discrete nature of the printout, the precise emission
times cannot be indicated and instead the ⊞ and + are placed at the
forthcoming time shown on the printout.   The instantaneous firing fre-
quency is evaluated only at the spike emission times and thus we have
discrete data points.   However, if there is a sufficient number of data
points to enable us to specify an appropriate continuous function that
fits these data points, we can describe the instantaneous firing frequency
response by a continuous function f(t).

In the first three cases in Figure 4-7 (a) - (c), the input
magnitude varies from a minimum just above the threshold current to a
variable maximum.   In the fourth case in (d), the input magnitude varies
about the threshold current.   For the response in (a), it is evident that
f(t) is a sinusoid in phase with i(t).   When the input amplitude is in-
creased in (b) and (c), f(t) remains essentially sinusoidal.   When the
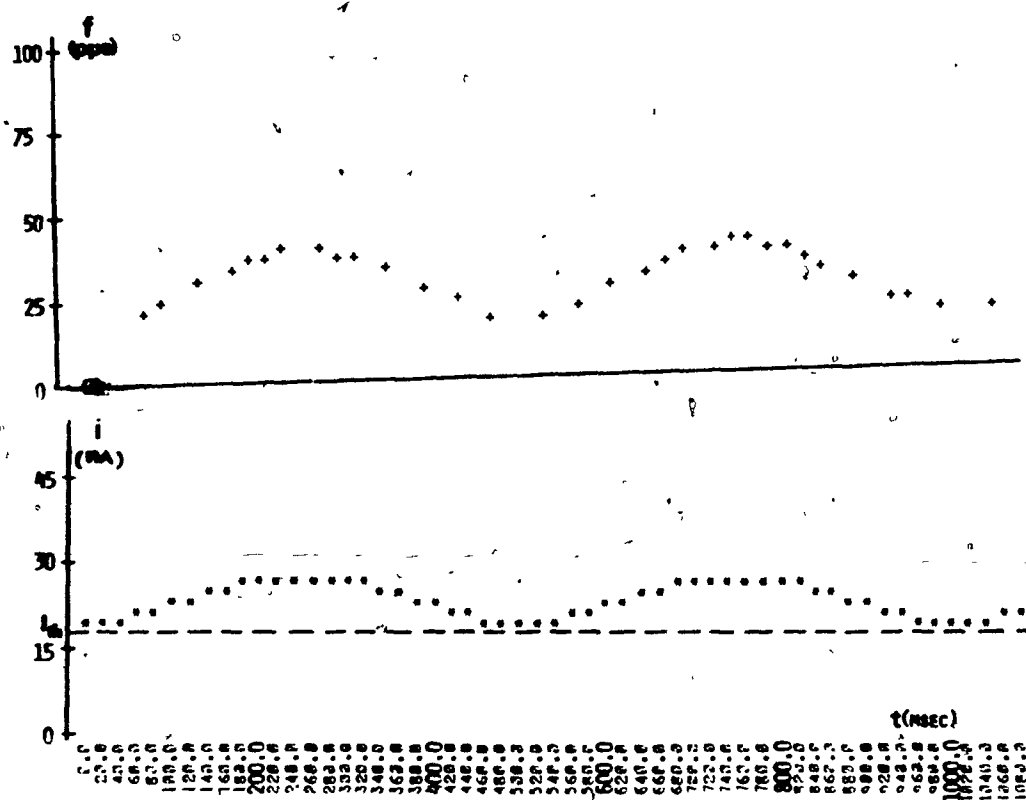input is such that during one portion of the cycle it is less than the

FIGURE 4-7(a) $i(t)=25-4\cos(2\Pi.2.t/1000)$

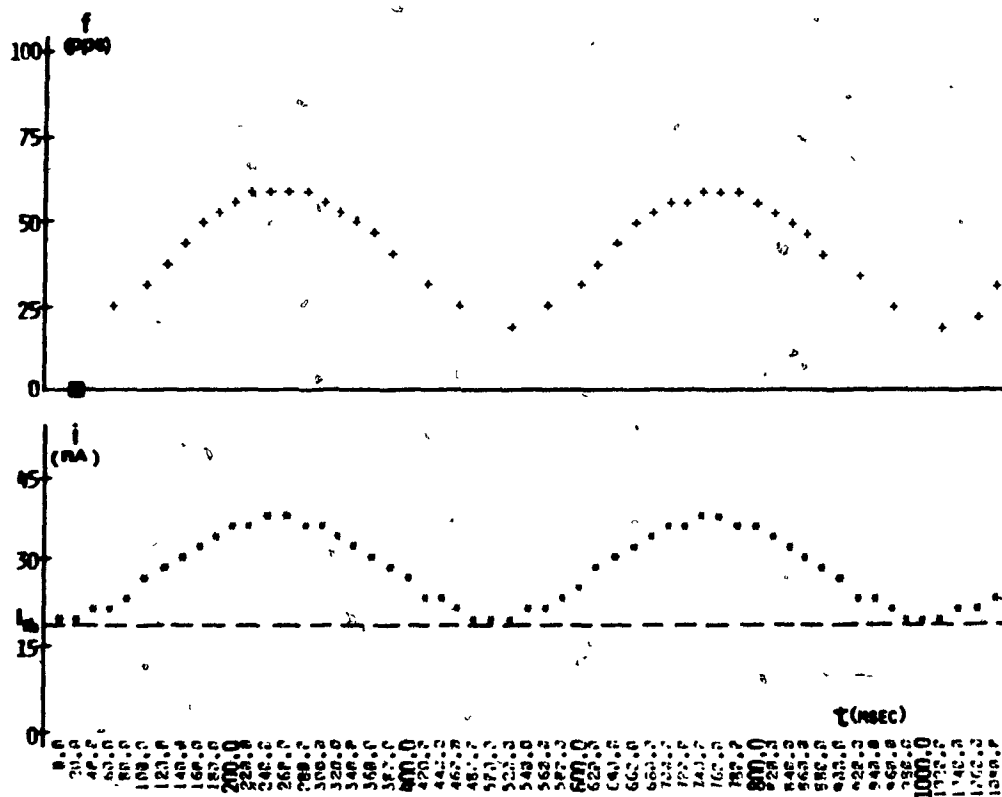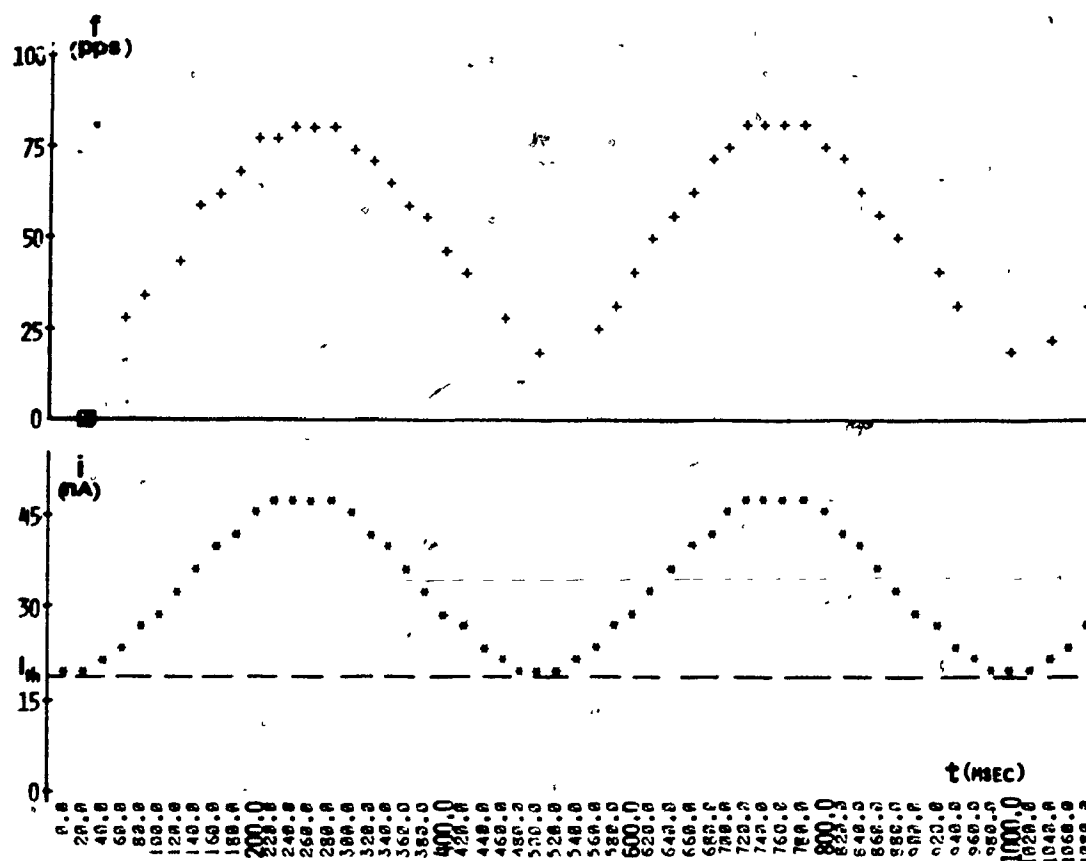
FIGURE 4-7(b) $i(t)=30-9\cos(2\Pi.2.t/1000)$

FIGURE 4-7(c) 1(t)=35-14cos(2Π.2.t/1000)
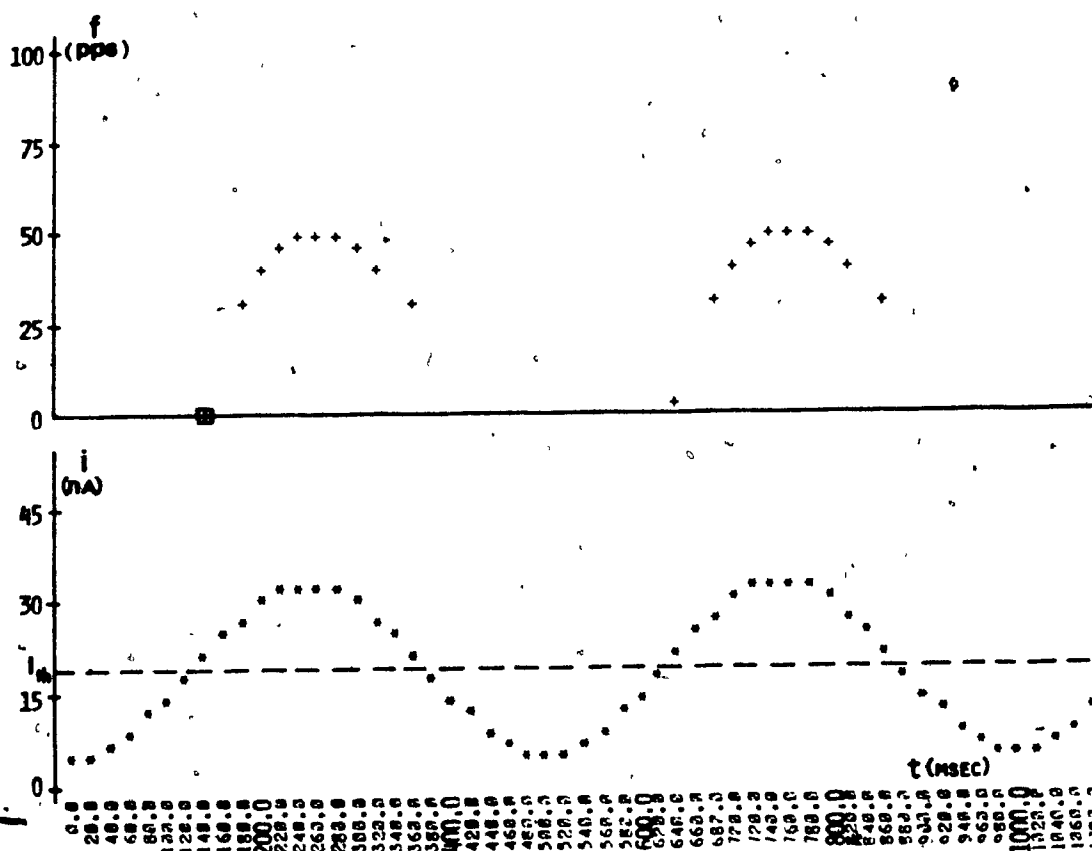
FIGURE 4-7(d) 1(t)=20-14cos(2Π.2.t/1000)

FIGURE 4-7 RESPONSE OF THE BASIC MODEL TO SINUSOIDAL INPUTS
WITH ONE FREQUENCY, 2Hz, AND DIFFERENT AMPLITUDE

threshold current as in (d), the spikes occur in groups or bursts followed by a period of no firing. The response at 2 Hz, then, is given by the expression,

$$f(t) = 2(i(t) - 20) + 20 \qquad i(t) > 20 \text{ nA}$$
$$= 0 \qquad\qquad i(t) \leq 20 \text{ nA} \qquad (4-9)$$

where, $f(t)$ is in pps and $i(t)$ is in nA. It is interesting to note that this expression is the same as expression (4-8) for the adapted or static relationship in Figure 4-5.

Now we vary the input frequency and keep the input amplitude constant. The simulation results are shown in Figure 4-8 (a) - (d) for the input frequencies .2, 5, 10, and 15 Hz, and in Figure 4-7(c) for the frequency 2 Hz. At .2 and 2 Hz, $f(t)$ is a sinusoid and in phase with $i(t)$. At the higher input frequencies, burst activity occurs and the trend is for the spikes to occur during the rising portion of the input. At 5 Hz, 4 spikes occur during the declining portion of the sinusoid compared to 6 spikes during the rising portion of the sinusoid. At 10 Hz, only one spike clearly occurs during the declining portion. At 15 Hz, all the pulses occur during the rising portion of the sinusoid. We particularly point out that, at the higher input frequencies, the "middle" of each burst of spikes does not occur at the time when the input is maximum, rather it is leading. We shall refer to this leading as a phase lead.

By examining the "internal" variables of the model, we can see why the burst of spikes occur with a phase lead at the input frequency of 15 Hz. The responses of these variables for two input amplitudes are shown in Figure 4-9 (a) and (b). Curve * represents the input current
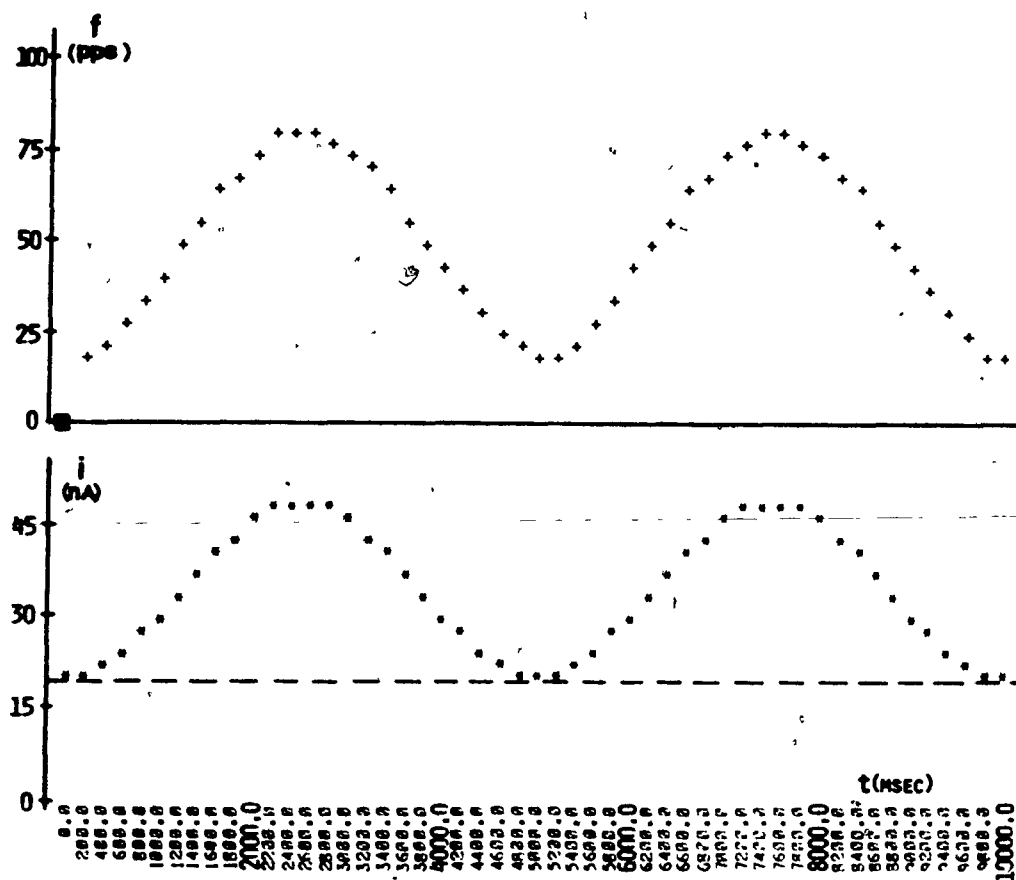
FIGURE 4-8(a)   i(t)=35-14cos(2Π..2.t/1000)
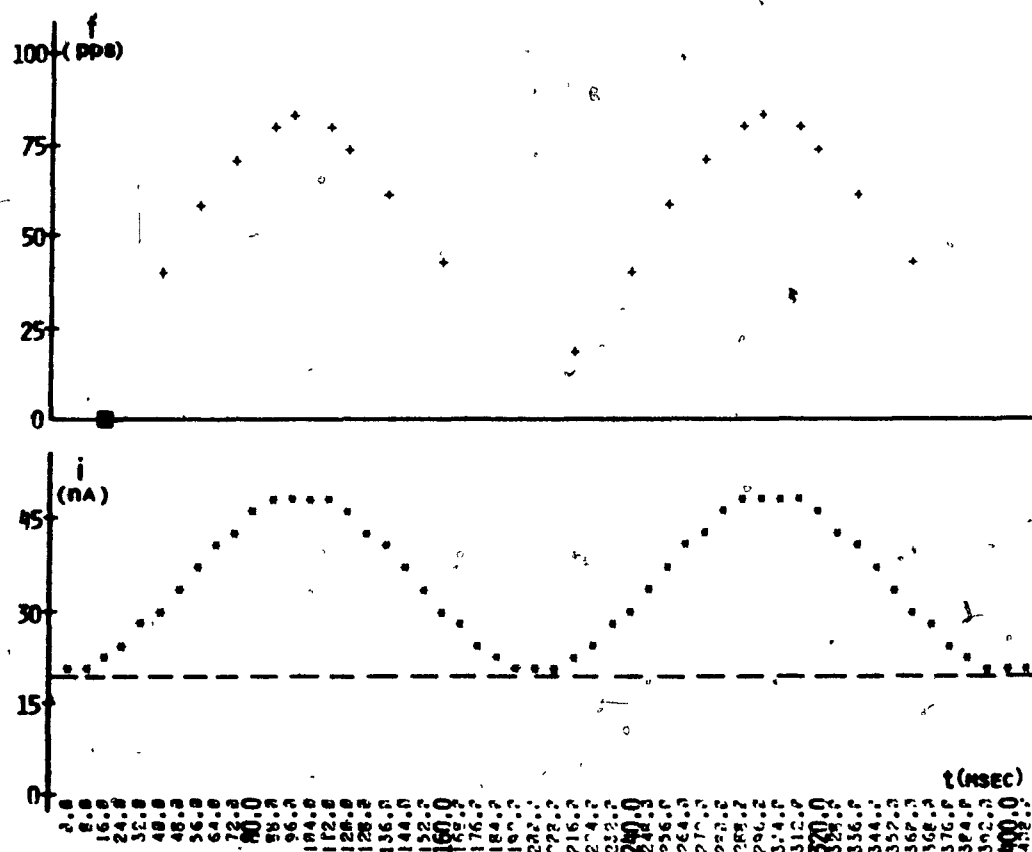
FIGURE 4-8(b)   i(t)=35-14cos(2Π.5.t/1000)
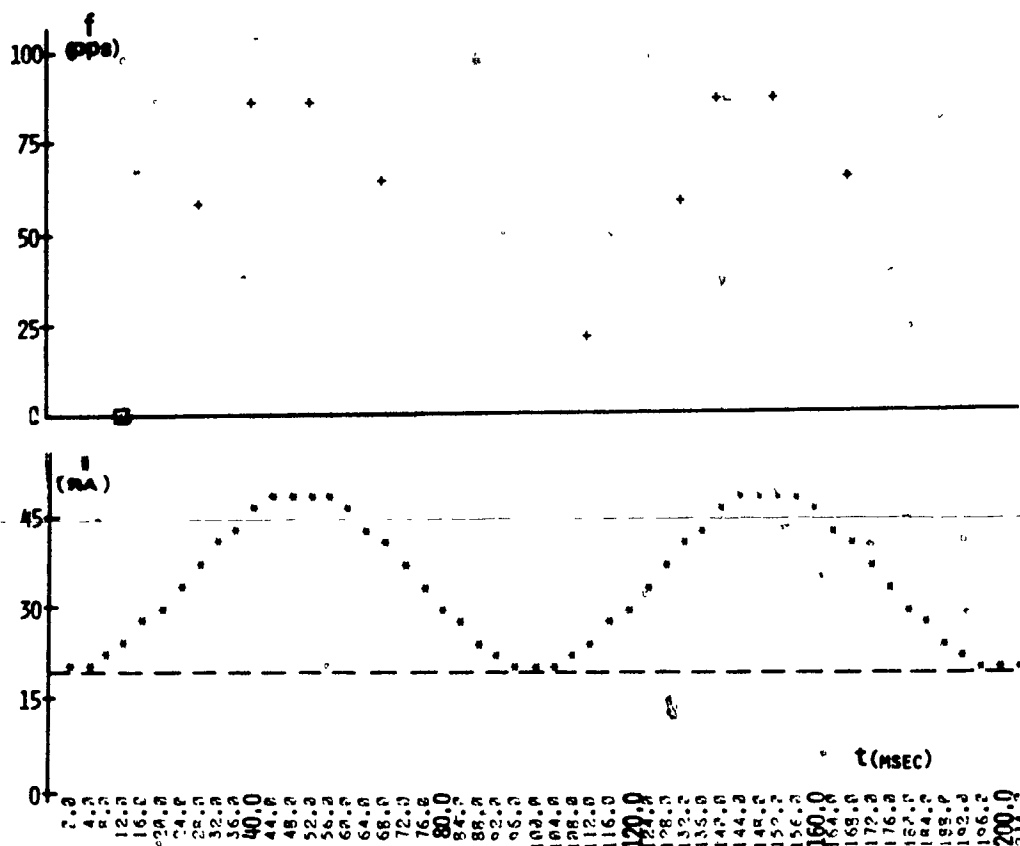
FIGURE 4-8(c) 1(t)=35-14cos(2Π.10.t/1000)
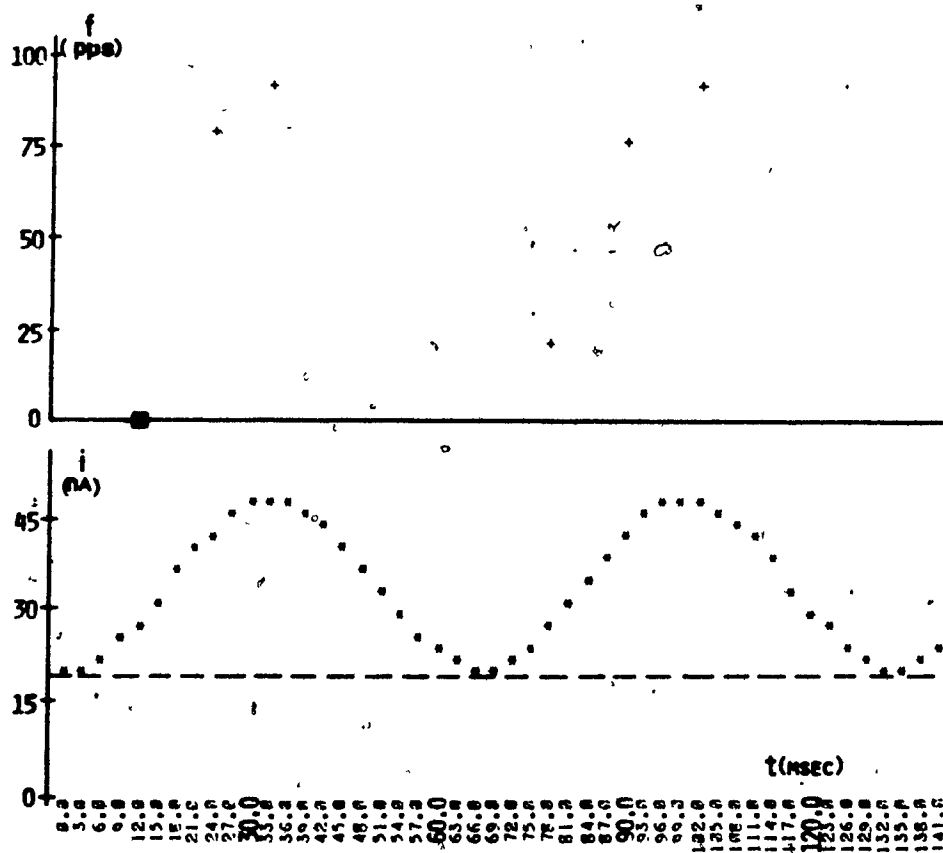
FIGURE 4-8(d) 1(t)=35-14cos(2Π.15.t/1000)

FIGURE 4-8 RESPONSE OF THE BASIC MODEL TO SINUSOIDAL INPUTS
WITH DIFFERENT FREQUENCY AND CONSTANT AMPLITUDE
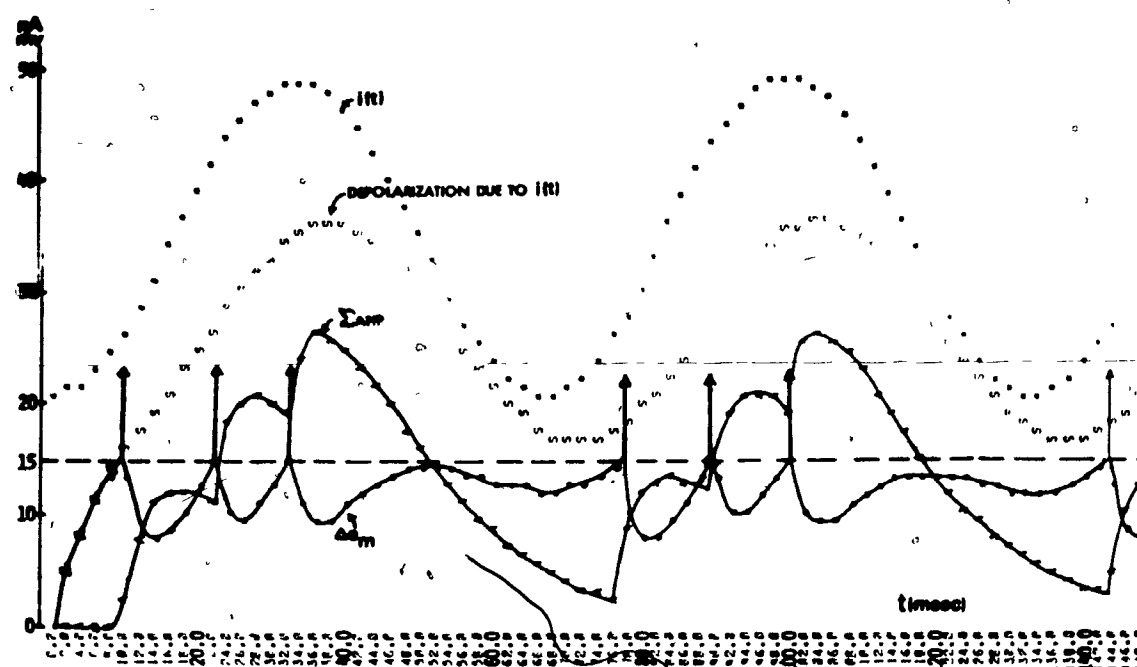
FIGURE 4-9(a)   LARGE AMPLITUDE INPUT i(t)=35-14cos(2π.15.t/1000)
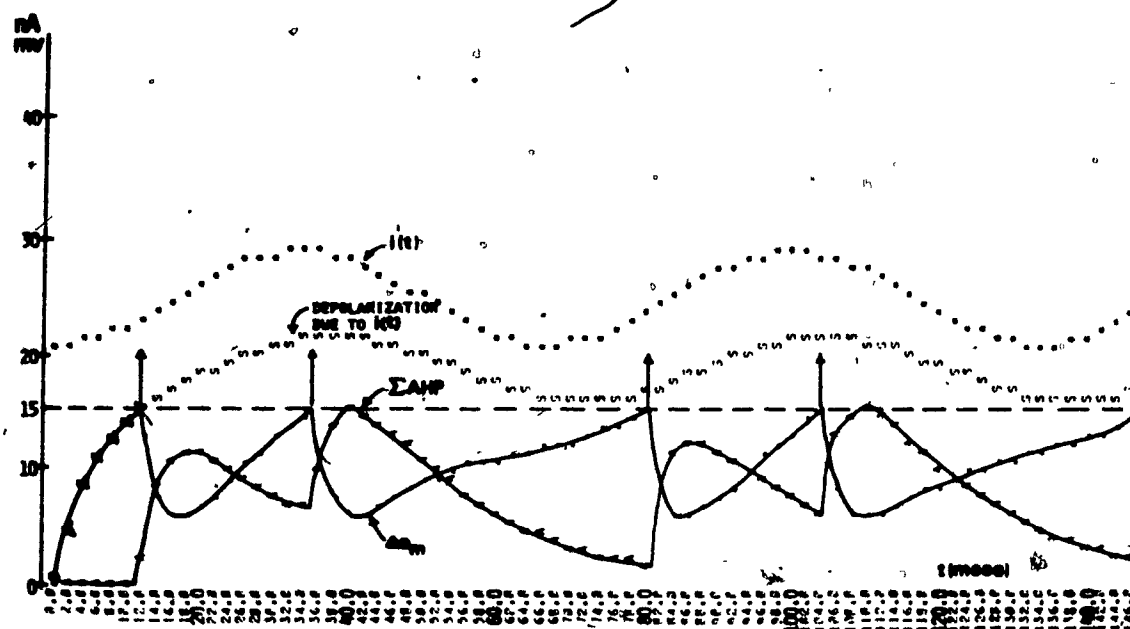
FIGURE 4-9(b)   SMALL AMPLITUDE INPUT i(t)=25-4cos(2π.15.t/1000)

FIGURE 4-9   DETAILS OF RESPONSES TO SINUSOIDAL INPUTS WITH FREQUENCY 15HZ

l(t).   Curve S represents the depolarization due to i(t).   Curve A represents the summated after-hyperpolarization due to the negative feedback current Δi_K.   Curve •, which represents Δe_m is the difference between curve S and curve A.   Clearly, the summated AHP holds Δe_m below the threshold during most of the falling portion of the input and, as a result, no spikes are emitted then.   We note that the phase lead is present for both inputs of different amplitude.

These simulation results suggest that the response is determined not only by the magnitude of the input but also by the rate of change of the magnitude of the input.   This property of the model will be confirmed through a mathematical analysis in the next chapter.

It would be desirable that the response of the model described above could be compared with experimental data.   Unfortunately, no experimental work has been reported where MNs were stimulated intracellularly with sinusoidal currents.   However, there are indications in experimental data obtained by synaptic stimulation of MNs that the response of the model for sinusoidal inputs is similar to that of the real MN.   By changing a muscle length l(t) sinusoidally, Rosenthal et al. (35) found that the firing frequency of MNs was in general sinusoidally modulated for small amplitudes of l(t), but burst activity did occur for either of the following conditions:

(i) The frequency of l(t) was higher than about 6 Hz.   Then, the bursts occurred with a phase lead with respect to the time when l(t) was maximum and this phase lead was more than the amount introduced by the muscle spindles.

(ii) The amplitude of l(t) was large.

Rosenthal et al. postulated in essence that, under conditions (i) and (ii), the sinusoidal 1(t) is transformed into a distorted i(t) of such a form that burst activity would occur, assuming the response of the MN is linearly proportional to the amplitude of i(t). However, based on our simulation results, it appears that the experimental results could occur even if i(t) remains sinusoidal: The response under condition (i) could be explained by the hypothesis that the response of the MN is determined by the magnitude i(t) and the rate of change of the magnitude di(t)/dt. For the response under condition (ii), the minimum i(t) during a large amplitude variation of 1(t) could drop below the threshold current during which time the MN does not emit spikes. Westbury (36) has also observed that, at the higher frequencies of stretch (2-15 Hz), spikes are emitted by the MN in advance of the peak depolarization produced by synaptic stimulation. The input frequencies for which a phase lead has been observed experimentally are in the same range as those for our model. In the simulations, the phase lead is dependent on the size of the MN. For a large MN (results in this chapter), the phase lead is evident for input frequencies above 5 Hz, while for a small MN (results in ChapterVI), the phase lead is evident for input frequencies as low as 1 Hz.

4.4 Summary

In this chapter, we have tested the basic model (for a large motoneuron) with step, ramp, and sinusoidal current stimuli and compared its responses with reported experimental results. The basic model reproduces the following primary properties which have been observed for

step inputs: (i) there is a fixed threshold current for repetitive firing, (ii) an initial adaptation of the firing frequency, (iii) the characteristic trajectory of the membrane potential between spikes, and (iv) similar values of the adapted firing frequency for the significant range of the input amplitude. The model, however, does not reproduce the following secondary properties which have been observed for step inputs: In the model, (i) there is no secondary range of firing, (ii) a few spikes are not emitted at the onset of input steps greater than the rheobase current but less than the threshold current, and (iii) the firing frequencies during the initial adaptation are larger than experimentally observed. For ramp inputs, the model and the motoneuron behave very similarly for ramps of different slope. For sinusoidal inputs, the model predicts that, for high input frequencies, the spikes occur with a phase lead relative to the input. Some experimental observations indicate that this prediction will be valid.

CHAPTER V

MATHEMATICAL ANALYSIS OF THE BASIC MODEL

During the simulation study of the model, it became evident to us that a mathematical analysis of the model could clarify the simulation results. Furthermore, we simulated the model only for a limited set of parameter values but the response of the model could be determined from a mathematical relation for a continuous range of parameter values. For these purposes, we performed the following mathematical analysis.

5.1 Simplification of the model

In order to be able to perform a mathematical analysis of the model, it is simplified in Figure 5-1 (a) - (d). The model in (b) is obtained from the model in (a) by replacing $K_m/(s + A_m)$ with K_m/A_m. This simplification is justified thus: If most of spectral content of the input to $K_m/(s + A_m)$ is below the cutoff frequency A_m, then we could replace $K_m/(s + A_m)$ by K_m/A_m. For most of spectral content of the input to $K_m/(s + A_m)$ to be below A_m, most of the spectral content of $i(t)$ and $\Delta i_K(t)$ must be below A_m. We can require that $i(t)$ satisfy this condition. The spectral content of Δi_K is difficult to find analytically. However, we do have some qualitative information about it. From the model, $\Delta i_K(t)$ is directly dependent on $\Delta g_K(t)$ and it is dependent on $\Delta e_m(t)$ through the multiplicative term $(E_K - E_r + \Delta e_m)$. Since when the model is emitting a series of spikes, Δe_m varies by at most 10 mv (e.g. see Figures 4-1(c), 4-4(b)-(c), 4-6, and 4-9) whereas (E_K-E_r)

$K_m = 1/C$

$A_m = 1/RC \equiv 1/T_m$

$A_K = 1/T_K$

$\Delta e_m = e_m + E_r$

(a)

(b)

$E_Z = TH + E_K - E_r$

(c)

(d)
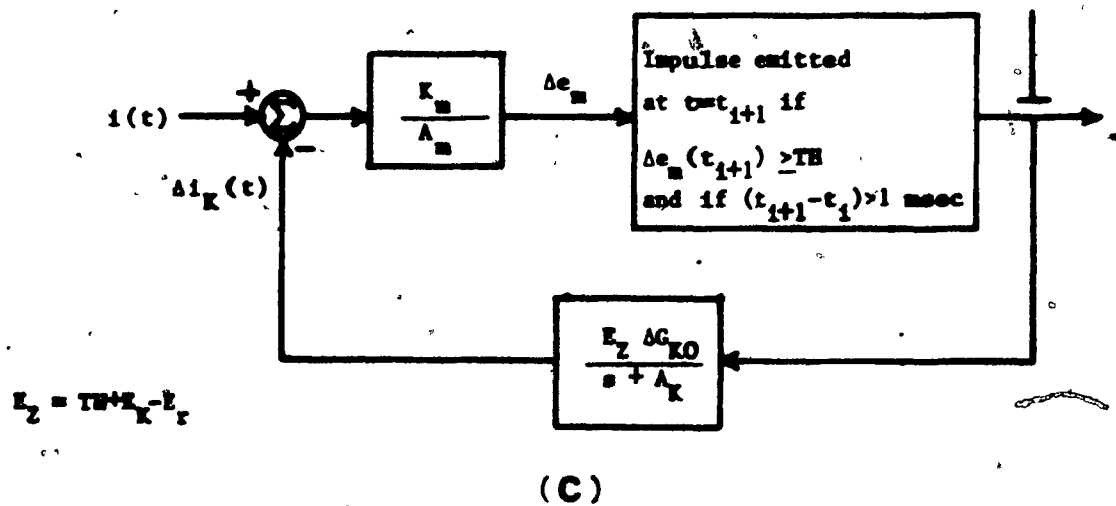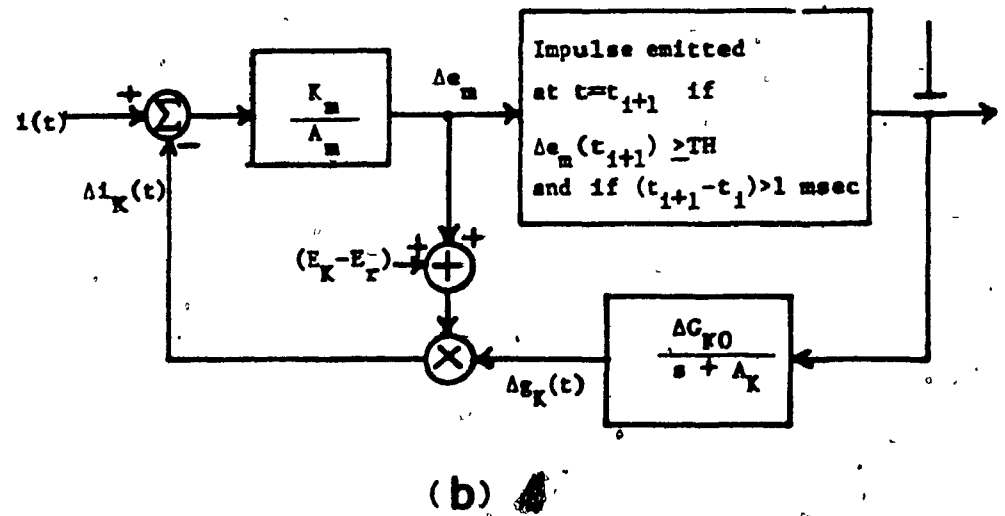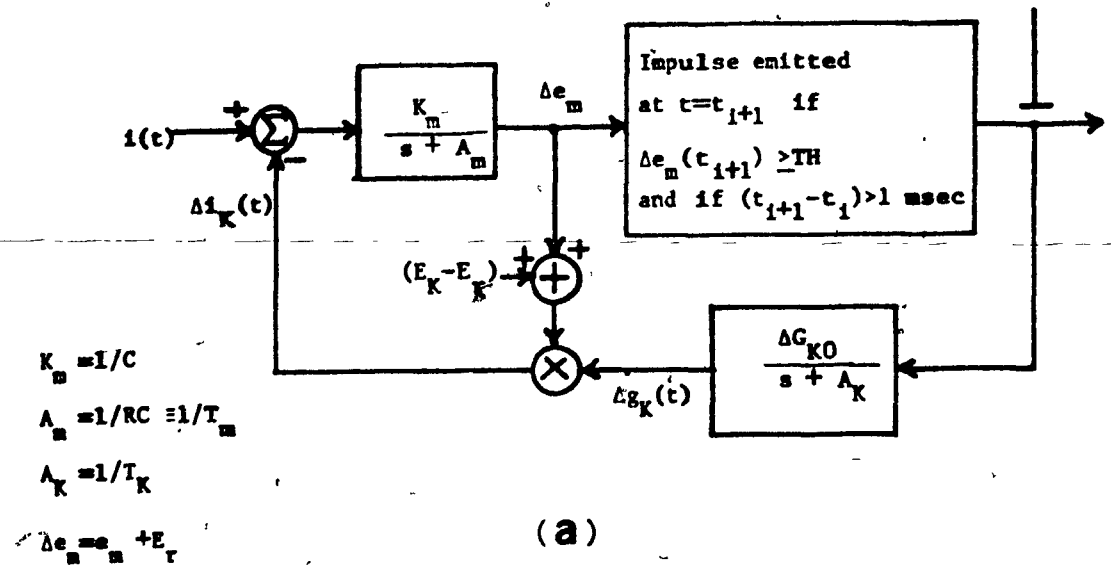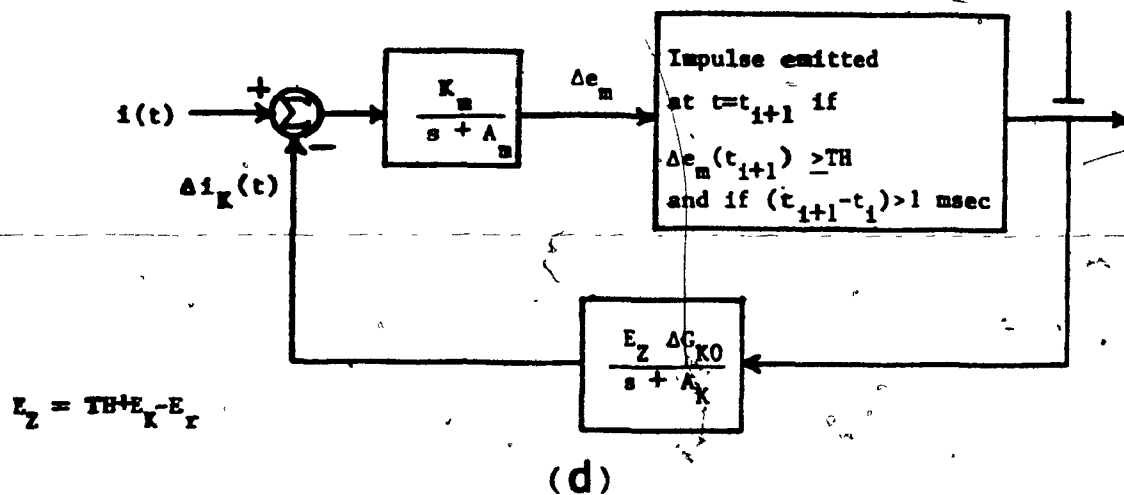
FIGURE 5-1   SIMPLIFICATION OF THE BASIC MODEL

$$E_Z = TH + E_K - E_r$$
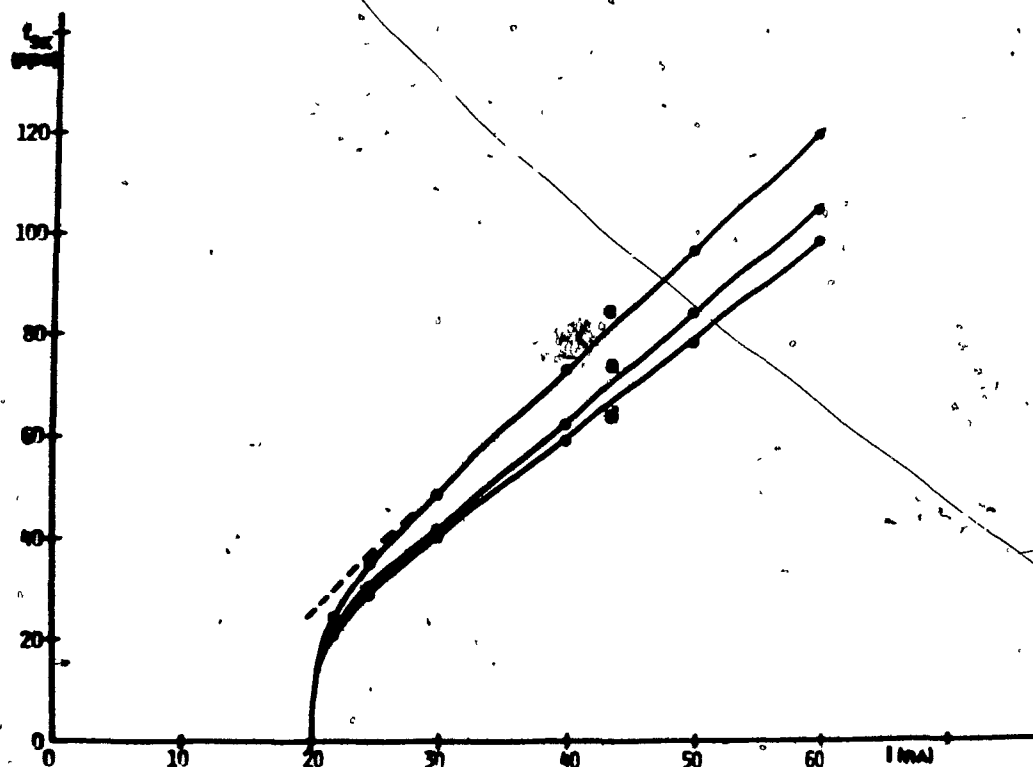
FIGURE 5-2   ADAPTED FIRING FREQUENCY f_{SK} VERSUS INTENSITY OF
STIMULATING STEP I FOR THE MODELS IN FIGURE 5-1

plus the steady change of Δe_m is more than 25 mv, therefore Δi_K is predominantly dependent on $\Delta g_K(t)$. We can have an indication of the spectral content of $\Delta g_K(t)$ and consequently of $\Delta i_K(t)$ by considering the case when only one spike is emitted so that $\Delta g_K(t) = \Delta G_{K0} e^{-t/T_K}$. The spectral content of this exponential waveform declines above the frequency A_K. We also know that the frequency A_m is substantially larger than the frequency A_K: for a large MN, A_m is three times A_K, and for a small MN, A_m is more than ten times A_K (see Chapter VI). Therefore, most of the spectral content of $\Delta g_K(t) = \Delta G_{K0} e^{-t/T_K}$ is below A_m. For the case when a series of spikes are emitted, we can expect that the spectral content of $\Delta g_K(t)$ below A_m remains large because, between the spike emission times, $\Delta g_K(t)$ still declines exponentially with the time constant T_K, and the temporal summation of $\Delta g_K(t)$ produces a large DC component.

The main condition for an impulse to be emitted at $t=t_{i+1}$ is,

$$\Delta e_m(t_{i+1}) \geq TH \qquad (5-1)$$

where, $\Delta e_m(t_{i+1})$ is the value of $\Delta e_m(t)$ at $t=t_{i+1}$

From Figure 5-1(b),

$$\Delta e_m(t_{i+1}) - (i(t_{i+1}) - \Delta i_K(t_{i+1}))\frac{K_m}{A_m} \qquad (5-2)$$

where, $i(t_{i+1})$ and $\Delta i_K(t_{i+1})$ are the values of $i(t)$ and $\Delta i_K(t)$ at $t=t_{i+1}$.

Substituting (5-1) into (5-2) we obtain,

$$(i(t_{i+1}) - \Delta i_K(t_{i+1})) \geq \frac{TH \; A_m}{K_m} \qquad (5-3)$$

Substituting (4-1) into (5-3), the main condition for a spike to be emitted at $t=t_{i+1}$ becomes,

$$(i(t_{i+1}) - \Delta i_K(t_{i+1})) \geq I_{th} \qquad (5-4)$$

The voltage across $\Delta g_K(t)$ at the instant when a spike is emitted at $t=t_{i+1}$ is equal to $(TH + E_K - E_r)$. Therefore,

$$\Delta i_K(t_{i+1}) = (TH + E_K - E_r) \Delta g_K(t_{i+1}) \qquad (5-5)$$

The multiplier can be removed by modifying the transfer function in the feedback path as shown in (c) where,

$$E_Z = TH + E_K - E_r \qquad (5-6)$$

In so doing, the spike emission times for the model in (c) remain the same as for the model in (b) because they are found for both cases from the same equations (5-4), (5-5), and (4-4). The relationship between the adapted firing frequency versus the intensity of an input current step for the model in (c) is shown in Figure 5-2 curve(c) and that for the original basic model is shown in Figure 5-2 curve(a).

The dynamics due to the membrane capacitance can be re-introduced as shown in Figure 5-1(d) and the f_{SK}-I curve generated by this model is shown in Figure 5-2 curve (d).

When only the multiplier is removed in (d), the AHP between spikes is enhanced as shown in Figure 5-3 in comparison with the response shown in Figure 4-4 (b) of the original basic model. However, the
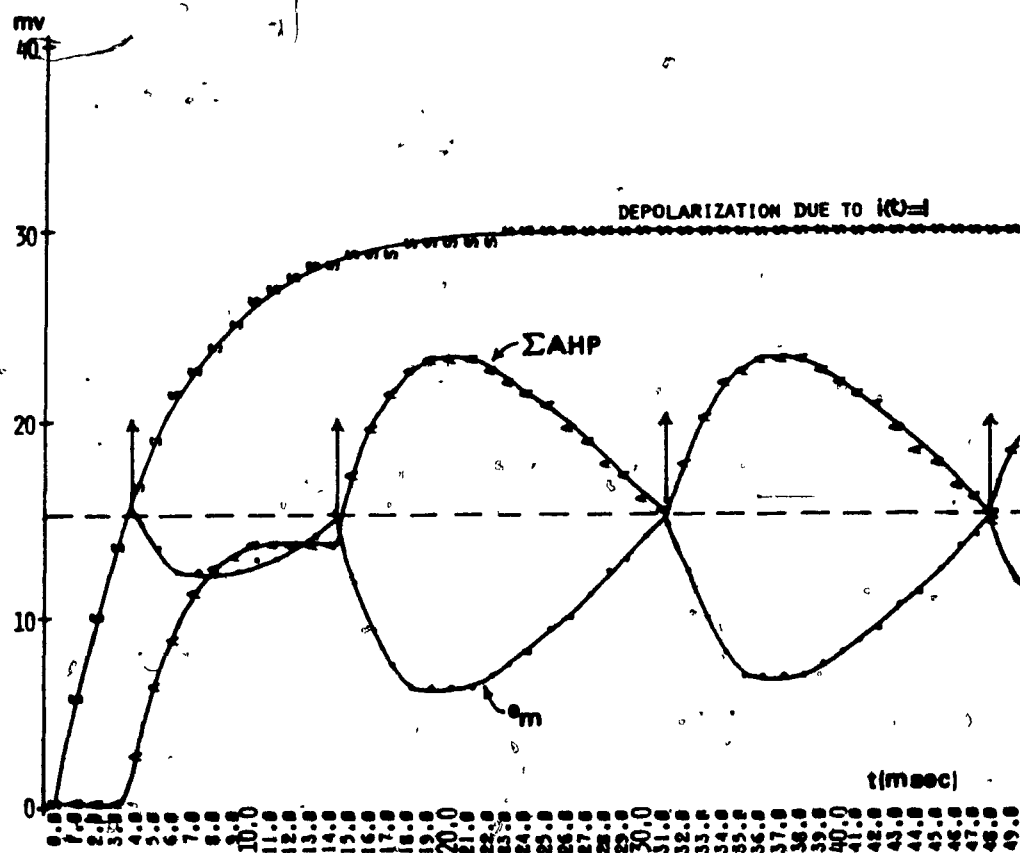
FIGURE 5-3 RESPONSE OF THE SIMPLER MODEL IN FIGURE 5-1(d) TO BE
            COMPARED TO THE RESPONSE IN FIGURE 4-4(b) OF THE
            ORIGINAL BASIC MODEL

firing frequencies shown in Figure 5-2 curve (d) of this simpler model are only slightly less than those shown in Figure 5-2 curve (a) of the original basic model. When the dynamics due to the membrane capacitance are also removed in (c), the firing frequencies are only increased by about 15% as shown in Figure 5-2 curve (c). The benefit of removing the multiplier is that, except for the spike emitter, the model is a linear model. When the dynamics due to the membrane capacitance are also neglected, it is easier to do a mathematical analysis of the model. The basic model in (a) compares the change in the membrane potential to a threshold voltage. However, since (5-4) gives approximately the condition for spike emission, the basic model operates approximately as a current comparator: The externally applied current minus the increased potassium current due to previous spikes is instantaneously compared to a threshold current.

5.2 Mathematical relation between the firing frequency and the input

We now proceed to derive a mathematical relation between the firing frequency and the input for the simpler model in Figure 5-1 (c). For convenience of presentation we shall first obtain the static relation and then include the effect of the dynamics. After the i th spike at $t = t_i$ the current $\Delta i_K(t)$ is given by,

$$\Delta i_K(t) = \sum_{j=0}^{\infty} E_Z \, \Delta G_{K0} \, e^{-(t-t_{i-j})/T_K} \qquad (5\text{-}7)$$

Substituting $t = t_{i+1}$ into (5-7),

$$\Delta i_K(t_{i+1}) = \sum_{j=0}^{\infty} E_Z \, \Delta G_{KO} \, e^{-(t_{i+1} - t_{i-j})/T_K} \qquad (5\text{-}8)$$

Substituting (5-8) into (5-4) we have,

$$i(t_{i+1}) - \sum_{j=0}^{\infty} E_Z \, \Delta G_{KO} \, e^{-(t_{i+1} - t_{i-j})/T_K} \geq I_{th} \qquad (5\text{-}9)$$

When the input is a step of current $I \geq I_{th}$, the steady-state or adapted firing frequency f_{SK} can be found from (5-9) by substituting $i(t_{i+1}) = I$ and the value $1/f_{SK}$ for the interval between two consecutive spikes thus,

$$I - \sum_{n=1}^{\infty} E_Z \, \Delta G_{KO} \, e^{-\frac{n}{f_{SK}T_K}} = I_{th} \qquad (5\text{-}10)$$

The inequality from (5-9) has been omitted because, in the steady-state, the equality is always satisfied (e.g. in Figure 4-4(c) $\Delta e_m = TH$ at the spike emission times in the steady-state). Using the geometric series expansion (5-10) reduces to,

$$I - E_Z \, \Delta G_{KO} \left(\frac{1}{1 - e^{-1/f_{SK}T_K}} - 1 \right) = I_{th}$$

or,

$$I - I_{th} = \frac{E_Z \, \Delta G_{KO}}{e^{1/f_{SK}T_K} - 1} \qquad (5\text{-}11)$$

The values of f_{SK} and I that satisfy (5-11) are shown as curve (c) in Figure 5-2. When the curve is extended as a straight line, it crosses $I = I_{th}$ approximately at $f_{SK} = f_m$ where f_m is given by (4-3). This linear static relation is given by,

$$f_{SK} - f_m = S_d (I - I_{th}) \qquad (5\text{-}12)$$

The slope $S_d = df_{SK}/dI$ of curve (c) can be found by differentiating (5-11) with respect to f_{SK} and inverting,

$$S_d = \frac{\left(e^{\frac{1}{f_{SK}T_K}} - 1\right)^2 T_K f_{SK}^2}{E_Z \Delta G_{KO} \; e^{\frac{1}{f_{SK}T_K}}} \qquad (5\text{-}13)$$

The slope of the linear part of curve (c) can be found by evaluating (5-13) at any point on the linear part of the curve which, for convenience, we choose $f_{SK} = 1/T_K$. Thus,

$$S_d = \frac{(e-1)^2}{E_Z \Delta G_{KO} \; e \; T_K}.$$

or,

$$S_d = \frac{1}{0.91 \; E_Z \Delta G_{KO} \; T_K} \qquad (5\text{-}14)$$

Substituting (5-14) into (5-12),

$$f_{SK} = \frac{1}{0.91 \; E_Z \Delta G_{KO} \; T_K} (I - I_{th}) + f_m \qquad I \geq I_{th} \qquad (5\text{-}15)$$

For an input below the threshold current there is no firing so that

$$f_{SK} = 0 \qquad I < I_{th} \qquad (5\text{-}16)$$

Equations (5-15) and (5-16) give the static relation.

We now proceed to include in the mathematical relation the effect of the dynamics. Since in the model of Figure 5-1(c) there is dynamics only in the feedback path, we have to understand how this feedback path behaves. To do so, we can first consider the hypothetical case when the model emits a train of spikes with constant frequency starting at time zero. Figure 5-4 shows that the resultant summation of the feedback current $\Delta i_K(t)$ summates with a time lag. Just before the emission time of the i th spike, the value of Δi_K is given by,
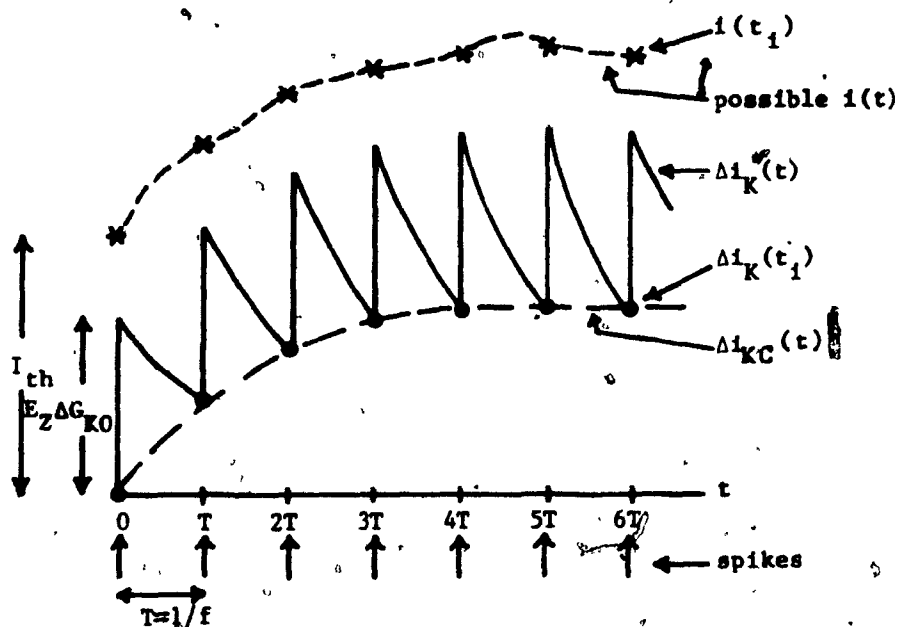
FIGURE 5-4 ILLUSTRATION OF THE DYNAMICS OF THE FEEDBACK PATH
IN THE MODEL SHOWN IN FIGURE 5-1(c)

$$\Delta i_K [(i-1)T] = 0 \qquad\qquad i = 1 \qquad (5\text{-}17)$$

$$= E_Z \cdot \Delta G_{KO} \sum_{m=1}^{i-1} e^{-mT/T_K} \qquad i \geq 2 \qquad (5\text{-}18)$$

where, $T = 1/f$ and f is a constant firing frequency.

The curve $\Delta i_{KC}(t)$ in Figure 5-4 which passes through these points is given by,

$$\Delta i_{KC}(t) = \frac{E_Z \ \Delta G_{KO}}{e^{T/T_K} - 1} (1 - e^{-t/T_K}) \qquad (5\text{-}19)$$

because,

$$\Delta i_{KC}(0) = 0$$

which corresponds to (5-17) and,

$$\Delta i_{KC} [(i-1)T] = \frac{E_Z \Delta \ G_{KO}}{e^{T/T_K} - 1} (1 - e^{-(i-1)T/T_K}) \qquad (5\text{-}20)$$

corresponds to (5-18) as it will be shown next. We have to show that the RHS of (5-18) is equal to the RHS of (5-20), or,

$$\left(\sum_{m=1}^{i-1} e^{-mT/T_K} \right) \left(e^{T/T_K} - 1 \right) = 1 - e^{-(i-1)T/T_K} \qquad (5\text{-}21)$$

Now,

$$\left(\sum_{m=1}^{i-1} e^{-mT/T_K} \right) \left(e^{T/T_K} - 1 \right) = \sum_{m=1}^{i-1} e^{(-m+1)T/T_K} - \sum_{m=1}^{i-1} e^{-mT/T_K}$$

$$= \sum_{m=2}^{i-1} e^{(-m+1)T/T_K} + 1 - \sum_{m=1}^{i-2} e^{-mT/T_K} - e^{-(i-1)T/T_K} \qquad (5\text{-}22)$$

Rewriting (5-22) by substituting $n = m-1$ into the first term of the RHS we have,

$$\left(\sum_{m=1}^{i-1} e^{-mT/T_K}\right)\left(e^{T/T_K} - 1\right) = \sum_{n=1}^{i-2} e^{-nT/T_K} + 1 - \sum_{m=1}^{i-2} e^{-mT/T_K} - e^{-(i-1)T/T_K}$$

$$= 1 - e^{-(i-1)T/T_K}$$

Thus, equation (5-21) is valid.

Substituting (5-11) into (5-15) and f for the dummy variable f_{SK} we have,

$$\frac{E_Z \, \Delta G_{K0}}{e^{\frac{1}{fT_K}} - 1} = 0.91 \, E_Z \, \Delta G_{K0} \, T_K(f - f_m) \qquad f > f_m \qquad (5\text{-}23)$$

Substituting (5-23) into (5-19),

$$\Delta i_{KC}(t) = 0.91 \, E_Z \, \Delta G_{K0} \, T_K(f - f_m)(1 - e^{-t/T_K}) \qquad (5\text{-}24)$$

Equation (5-24) gives the response $\Delta i_{KC}(t)$ for an input which can be considered to be a step of frequency $(f - f_m)$. The response of a system with such a step response to an input $(f(t) - f_m)$ is given by,

$$\Delta i_{KC}(t) = \int_0^t 0.91 \, E_Z \, \Delta G_{K0} \, e^{-(t-\tau)/T_K} \, [f(\tau) - f_m] \, d\tau \qquad (5\text{-}25)$$

We assume that by substituting $t = t_i$ in (5-25) we obtain approximately the value of $\Delta i_K(t_i)$ for a spike train with time-varying firing frequency $f(t)$. Furthermore, since for the simulation results the instantaneous firing frequency is evaluated at the spike emission times (data points), there must be a sufficient number of data points in order to specify an appropriate continuous function $f(t)$ that fits these data points (e.g. see Figure 4-8(a) versus Figure 4-8(d)). Nevertheless, in the subsequent

analysis we use (5-25) without any restrictions because, in the next

section, it will be possible to make a meaningful comparison between the

resultant mathematical expression and the simulation results even when

it is not possible to specify an appropriate continuous function $f(t)$.

We have described the dynamics of the feedback path and now
we investigate how these dynamics affect the input-output relation.
Let us consider again the case when the model emits a train of spikes
with constant frequency as illustrated in Figure 5-4. To generate this
output, the input can be any member of the class of inputs specified by:

i. The values of the input $i(t)$ at the spike emission times,

$i(t_i)$, must satisfy the condition $i(t_i) - \Delta i_K(t_i) = I_{th}$

from (5-4). (The inequality condition in (5-4) may be

satisfied during large abrupt changes of the input (e.g.

see Figure 4-3(c)). However, we have already restricted

our mathematical analysis to inputs with low-frequency

spectral content.

ii. Between the spike emission times, the input is constrained

only by the inequality $i(t) - \Delta i_K(t) < I_{th}$ from (5-4).

By restricting our analysis to inputs with low-frequency spectral content,
we are limiting the class of inputs further:

iii. Between any two consecutive spike emission times t_i and t_{i+1},

the input does not deviate significantly from the straight

line joining $i(t_i)$ and $i(t_{i+1})$. Otherwise, $i(t)$ would have

large-amplitude high-frequency fluctuations. In Figure

5-4, we see that the admissable $i(t)$ is similar in shape to

$\Delta i_{KC}(t)$. Thus, $i(t)$ and $\Delta i_{KC}(t)$ are related approximately

by,

$$i(t) - \Delta_{KC}(t) = I_{th} \tag{5-26}$$

Since requirements (i), (ii), and (iii) above are applicable in general, we can use (5-25) and (5-26) to obtain a general relation.

Substituting (5-25) into (5-26),

$$i(t) - \int_0^t 0.91E_Z \, \Delta G_{KO} \, e^{-(t-\tau)/T_K} \, [f(\tau) - f_m] \, d\tau = I_{th} \tag{5-27}$$

Differentiating (5-27) with respect to t we have,

$$\frac{di}{dt} - e^{-t/T_K} 0.91E_Z \Delta G_{KO} e^{t/T_K}(f(t) - f_m) + \frac{1}{T_K} e^{-t/T_K} \int_0^t 0.91E_Z \Delta G_{KO} e^{\tau/T_K}(f(\tau) - f_m) d\tau = 0 \tag{5-28}$$

By using (5-27) and (5-28) we get,

$$\frac{di(t)}{dt} - 0.91E_Z \, \Delta G_{KO} \, [f(t) - f_m] + \frac{1}{T_K}[i(t) - I_{th}] = 0 \tag{5-29}$$

Rearranging (5-29),

$$f(t) = \frac{1}{0.91E_Z \Delta G_{KO}}\left(\frac{1}{T_K}[\, i(t) - I_{th}] + \frac{di(t)}{dt}\right) + f_m \quad i(t) \geq I_{th} \tag{5-30}$$

For an input below the threshold current there is no firing so that

$$f(t) = 0 \qquad i(t) < I_{th} \tag{5-31}$$

Equations (5-30) and (5-31) include the effect of dynamics. These equations reduce to the static equations (5-15) and (5-16) when $i(t) = I$ is substituted.

5.3   Comparison between the mathematical relation and the simulation

results

The mathematical relation (5-30) reveals that $f(t)$ is proportional to the magnitude $i(t)$ and the rate of change of the magnitude $di(t)/dt$ of the input. In view of this result, we can now have a better understanding of the simulation results.

For step inputs, the steady-state f found from (5-30) is linearly related to the magnitude of the step as in the simulation results. The derivative term in (5-30) introduces an impulse in $f(t)$ at the onset of the step. Although we restricted our mathematical analysis to inputs with low-frequency spectral content which is not the case at the onset of a step, this impulse in $f(t)$ that we nevertheless find from (5-30) could be considered as the high instantaneous firing frequency during the quick initial adaptation in the simulation results. For ramp inputs, $f(t)$ found from (5-30) is dependent on the slope of the ramp. This effect is also observed in the simulation results since, in Figure 4-5(c), when $i(t)$ = 48 nA a spike is emitted and the previous instantaneous firing frequency is 140 pps, while in Figure 4-5(b) where the input has a smaller slope, when $i(t)$ = 48 nA, the frequency is only about 90 pps.

In order to illustrate the effect of the derivative term for sinusoidal inputs, equation (5-30) can be rearranged as follows,

$$f(t) = \left(\frac{i(t) - I_{th}}{0.91 E_Z \Delta G_{KO} T_K} + f_m \right) + \frac{1}{0.91 E_Z \Delta G_{KO}} \frac{di(t)}{dt} \qquad (5\text{-}32)$$

We denote the first term in (5-32) as f_a and the second term as f_v so that $f = f_a + f_v$. Plots of f_a, f_v, and f are shown in Figure 5-5 (a) – (c) for three sinusoidal inputs that were used in the simulations.

For the low input frequency in (a), f is determined chiefly by the magnitude of the input. As the input frequency is increased in (b) and (c), the derivative term becomes significant, and f occurs with a phase lead with respect to the input $i(t)$ or the f_a curve.

The effect can be analyzed more easily with a Bode plot. The Laplace transform of Equation (5-30) is shown as a block diagram in Figure 5-6(a). This transfer function is valid when the input current is above the threshold current at all times. The input is transformed only by $H_K(s)$ which is defined in the figure. The magnitude and phase curves of the Bode plot of $(0.91E_Z \Delta G_{KO} T_K) H_K(s)$ are shown in Figure 5-6 (b). In this Figure, the data marked (X) are calculated from the simulation results of the basic model which were shown in Figure 4-7(c) and Figure 4-8. We recall that, for low-input frequencies, the instantaneous firing frequency varied sinusoidally. However, for high input frequencies, the spikes occurred in bursts so that the instantaneous firing frequency did not vary sinusoidally. Consequently, the standard method of calculating the gain and the phase is not applicable for high input frequencies. Nevertheless, we can establish a reasonable method of calculating the data. Let us reconsider the simulation result shown in Figure 4-8(d) for which the burst effect is most pronounced. As discussed in Section 4.3, the output spikes occur with a phase lead relative to the input. A measure of this phase lead can be found by locating the centre of the spikes in each cycle and the phase lead of this centre with respect to the input maximum. The gain can be found by using the maximum and minimum firing frequency. We define for one complete cycle in the steady state:
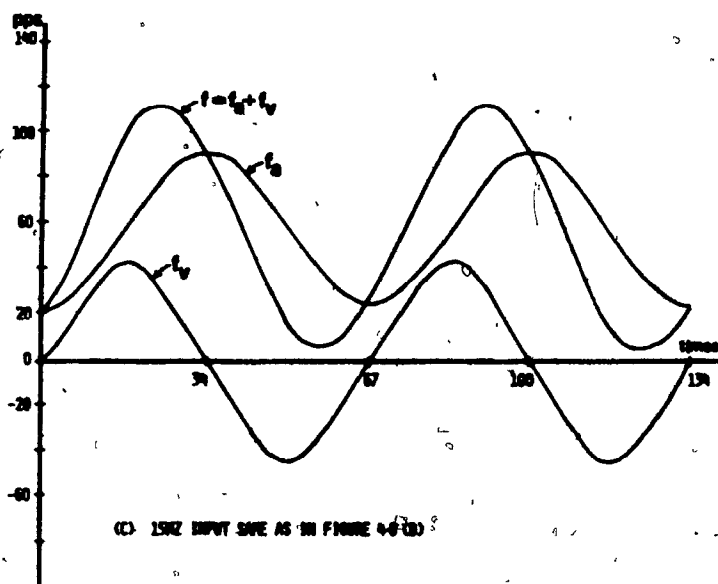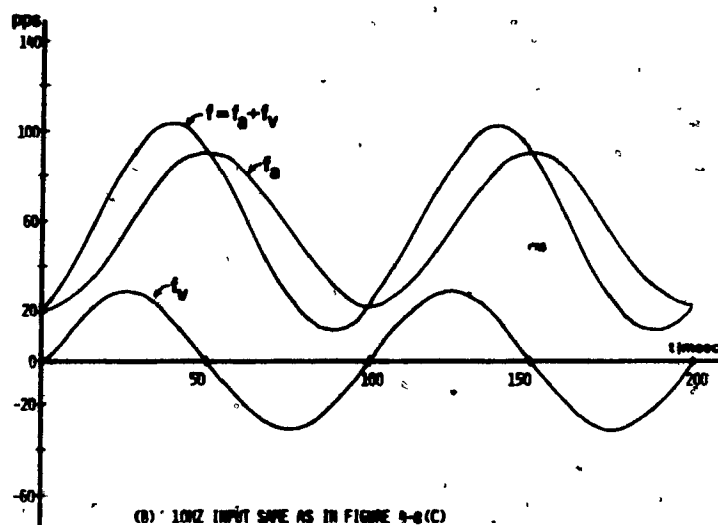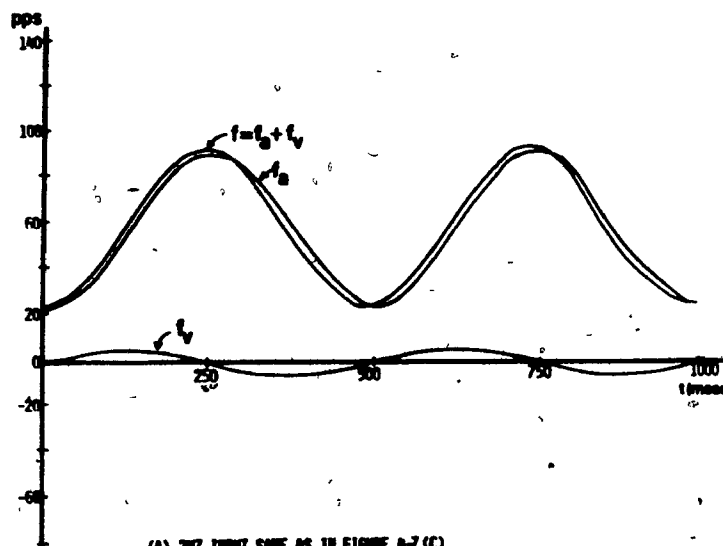
FIGURE 5-5 ILLUSTRATION OF SENSITIVITY OF THE RESPONSE TO THE MAGNITUDE
AND THE RATE OF CHANGE OF THE MAGNITUDE OF A SINUSOIDAL INPUT
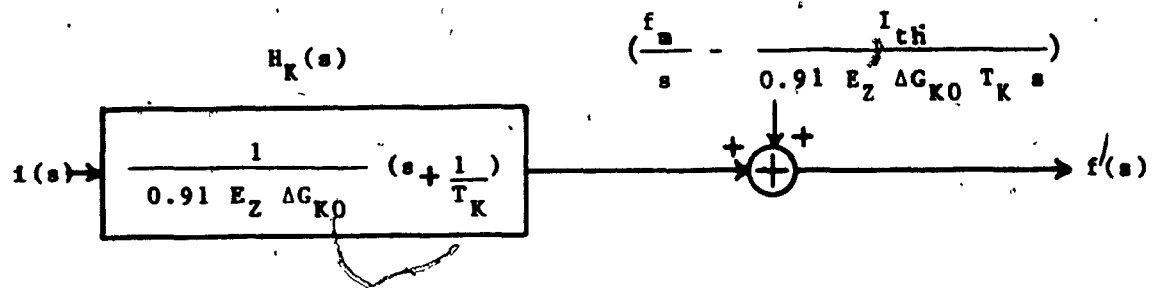
FIGURE 5-6(a)   TRANSFER FUNCTION FOR THE BASIC MODEL VALID
FOR OPERATION ABOVE THRESHOLD
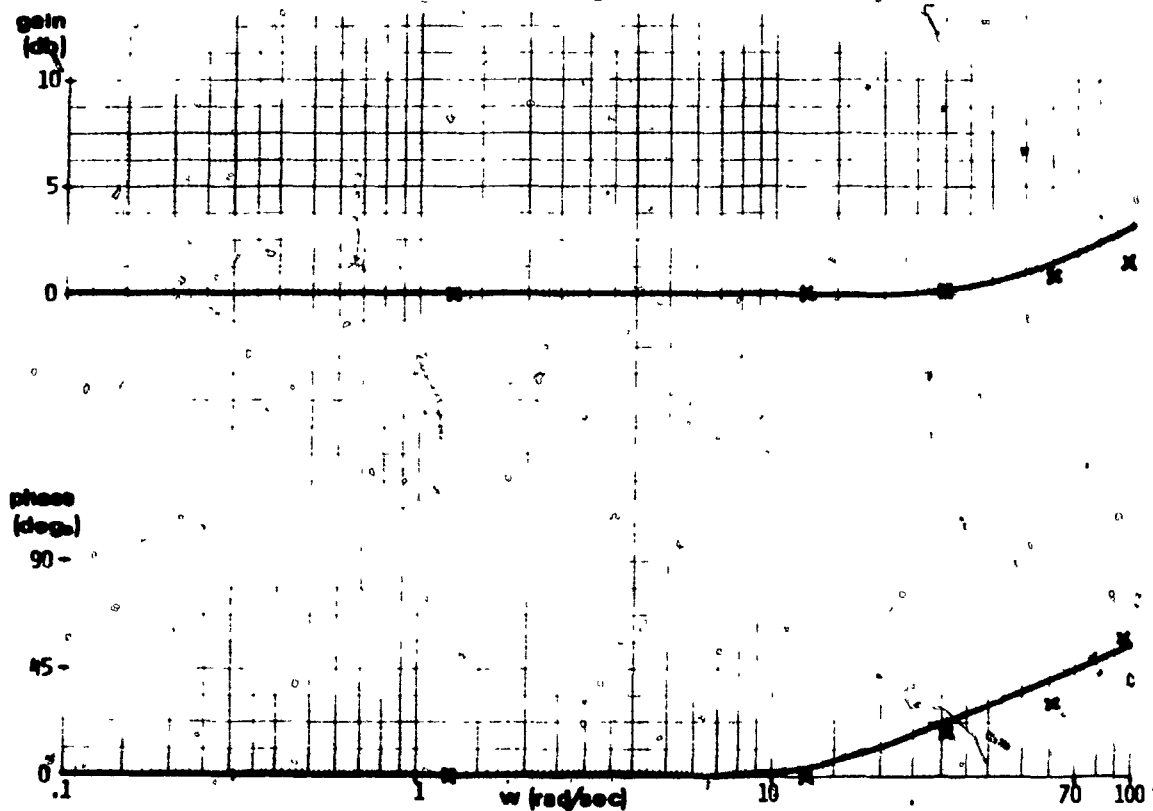
FIGURE 5-6(b)   BODE PLOT OF $0.91 E_Z \Delta G_{KO} T_K H_K(s)$ AND DATA(X) FROM
SIMULATIONS OF BASIC MODEL WITH $d=79 \mu m$

t_c in msec = the average of the emission times of the spikes in the cycle (location of the centre)

t_m in msec = time when the input is maximum

t_p in msec = period of the cycle

I_{pp} in nA = twice the amplitude of the input

f_{max} in pps = maximum instantaneous firing frequency

f_{min} in pps = minimum instantaneous firing frequency

Then, the gain and the phase are found from,

$$\text{gain} = 20 \log \left(\frac{f_{max} - f_{min}}{I_{pp}} \right) - 20 \log \left(\frac{f_{max} - f_{min}}{I_{pp}} \right)_{w \to 0} \quad \text{in db} \quad (5\text{-}33)$$

$$\text{phase} = 360 \times \frac{t_m - t_c}{t_p} \quad \text{in degrees} \quad (5\text{-}34)$$

We chose (5-33) and (5-34) because these equations comprise the standard method of calculating the gain and phase when the response $f(t)$ is a sinusoid. In this way, for low input frequencies the method is the same as the standard method since the response is a sinusoid and t_c is equivalent to the time when the sinusoid is maximum. The data calculated with this method is shown in Figure 5-6(b). It is evident from this figure that the curve for the mathematical relation agrees with the data. Thus, in order to clarify the phase lead for high input frequencies observed in the simulations of the model we can examine the mathematical relation (5-30). The phase lead found from the mathematical relation is due to its derivative term which arose when the dynamics in the feedback path of the basic model were included in the analysis. Consequently, the phase lead is due to the dynamics in the feedback path.

The mathematical analysis has been used to clarify the simulation

results presented thus far.   It will also be useful in the next two

chapters.

CHAPTER VI

RESPONSE OF THE BASIC MODEL FOR NEURONS OF

DIFFERENT SIZE AND TO SYNAPTIC STIMULATION

In the previous chapters, we have studied the encoding mechanism of the basic model by using the parameter values of a large motoneuron and by comparing its response mainly to experimental results reported for stimulation with an intracellular microelectrode. Since motoneurons in the spinal cord are of different size and since the model is to be used for studying the cooperation of motoneurons as a system, in this chapter we shall express the parameters of the basic model as a function of the size of the motoneuron and investigate how the size affects its response. Furthermore, since in the real system, the motoneuron is stimulated by a spatio-temporal pattern of spikes converging at the synapses, we shall include this synaptic stimulus in the model.

6.1   Response for neurons of different size

6.1.1   Expressions for the parameters as a function of cell size

Although the MN is a very complex structure, the overall size can be specified by only one variable. The extent of the dendritic tree is directly related to the size of the soma which can be specified by measuring an average diameter d (38). Spinal MNs are known to have d varying from 25 μm for the smallest to 90 μm for the largest (38). There

has been a sufficient number of experimental observations to enable us to express indirectly the parameters of the model, R, C, T_K, and ΔG_{KO} as a function of d. The other parameters E_K, E_r, and TH are independent of d (26 and read below).

Kernell (38) has measured the total effective resistance R of the MN as a function of the conduction velocity V_a of its axon. The resistance R is defined as the ratio of the steady-state subthreshold change of the membrane potential to the intensity of the stimulating current step. The data is shown in Figure 6-1 and a straight line was fitted through the data points which were measured by two different techniques. The resistance R is linearly proportional to the reciprocal of the square of the conduction velocity, $1/V_a^2$. The equation of this straight line is,

$$R = 3.74 \times 10^4 \times \left(\frac{1}{V_a^2}\right) - 2.54 \qquad (6-1)$$

where R is in $M\Omega$ and V_a is in m/sec.

The samples are representative of α-MNs of all sizes because the values of V_a cover the entire range of the conduction velocity of the α-MN axons (39). Since V_a is directly proportional to d, the resistance R is inversely proportional to d (38). Only two data points were obtained from a small MN because it is difficult to do experiments on small MNs with an intracellular microelectrode.

The surface area of the soma is proportional to d^2 and the surface area of the dendritic tree is proportional to the surface area of the soma (38) so that the total surface area of the MN is proportional to d^2. The resistance R presented by the MN to the flow of current from
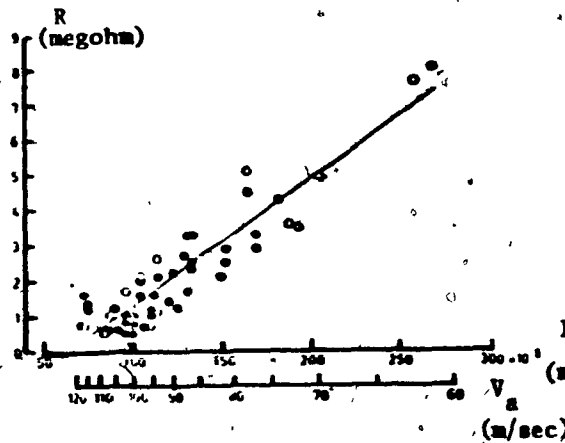
FIGURE 6-1   RESISTANCE R VERSUS
            CONDUCTION VELOCITY V_a (38)
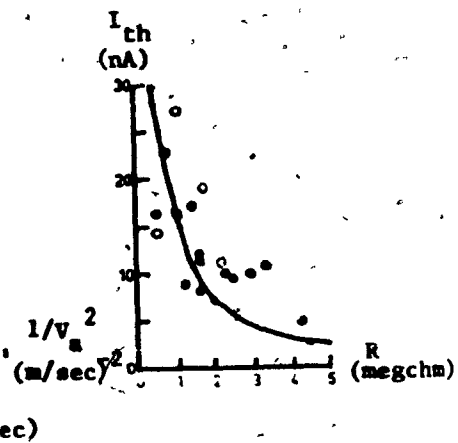
FIGURE 6-2 I_{th} VERSUS R
ASSUMING TH IS INDEPENDENT
OF SIZE; EXP. DATA FROM (38)
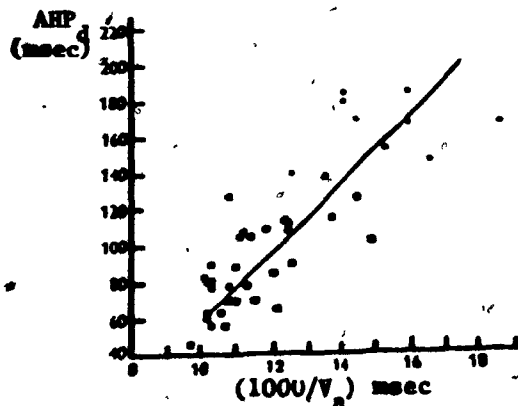
FIGURE 6-3 AHP_d VERSUS $1000/V_a$ (40)

an intracellular electrode to an extracellular reference electrode should
be inversely proportional to the available surface area through which the
current may pass.   Thus we assume the simple relation,

$$R = constant/d^2 \qquad (6-2)$$

Given that the range of d is from 25 to 90 µm, according to Equation (6-2),
the value of R for the smallest MN would be 13 times larger than the value
of R for the largest MN.   The range of R shown in Figure 6-1 is from

.5 MΩ to 8 MΩ , so that the smallest MN has a resistance 16 times larger
than the largest MN.   Since there is good agreement between the theore-
tical and experimental limits, we assume that expression (6-2) is valid
for the entire range of d.   In order to evaluate the constant in (6-2),
we set for convenience R = .58 MΩ for the largest MN with d = 90 μm, so
that the constant equals .58 x 90^2 = 4700.   Consequently,

$$R = 4700/d^2 \qquad (6-3)$$

where R is in MΩ and d is in μm.

For the smallest MN with d = 25 μm, R = $4700/25^2$ = 7.5 MΩ .   Thus, the
theoretical range of R will be from .58 MΩ to 7.5 MΩ and it is within
the experimental range which is from .5 MΩ to 8 MΩ .

        We now turn to the next parameter, the capacitance C.   Since
in general the capacitance of a capacitor is proportional to the area of
the capacitor, we assume that,

$$C = \text{constant} \cdot d^2 \qquad (6.4)$$

The time constant of the membrane T_m is given by,

$$T_m = RC \qquad (6-5)$$

Substituting (6-2) and (6-4) into (6-5) we find that, theoretically, T_m
is a constant independent of size, which has also been observed experi-
mentally (24).   Substituting T_m = 5 msec (24) and R from (6-3) into (6-5),
we have,

$$C = 1.06 \times 10^{-6} \times d^2 \qquad (6-6)$$

where C is in μf and d is in μm.

The threshold current for MNs of different size as measured by
Tannell (38) is shown in Figure 6-2. The threshold current varies in-
versely with the resistance but the data points are too few and too widely
scattered to enable a precise determination of the relationship (38).
Nevertheless, if we assume that the threshold voltage TH is independent
of size, the threshold current I_{th} in the model as given by (4-1) varies
according to the curve shown in Figure 6-2. This curve provides an
acceptable fit to the data and we do not have to express the parameter
TH as a function of size.

Eccles et al. (40) observed that the duration of the after-
hyperpolarization AHP_d varies inversely with the size of the MN. Their
data is shown in Figure 6-3 where AHP_d was plotted versus the inverse of
the conduction velocity, $1/V_a$. A straight line was fitted by Eccles
et al. in order to describe the general trend. The equation of this
straight line is,

$$AHP_d = \frac{19,200}{V_a} - 137 \qquad (6\text{-}7)$$

where AHP_d is in msec and V_a is in m/sec.
Substituting (3-3) into (6-7), we have

$$T_K = \frac{6400}{V_a} - 45.7 \qquad (6\text{-}8)$$

where T_K is in msec and V_a is in m/sec.
Solving (6-1) for V_a ,

$$V_a = \frac{193}{\sqrt{R + 2.54}} \qquad (6\text{-}9)$$

By substituting (6-9) into (6-8),

$$T_K = 33\sqrt{R + 2.54} - 45.7 \qquad (6\text{-}10)$$

where R is in MΩ and T_K is in msec.

Finally substituting (6-3) into (6-10),

$$T_K = 33\sqrt{\frac{4700}{d^2} + 2.54} - 45.7 \qquad (6\text{-}11)$$

where T_K is in msec and d is in μm.

Now the only remaining parameter that is to be correlated to the size is ΔG_{KO}. We shall find this relation by using the experimental observation that the maximum magnitude of the after-hyperpolarization is 5 mv and independent of the MN size (26). During the AHP, the equation for the basic circuit in Figure 3-4(b) is,

$$C\frac{d\,\Delta e_m}{dt} + \frac{\Delta e_m}{R} + (\Delta e_m + E_K - E_r)\,\Delta G_{KO}\,e^{-t/T_K} = 0 \qquad (6\text{-}12)$$

Let t_{max} be the time when the magnitude of the AHP is maximum. Then, we have $\Delta e_m = -5$ mv and $\dfrac{d\,\Delta e_m}{dt} = 0$. Substituting these constraints and $E_K - E_r = 20$ mv, we have

$$\frac{-5}{R} + (-5 + 20)\,\Delta G_{KO}\,e^{-t_{max}/T_K} = 0 \qquad (6\text{-}13)$$

Rearranging (6-13) we obtain,

$$\Delta G_{KO}R = \frac{1}{3}\,e^{t_{max}/T_K} \qquad (6\text{-}14)$$

The variable t_{max} can be expressed as a function of T_K. To do so, the model was simulated for four MNs of different size. In the simulations $\Delta G_{KO}R$ was varied until the resultant maximum magnitude of the AHP was equal to 5 mv. The values of $\Delta G_{KO}R$ and t_{max} found from the simulations are given in Table 6-1. It is apparent that t_{max} is inversely related

to the size and this result agrees with the experimental observation by Kuno

(26).   An expression for t_{max} which approximately fits the simulation

results is the following,

$$t_{max} = .133 T_K + 8.34 \tag{6-15}$$

where t_{max} and T_K are in msec.

Substituting (6-15) into (6-14) we have,

$$\Delta G_{KO} = \frac{.333}{R} e^{(.133T_K + 8.34)/T_K} \tag{6-16}$$

The values of t_{max} and ($\Delta G_{KO}R$) calculated from (6-15) and (6-16) res-

pectively are approximately equal to the values found from the simulations

as shown in Table 6-1.

In summary, the parameters of the model which are dependent on

the MN size are R, C, T_K, and ΔG_{KO}.   Given the diameter d, these

parameters can be calculated from (6-3), (6-6), (6-11), and (6-16).   All

the other parameters of the model are independent of the MN size and

these are: TH = 15 mv, E_K = 90 mv,   and E_r = 70 mv.   In the next two

sections, the response of the model for MNs of different size will be

described.

TABLE 6-1

MN size	$d(\mu m)$	$R(M\Omega)$	T_K(msec)	$(\Delta G_{K0}R)$	t_{max}(msec)	t_{max}(msec)	$(\Delta G_{K0}R)$	$(\Delta G_{K0}R)T_K$	S_d
		(6-3)	(6-11)	(in simulation of AHP)	(in simulation of AHP)	(6-15)	(6-16)	(6-16) and (6-11)	(5-14)
smallest	25	7.52	61.3	.44	15.8	16.1	.44	27.0	8.75
medium	60	1.31	19.0	.61	11.5	10.9	.59	11.2	3.65
exemplary MN used in the previous sections	79	0.75	14.2	.68	10.4	10.2	.68	9.7	2.43
largest	90	0.58	12.5	.72	10.0	10.0	.74	9.3	1.96

6.1.2 Response to stimulation by steps of current

The relationship between the adapted firing frequency versus the intensity of the current step for MNs of different size are shown in Figure 6-4. The curves marked with ● are obtained from computer simulations of the basic model, while the curves marked with O are reported experimental results. In the following, we describe how the threshold current, the minimum firing frequency, the range of firing frequencies, and the slope of the curves are correlated to the size of the MN both for the model and the real MN.

The threshold current I_{th} is given by Equation (4-1) and it is directly proportional to the size. This result agrees with Kernell's experimental result (38). The minimum firing frequency f_m found by extending the linear portion of the simulation curves up to the threshold current is given by Equation (4-3) and it is directly proportional to the size. This result agrees with the real case, since Kernell has observed that f_m is inversely proportional to the duration of the AHP (30) which is inversely proportional to the size (40) so that f_m is directly proportional to the size. The firing frequency of a MN for a current intensity $I = PI_{th}$, where P is a constant, can be meaningfully compared to the firing frequency of another MN for the current intensity $I = PI_{th}$ when P is the same for both MNs whereas I_{th} is dependent on the MN size. Substituting $I_{th} = TH/R$ and $I = PI_{th}$ into (5-15) we obtain,

$$f_{SK} = \frac{TH}{0.91\ E_Z\ (\ \Delta G_{KO}R)T_K}\ (P-1) + f_m \qquad (6\text{-}17)$$

The term ($\Delta G_{KO}R)T_K$ in the denominator of (6-17) is inversely proportional to the size as shown in Table 6-1. Therefore, both terms in

(6-17) are directly proportional to the size so that the frequency f_{SK} is directly proportional to the size for any value of P. Few experimental curves have been reported and three of these are included in Figure 6-4 for comparison with the simulation results. The experimental results and the simulation results agree in the sense that the firing frequencies are directly proportional to the size, but the firing frequencies of the model for any particular MN are larger than the experimental values.

We can extract from Figure 6-4 more information about the firing frequencies by comparing the slopes of the curves of the model to the slopes of the experimental curves. For the curves of the model, the slope is inversely proportional to the size. The slopes calculated from Equation (5-14) also show the same correlation (see Table 6-1). Kernell concluded from his experimental data that the slope was not correlated to the size (29) and, in a subsequent paper, he concluded from a smaller number of tests that the slope was directly proportional to the size (38). His latter conclusion is the opposite of the correlation found from the simulations. To clarify this contradiction, we compare the simulation results with the range of the slopes observed by Granit et al. (41, Figure 8) shown in the inset of Figure 6-4. The largest slope observed is 3.59, and the curve for the MN is located in Figure 6-4 next to the model for a MN with d = 25 µm. Unfortunately, the data obtained by Granit et al. was not correlated to the size because this was not their reason for obtaining the data. However, we can assume that the real MN with slope 3.59 is one of the smallest for three reasons:

　　1.　its threshold current is small
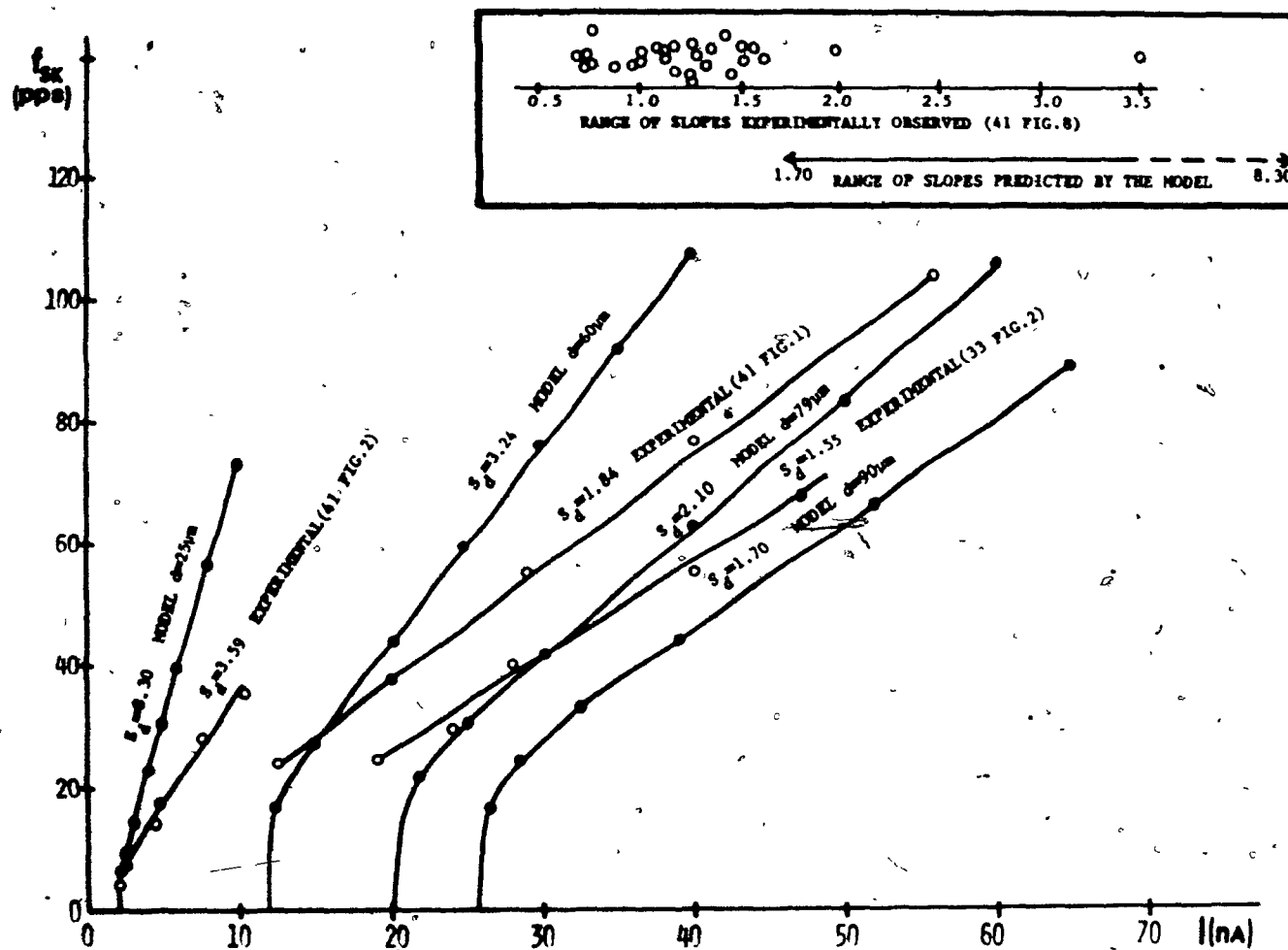
FIGURE 6-4 ADAPTED FIRING FREQUENCY f_{SK} VERSUS INTENSITY OF STIMULATING STEP I
FOR THE BASIC MODEL AND FOR REAL MOTONEURONS OF VARIOUS SIZES

- ii. its minimum firing frequency is small

iii. only one MN was tested with such a comparatively
large slope presumably because of the difficulty
of experimenting on small MNs with an intracellular
microelectrode.

The ratio of the slope of the model for the smallest MN (8.30) and the
largest experimental slope (3.59) is 2.3. The ratio of the slope of
the model for the largest MN (1.70) and the smallest experimental slope
(0.7) is 2.4 . Thus, although the slopes predicted by the model are
larger than the experimental slopes, it is significant that they are
larger by about the same factor 2.3 at both ends of the range. From
these observations, it appears that the slope is inversely proportional
to the MN size. In view of this conclusion, it would be worthwhile to
clarify the contradiction with Kernell's conclusion by further experi-
mental work.

6.1.3 Response to stimulation by sinusoids of current

It was shown in section 5.3 that the response of the model is
proportional to the magnitude and the rate of change of the magnitude of
the input. The latter factor begins to become significant when the fre-
quency of a sinusoidal input is approximately equal to the cut-off fre-
quency $1/T_K$ of the transfer function $H_K(S)$. Since T_K is inversely pro-
portional to the size as indicated by (6-11), the frequency at which the
rate factor becomes evident is directly proportional to the size. For
example, Figure 6-5 shows the response of the model for the smallest MN

for an input with a frequency of 4 Hz.
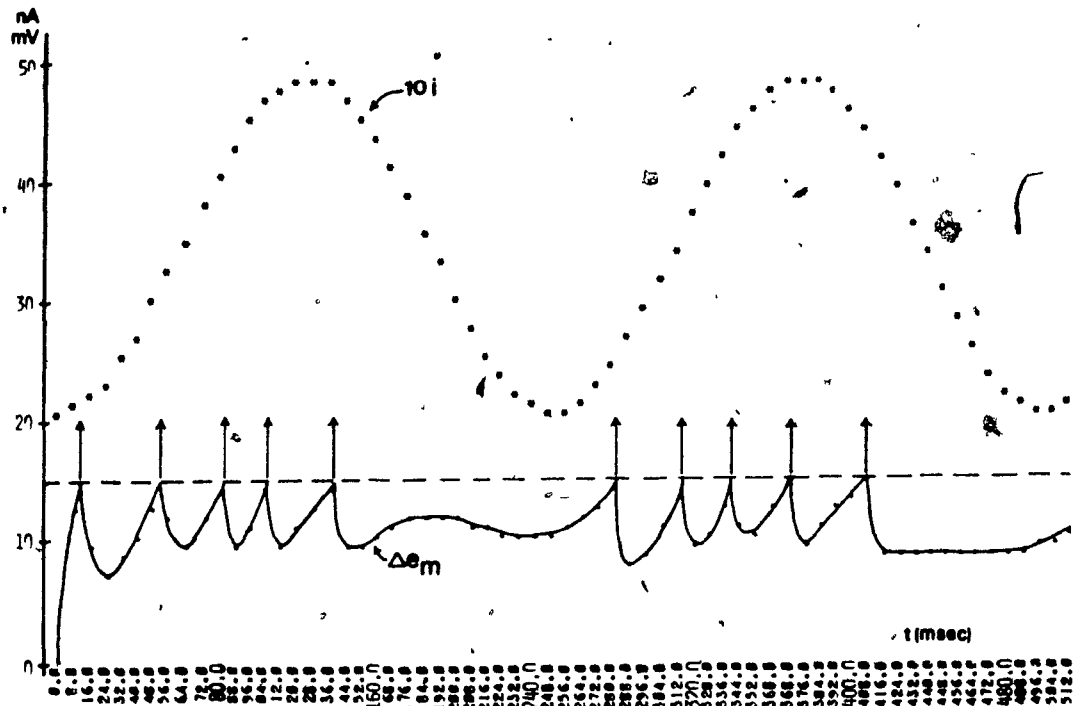
FIGURE 6-5   RESPONSE OF THE BASIC MODEL (d=25μm) TO THE INPUT
            i(t)=3.5-1.4cos(2Π.4.t/1000)

Most of the spikes occur during the rising portion of the input.   This
behaviour was observed in the model for a large MN for higher input fre-
quencies of 10-15 Hz (see Section 4.3).   In Figure 6-6 are shown the
Bode plot of the mathematical relation $(0.91 \ E_Z \ \Delta G_{K0}T_K)H_K(s)$, where $H_K(s)$
is defined in Figure 5-6(a), and the data (X) calculated according to
(5-33) and (5-34) by using the simulation results of the model for the
smallest MN.   By comparing the results in Figure 6-6, it is evident that
the mathematical relation describes well the general trend in the simula-
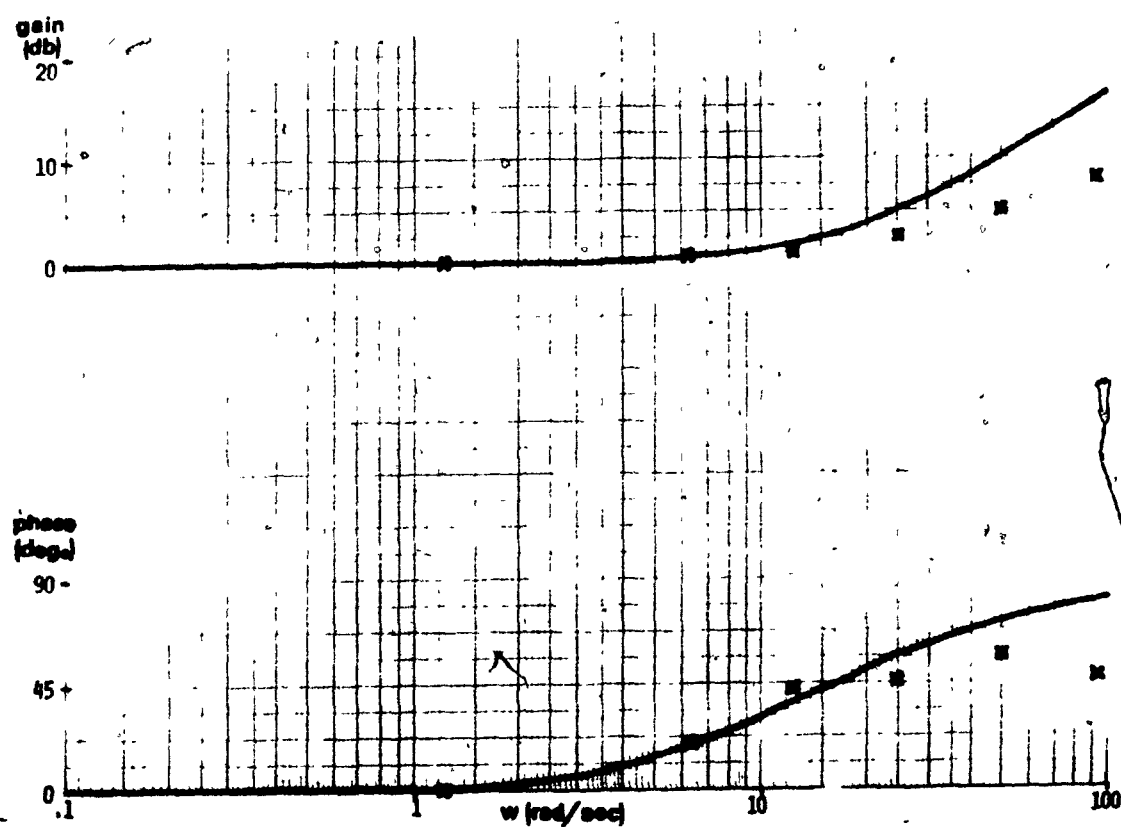
FIGURE 6-6   BODE PLOT OF $0.91E_Z \Delta G_{KO} T_K H_K(s)$ AND DATA(X) FROM
SIMULATIONS OF BASIC MODEL WITH $d=25\mu m$

tion results. The responses of the model for sinusoidal inputs have been compared to experimental observations in section 4.3 .

6.2   Synaptic stimulation

In the natural state, the motoneuron is stimulated by trains of spikes arriving at the synapses.   In order to represent the motoneuron in this natural state, in this section we shall include synaptic inputs in the basic model.

Briefly, the trains of spikes travel along many parallel excitatory and inhibitory fibers.   Each spike arriving at the synapses of an excitatory fiber causes a very brief pulse of current to flow across the membrane, and this current in turn produces a transient depolarization of the membrane at the soma called the miniature excitatory postsynaptic potential (mEPSP).   When a spike is elicited simultaneously in many parallel excitatory fibers, the mEPSP summate and the summated depolarization is called the excitatory postsynaptic potential(EPSP).   The time course of both the mEPSPs and the EPSP depend on the location of the synapses over the surface of the MN.   On the average, the mEPSPs and the EPSP reach a peak in 1 msec and decline with a time constant of 5 msec (42), which is the recently measured value of the time constant T_m of the membrane (24).   Likewise, the spikes in the inhibitory fibers produce an inhibitory postsynaptic potential (IPSP) which has a time course similar to the EPSP (16).   In Figure 6-7 we have included the synaptic inputs.   The spikes in each fiber and the very brief synaptic currents are represented by impulses.   The mEPSP and mIPSP are the impulse res-

ponse of the transfer function $K_m/(s+A_m)$.
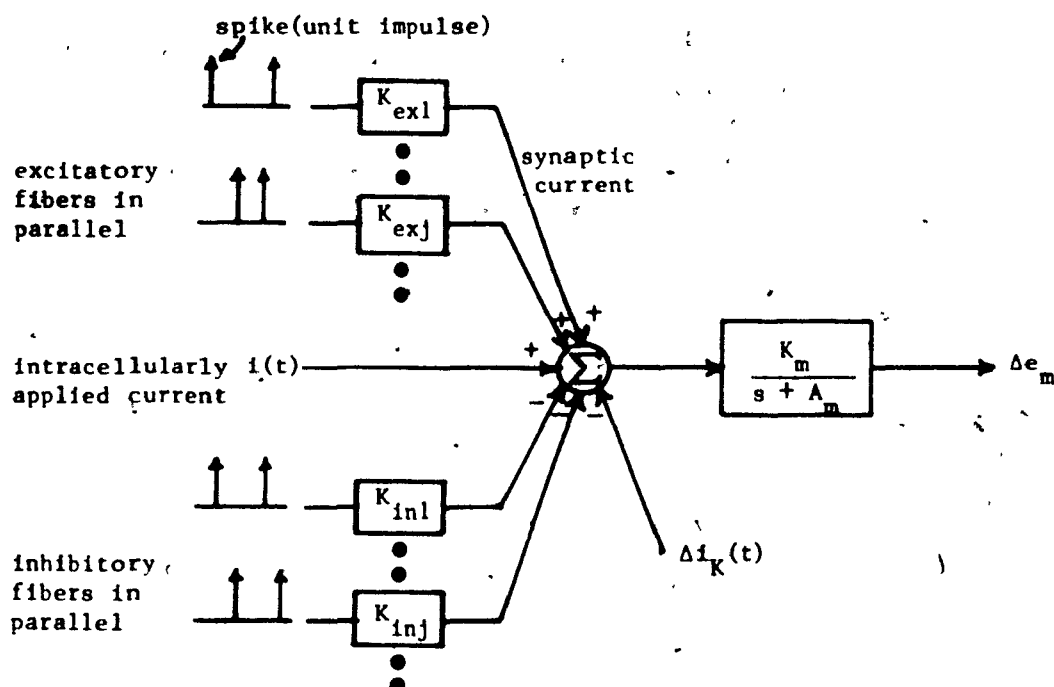
FIGURE 6-7 SYNAPTIC INPUTS ARE INCLUDED

The magnitude of the mEPSP and mIPSP can be varied for each fiber but, unlike the biological case, the time course of the mEPSP and the mIPSP cannot be varied. However, the time constant of the decline of mEPSP and mIPSP is equal to the experimentally observed average value T_m .

When the gains K_{ex} and K_{in} are set, we have to take into account the fact that the magnitude of the IPSP is dependent on the membrane potential: The magnitude of the IPSP when the membrane potential is biased at the threshold level is 2.5 times the magnitude at the resting potential (16). On the other hand, the EPSP remains the same. In order for the IPSP to be dependent on Δe_m , we must vary K_{in} as a function of Δe_m. However, for the purpose of determining how the inhibition affects the spike emission times, we can set K_{in} constant at the value that pro-

duces the magnitude of the IPSP at the threshold level for the following reason:

Under natural conditions, the mEPSPs and mIPSPs occur asynchronously and summate to produce a smooth change of the membrane potential (34). Since a smooth change can also be produced by a continuous intracellular current $i(t)$, we can think of the summated synaptic current as being equivalent to an intracellular current $i(t)$. Thus, we have an excitatory input $i_{ex}(t)$, and an inhibitory input $i_{in}(t)$ which is given by,

$$i_{in}(t) = C [\Delta e_m(t)] i_{inr}(t) \qquad (6-18)$$

where, C is a variable dependent on Δe_m

and, $i_{inr}(t)$ is the equivalent inhibitory input at the resting potential. From the mathematical analysis in Chapter V, we know that the spike emission times t_i , $i = 1, 2 \ldots$, can be found approximately from,

$$i_{ex}(t_i) - i_{in}(t_i) - \Delta i_K(t_i) = I_{th} \qquad (6-19)$$

where $\Delta i_K(t)$ is given by (4-4).

Substituting (6-18) into (6-19) we have,

$$i_{ex}(t_i) - C[\Delta e_m(t_i)]i_{inr}(t_i) - \Delta i_K(t_i) = I_{th} \qquad (6-20)$$

Substituting $\Delta e_m(t_i) = TH$ into (6-20), we obtain

$$i_{ex}(t_i) - C(TH)i_{inr}(t_i) - \Delta i_K(t_i) = I_{th} \qquad (6-21)$$

Now suppose that instead of the inhibitory input $i_{in}(t) = C[\Delta e_m(t)]i_{inr}(t)$, we have the inhibitory input $i_{in}(t) = C(TH)i_{inr}(t)$. Then we can write directly (6-21) as the equation from which the spike emission times for the latter input can be found. Consequently, given the same $i_{ex}(t)$ and

$i_{inr}(t)$, the spike emission times found from (6-21) are the same for both inhibitory inputs. Equivalent to having $i_{in}(t)$ equal to $C(TH)i_{inr}(t)$ instead of $C[\Delta e_m(t)]i_{inr}(t)$, we set K_{in} constant at the value that produces the magnitude of the IPSP at the threshold level.

Our model of the encoding mechanism has been based on experimental data obtained by stimulating the MN with a microelectrode. During synaptic stimulation, the trajectories of the membrane potential between spikes are similar to those observed during intracellular stimulation (27). Furthermore, the firing frequencies for synaptic stimulation are similar to those for intracellular stimulation since small MNs fire with frequencies generally below 25 pps while large MNs fire with frequencies above 25 pps (43). Because of the similar trajectories and firing frequencies, we expect that intracellular current and synaptic currents are both encoded essentially in the manner described by the basic model. However, we can also expect some differences. In the stretch reflex, the firing frequency of a small MN saturates, instead of increasing, as the stretch is increased (44). On the other hand, for the model, the firing frequency increases linearly as the stimulating current is increased. Granit postulated in his book (44) that this saturation may be caused, in part, by Kernell's observation that the slope of the f_{SK} - I curve for intracellular stimulation is small for small MNs. The analysis in Section 6.1.2 of this thesis indicated that the slope may actually be large, so that this factor may not account for saturation. Granit also postulated that the inhibition from the Renshaw cells in the system may be another factor that limits the firing frequency. Preliminary simulations of our model of the motoneuron-Renshaw cell

system (56) indicate that this factor may not be significant.

Another possibility is suggested by Kernell's observation that synaptic stimulation, depending on its source, modifies the time course of the after-hyperpolarization and also the slope of the $f_{SK} - I$ curve determined by adding synaptic and intracellular stimulation. Thus, the synaptic inputs may interact with themselves or with the encoding mechanism by modifying the characteristics of the potassium conductance process. Unfortunately, there is little known about such interactions and none have been included in the model.

CHAPTER VII

EXTENDING THE BASIC MODEL BY MODELLING THE ELECTROGENIC

SODIUM PUMP PROCESS - GENERAL MODEL AND ITS ANALYSIS

7.1   Introduction

The electrogenic Na and K pumps of the membrane shown in

Figure 2-2 are believed to be involved in the maintenance of equilibrium

in a neuron at rest (11a, 12, 45).   These pumps have been referred to

simply as the electrogenic Na pump (45), presumably because the operation

of each pump is dependent on the operation of the other (12).   During

an action potential, Na ions enter the cell and K ions leave the cell so

that there is change in the concentrations of the ions across the membrane

and the equilibrium is unbalanced.   It is believed that the

electrogenic Na pump re-establishes the equilibrium, and while doing

so, the membrane potential is hyperpolarized(11c). , It has been

suggested that, in the crayfish stretch receptor and in the pyramidal

tract cell, both the increased potassium conductance and the electrogenic

Na pump are involved in producing the after-hyperpolarization (46, 47).

However, it appears that the importance of both processes in determining

other properties of the encoding mechanism has not been recognized.

The properties for the motoneuron have been discussed solely in terms of

the increased potassium conductance (8, 12, 22, and previous chapters of

this thesis).   On the other hand, Sokolove has recently attempted to

explain all his experimental results for the crayfish stretch receptor

neuron in terms of the effect of the electrogenic Na pump (10, 45).   In

this chapter, we extend the basic model, which included the potassium conductance process, by modelling also the electrogenic Na pump process. The analysis of the entire model (called the general model) and the previous analysis of the basic model together show which properties of the encoding mechanism are due to each process. These properties will be classified in the next chapter.

7.2   Formulation of the general model

Sokolove and Cooker (45) found that certain experimental results for the crayfish stretch receptor neuron were modified considerably when the activity of the electrogenic Na pump was depressed by several methods. For example, normally when the neuron was stimulated by current steps, the firing frequency declined exponentially with a time constant of about 5 seconds to a steady-state value equal to one-half of the initial value. However, when the pump was depressed, the firing frequency remained constant at the initial value. They postulated that, when spikes are emitted, the increased activity of the pump produces an inhibitory current which counteracts the stimulating current. Sokolove has proposed a model (10, see Section 1.2 of this thesis) in which he assumed that the inhibitory current is a temporal summation of component currents, each of which is produced by a spike and declines from a maximum at the time of the spike exponentially with a time constant of 10 seconds. His model reproduces some experimental observations but it has limitations which will be described after we propose our general model (see Section 8.6). Our

general model is shown in Figure 7-1.
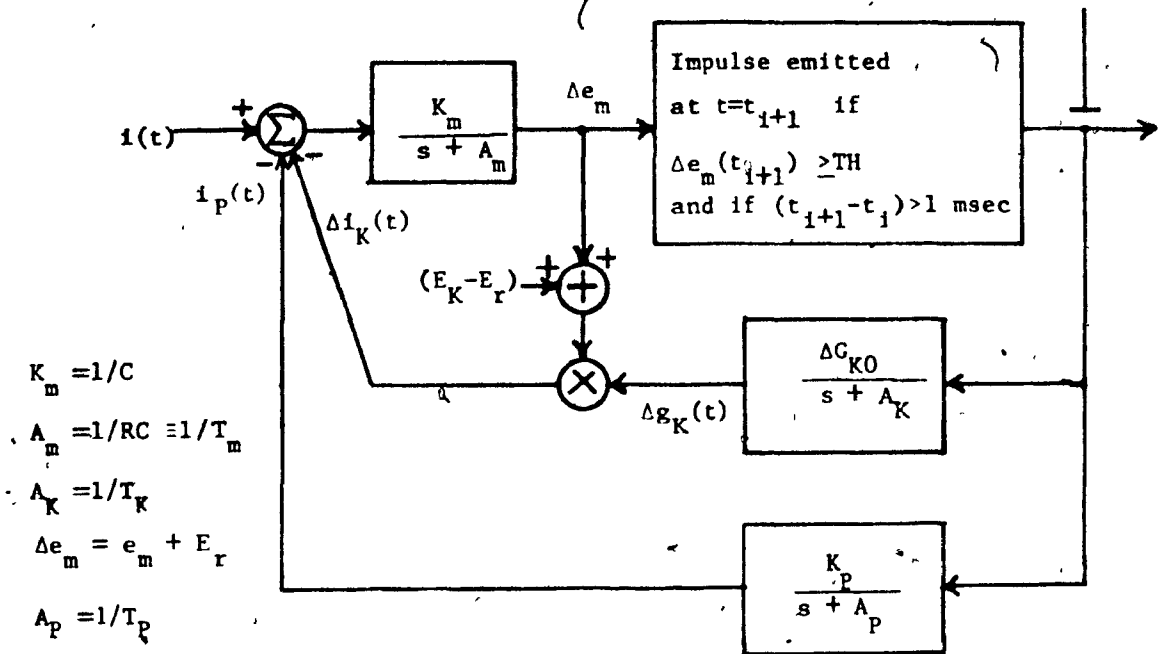
FIGURE 7-1   GENERAL MODEL OF THE NEURONAL ENCODING MECHANISM

We have added to our basic model another feedback path in order to in-
clude the electrogenic Na pump process.   In modelling this process with
a negative feedback path containing the transfer function $K_p/(s+A_p)$, we
have adopted the same assumptions made by Sokolove and Cooke (stated
above).

7.3   Response to stimulation by steps of current

In this and the following sections, we shall compare the response
of our model with the experimental results obtained by Sokolove et al.
Thus, unless otherwise stated, the simulation results have been obtained
with the parameters of the model set equal to those of the smallest MN
because the crayfish neurons tested by Sokolove et al. had firing fre-

quencies and current intensities in the range of those for the smallest
MN (see data in (45) and in this thesis). The new parameter A_p in the
outer feedback path was set as $T_p = 1/A_p = 10$ sec, while K_p was found
from Equation (7-11).

When a step input equal to two times the threshold current is
applied to the general model, the instantaneous firing frequency $f(t)$ is
shown in Figure 7-2. This response of the general model is equal to the
response of the basic model with the input equal to $[I - i_p(t)]$, where I
is the magnitude of the step input and $i_p(t)$ is the inhibitory current
due to the electrogenic Na pump process. As shown in the figure, during
the first few hundred milliseconds, $i_p(t)$ is approximately zero and the
general model reduces approximately to the basic model. Therefore, as
explained in the previous chapters, the instantaneous firing frequency
adapts within the first few spikes to the value f_{SK}, due to the summation
of the potassium conductance (Δg_K) process. As time increases, $i_p(t)$
summates temporally, with small deviations from the continuous curve
shown in the figure. Meanwhile $f(t)$ declines exponentially with a time
constant of 5 sec to a steady-state value f_{SP} equal to about one-half
of f_{SK}. The gradual adaptation of the firing frequency with a time con-
stant of 5 sec due to the electrogenic Na pump process is in agreement
with the experimental observation of Sokolove et al. The response of
the model has, in addition, an initial adaptation within the first few
spikes due to the summation of the Δg_K process, whereas Sokolove et al.
did not report if any initial adaptation of the firing frequency was pre-
sent in the crayfish sensory neuron. However, it is reasonable to ex-
pect that there is an initial adaptation because another of their experi-

mental observations can only be explained by the summation of the Δg_K process as we shall show in the next section. The adapted firing frequency f_{SP} is equal to about one-half of f_{SK} for all values of the input I greater than 2.5 nA as shown in Figure 7.3 This latter property has also been observed experimentaly by Sokolove et al.

Let us extend the mathematical analysis of Chapter V for the same purposes which we discussed at the beginning of that chapter. If a spike train with a constant spike frequency f is applied to $K_p/(s + A_p)$ at t = 0, then, analagous to the behaviour of the transfer function $E_Z \Delta G_{KO}/(s + A_K)$ shown in Figure 5-4 and the derivation of Equation (5-19), the curve passing through the minimum values of $i_p(t)$ is described by the equation,

$$i_{PC}(t) = \frac{K_P}{e^{1/fT_P} - 1} (1 - e^{-t/T_P}) \tag{7-1}$$

Since the values of 1/f are of the order of 50 msec, they are much less than T_p which equals 10 sec. Therefore, $1/fT_p \ll 1$ and approximately,

$$i_{PC}(t) = K_P T_p f(1 - e^{-t/T_P}) \tag{7-2}$$

The value of $i_p(t)$ is approximately equal to $i_{PC}(t)$ because the increment K_p added by each spike is much less than the summated $i_{PC}(t)$ (except initially when only a few spikes have been emitted). Thus approximately,

$$i_p(t) = K_P T_p f(1 - e^{-t/T_P}) \tag{7-3}$$

Equation (7-3) gives the response of $K_p/(s + A_p)$ for an input which can be considered to be a step of frequency f. For a system with such a step response, the Laplace transform of the response for a time-varying input f(t) is related to the Laplace transform of the input by,

f(t) FOR THE FIRST INTERVAL
IS 1000 PPS AND FOR SUBSEQUENT
INTERVALS IT IS $f(t) \doteq f_{SP}(1 + e^{-t/S})$

$i_p(t) \doteq i_{PS}(1 - e^{-t/S})$
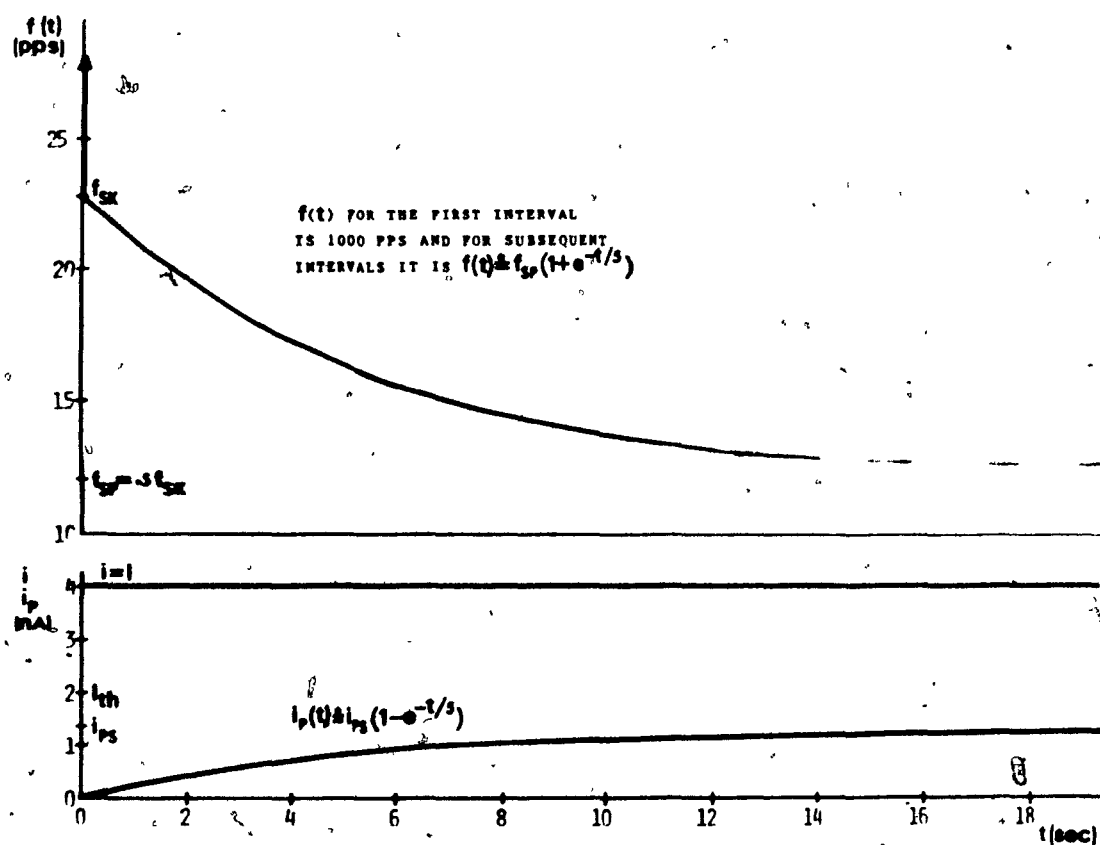
FIGURE 7-2   RESPONSE OF THE GENERAL MODEL TO A STEP INPUT
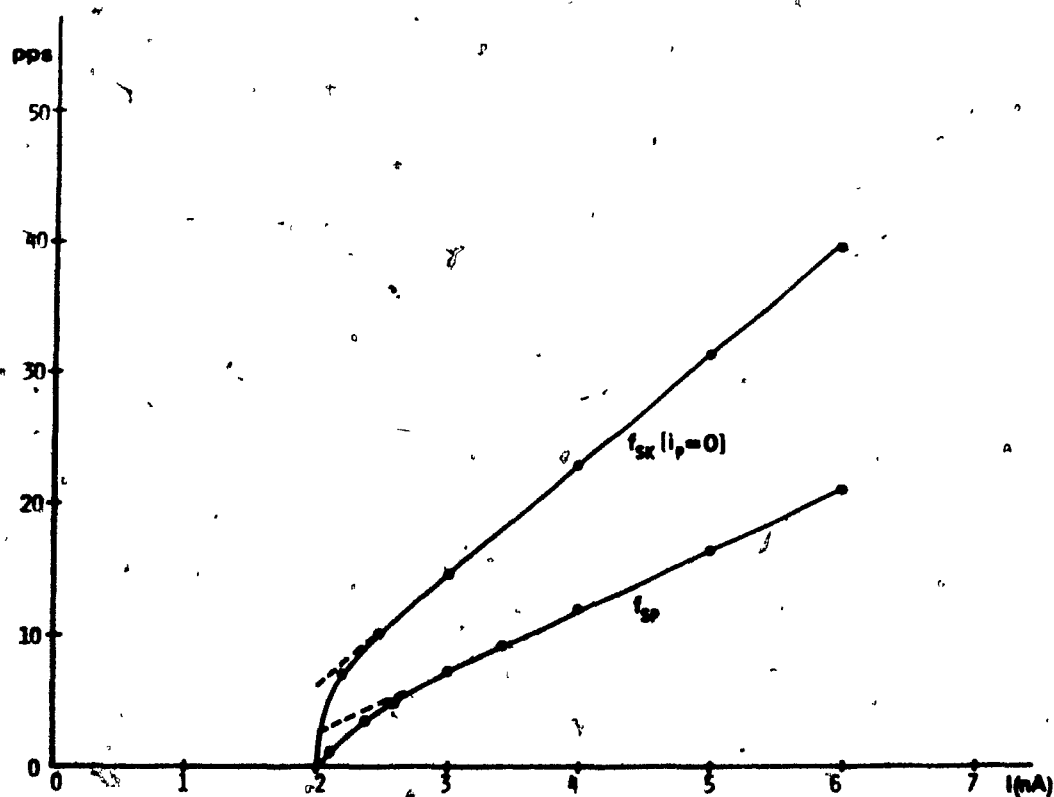

$f_{SK}(i_p = 0)$

f_{SP}

FIGURE 7-3   ADAPTED FIRING FREQUENCY OF THE GENERAL MODEL WITH
AND WITHOUT THE EFFECT OF THE ELECTROGENIC SODIUM PUMP

$$i_p(s) = \frac{K_P}{s + A_P} f(s) \qquad (7-4)$$

Substituting $[i(t)-i_p(t)]$ for $i(t)$ in Equation (5-30) we obtain,

$$f(t) = \frac{1}{0.91E_Z \Delta G_{KO}}\left[\frac{1}{T_K}[i(t)-i_p(t)-I_{th}] + \frac{d[i(t)-i_p(t)]}{dt} + f_m\right] \qquad (7-5)$$

Taking the Laplace transform of (7-5) and substituting (7-4),

$$f(s) = \frac{1}{0.91E_Z \Delta G_{KO}}\left[\frac{1}{T_K}\left(i(s) - \frac{K_P f(s)}{s + A_P} - \frac{I_{th}}{s}\right) + si(s) - \frac{sK_P f(s)}{s + A_P}\right] + \frac{f_m}{s} \qquad (7-6)$$

Solving (7-6) for $f(s)$,

$$f(s) = \frac{0.91E_Z \Delta G_{KO}T_K(s+A_P)\left\{\dfrac{1}{0.91E_Z \Delta G_{KO}}\left[\dfrac{1}{T_K}\left(i(s) - \dfrac{I_{th}}{s}\right) + si(s)\right] + \dfrac{f_m}{s}\right\}}{\left(0.91E_Z \Delta G_{KO}T_K + K_P T_K\right)\left(s + \dfrac{0.91E_Z \Delta G_{KO}T_K A_P + K_P}{0.91E_Z \Delta G_{KO}T_K + K_P T_K}\right)} \qquad (7-7)$$

For a step input $i(t)=I$ or $i(s)=I/s$, the steady-state value of $f(t)$, denoted f_{SP}, is

$$f_{SP} = \lim_{s \to 0} sf(s)$$

$$= \frac{0.91E_Z \Delta G_{KO}T_K A_P\left[\dfrac{1}{0.91E_Z \Delta G_{KO}}\left(\dfrac{I - I_{th}}{T_K}\right) + f_m\right]}{\left(0.91E_Z \Delta G_{KO}T_K + K_P T_K\right)\left(\dfrac{0.91E_Z \Delta G_{KO}T_K A_P + K_P}{0.91E_Z \Delta G_{KO}T_K + K_P T_K}\right)}$$

$$= \frac{\dfrac{1}{0.91E_Z \Delta G_{KO}}\left(\dfrac{I - I_{th}}{T_K}\right) + f_m}{1 + \dfrac{K_P}{0.91E_Z \Delta G_{KO}T_K A_P}} \qquad (7-8)$$

Substituting f_{SK} (from (5-15) for the numerator of (7-8) we get,

$$f_{SP} = \frac{f_{SK}}{1 + \frac{K_P}{0.91E_Z \Delta G_{KO} T_K A_P}} \qquad (7-9)$$

Solving for K_P ,

$$K_P = \left(\frac{f_{SK}}{f_{SP}} - 1\right) 0.91E_Z \Delta G_{KO} T_K A_P \qquad (7-10)$$

In the simulations, $f_{SP} = .5 f_{SK}$ because we chose K_P as

$$K_P = 0.91E_Z \Delta G_{KO} T_K A_P \qquad (7-11)$$

Since ΔG_{KO} and T_K have been expressed as a function of size, then K_P also depends on the size. In general,

if the maximum $\frac{f_{SK}}{f_{SP}} = 10$ and since $T_K A_P \approx 1/100$,

then,

$$\text{maximum } K_P = \frac{9}{100} (0.91E_Z \Delta G_{KO})$$

so that,

$$K_P << 0.91E_Z \Delta G_{KO} \qquad (7-12)$$

Thus, the parameters of the two feedback paths in the general model are substantially different. The gain K_P of the electrogenic Na pump process is much less than the gain $E_Z \Delta G_{KO}$ of the Δg_K process. The time constant T_P is more than 100 times larger than T_K .

By substituting (7-10) into (7-7),

$$f(s) = \frac{0.91E_Z\Delta G_{KO}T_K(s+A_P)\left\{\frac{1}{0.91E_Z\Delta G_{KO}}\left[\frac{1}{T_K}\left[i(s)-\frac{I_{th}}{s}\right]+si(s)\right]+\frac{f_m}{s}\right\}}{\left(0.91E_Z\Delta G_{KO}T_K+K_PT_K\right)\left(s+\frac{0.91E_Z\Delta G_{KO}T_KA_Pf_{SK}/f_{SP}}{0.91E_Z\Delta G_{KO}T_K+K_PT_K}\right)} \quad (7-13)$$

Utilizing (7-12) we have,

$$f(s) = \frac{(s+A_P)}{\left(s+A_P\frac{f_{SK}}{f_{SP}}\right)}\left\{\frac{1}{0.91E_Z\Delta G_{KO}}\left[\frac{1}{T_K}\left[i(s)-\frac{I_{th}}{s}\right]+si(s)\right]+\frac{f_m}{s}\right\} \quad (7-14)$$

where, f_{SK}/f_{SP} is related to the parameters of the model by Equation (7-9). Thus, the additional feedback path introduced in order to account for the electrogenic Na pump simply introduces a term that multiplies the expression for the basic model. The block diagram for Equation (7-14) is shown in Figure 7-4. As shown in Figure 7-5, when the input is a step $i(t) = I$, the output of the transfer function due to the Δg_K process is $f_{SK}u(t) + \frac{I\,\delta(t)}{0.91E_Z\Delta G_{KO}}$. The unit-step response of the transfer function

$$(s+A_P)/(s+A_P\frac{f_{SK}}{f_{SP}})$$

is

$$\left[\frac{f_{SP}}{f_{SK}}+\left(1-\frac{f_{SP}}{f_{SK}}\right)e^{-A_P\frac{f_{SK}}{f_{SP}}t}\right]u(t)$$

and the impulse response is

$$\delta(t)+A_P\left(1-\frac{f_{SK}}{f_{SP}}\right)e^{-A_P\frac{f_{SK}}{f_{SP}}t}\,u(t)$$

Therefore, the step response of the transfer function for the general model is given by,
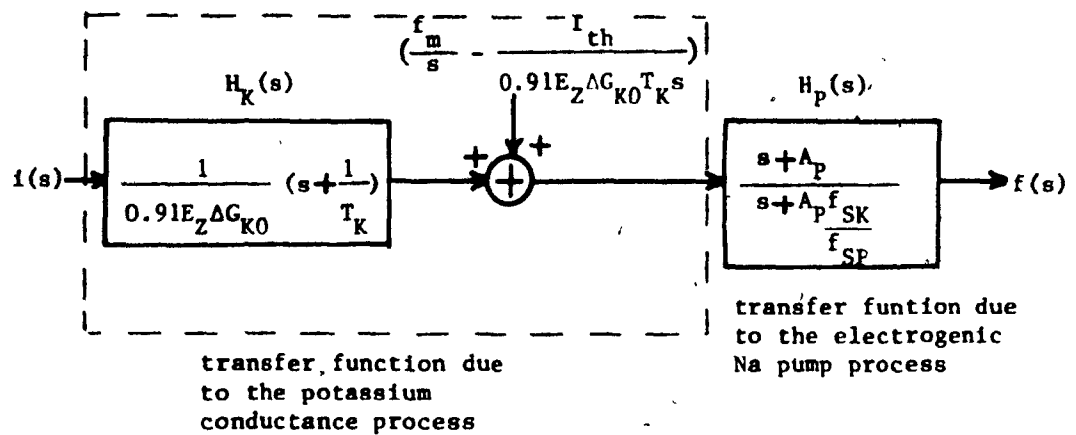
FIGURE 7-4 TRANSFER FUNCTION FOR THE GENERAL MODEL VALID
FOR OPERATION ABOVE THRESHOLD
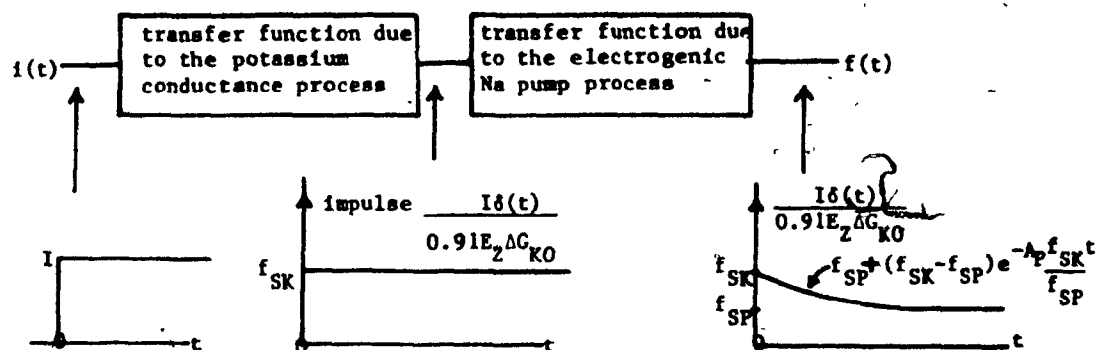
FIGURE 7-5 OUTPUTS OF THE TRANSFER FUNCTIONS IN FIGURE 7-4
FOR A STEP INPUT

$$f(t) = \left[f_{SP} + (f_{SK} - f_{SP}) e^{-A_P \frac{f_{SK}}{f_{SP}} t} \right] u(t) + \frac{I \delta(t)}{0.91 E_Z \Delta G_{KO}} + \frac{I A_P}{0.91 E_Z \Delta G_{KO}} \left(1 - \frac{f_{SK}}{f_{SP}} \right) e^{-A_P \frac{f_{SK}}{f_{SP}} t} u(t)$$

$$(7-15)$$

Since,

$$I < (3 I_{th} = 3 \times 15 \text{ mv/R}), \quad \Delta G_{KO} > .45/R, \quad A_P = 1/10 \text{ sec, and}$$

$$E_Z = 35 \text{ mv},$$

Therefore,

$$\frac{I\,A_P}{0.91E_Z\Delta G_{KO}}\left(1 - \frac{f_{SK}}{f_{SP}}\right) < \left\{\frac{3 \times 15}{0.91 \times 35 \times .45 \times 10}\left(1 - \frac{f_{SK}}{f_{SP}}\right) = .31\left(1 - \frac{f_{SK}}{f_{SP}}\right) \text{ pps}\right\}$$

(7-16)

Since, $f_{SP} \gg .31$ pps

Therefore,

$$\frac{I\,A_P}{0.91E_Z\Delta G_{KO}}\left(1 - \frac{f_{SK}}{f_{SP}}\right) \ll \left\{f_{SP}\left(1 - \frac{f_{SK}}{f_{SP}}\right) = -(f_{SK} - f_{SP})\right\}$$

(7-17)

Because of the inequality in (7-17), the last term in (7-15) can be neglected, so that,

$$f(t) = \left[f_{SP} + (f_{SK} - f_{SP})\,e^{-A_P\frac{f_{SK}}{f_{SP}}t}\right]u(t) + \frac{I\,\delta(t)}{0.91E_Z\Delta G_{KO}}$$

(7-18)

The first term in (7-18) corresponds to the gradual adaptation of the firing frequency due to the electrogenic Na pump process, and the second term corresponds to the quick initial adaptation of the firing frequency due to the potassium conductance process (see Section 5.3).

7.4 Resetting of repetitive firing by inserting spikes

In the previous section we have shown that the feedback path due to the electrogenic Na pump process must be present in order to account for the gradual adaptation of the firing frequency as observed in the crayfish stretch receptor neuron by Sokolove et al.   We now show that the feedback path due to the potassium conductance process must also be present in order

to account for another experimental observation made by Sokolove et al.

Sokolove et al(45) reset the repetitive firing of a crayfish stretch receptor neuron by artificially inserting one or two spikes as illustrated in Figure 7-6. The neuron under study had a relatively stable interspike period T_0 of about 79 msec (Figure 7-6(a)). In experiment 1 (Figure 7-6(b)), a spike was artificially initiated T_1 msec after a spontaneous spike and the time T_2 that elapsed until the next spontaneous spike occurred was measured. In experiment 2 (Figure 7-6(c)), a spike was artificially initiated T_1 msec after a spontaneous spike, and a second spike was artificially initiated 18 msec later. The time T_2 was again measured. Plots of the data T_2 versus T_1 for both experiments are shown in Figure 7-7. In both experiments, T_2 was greater than T_0 except for a few data points of experiment 1.
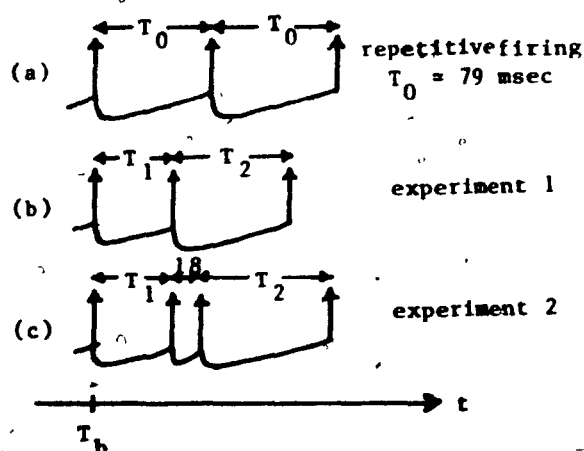
FIGURE 7-6 RESETTING OF REPETITIVE
FIRING BY INSERTING ONE OR TWO SPIKES
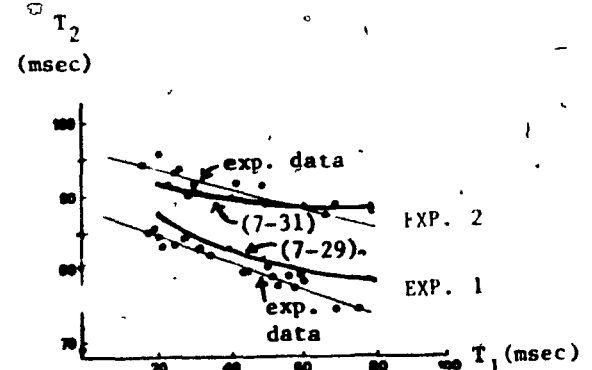
FIGURE 7-7 DATA(45) FROM EXPERI-
MENTS IN FIG. 7-6 AND RESULTS OF
MATHEMATICAL ANALYSIS

First we shall show mathematically that the negative feedback current due to the electrogenic Na pump process is not the cause of T_2 being greater than T_0. The value of $i_p(t)$ immediately after the spike at $t = T_b$ is given by,

$$i_p(T_b) = \frac{K_p}{A_p T_0} + K_p \qquad (7\text{-}19)$$

where, the first term is the accumulated i_p due to the spikes prior to $t = T_b$ found by substituting $f = 1/T_0$ and $t = T_b \gg T_p$ in (7-2) and, the second term is the increment added by the spike at $t = T_b$.

In experiment 1, $i_p(T_b + T_1)$ is given by,

$$i_p(T_b + T_1) = i_p(T_b) e^{-T_1/T_p} + K_p \qquad (7\text{-}20)$$

where, the first term is the output of $K_p/(s + A_p)$ for zero input and initial condition $i_p(T_b)$,

and, the second term is the increment added by the spike at $t = T_b + T_1$.

By substituting (7-19) into (7-20),

$$i_p(T_b + T_1) = K_p\left[\left(\frac{1}{A_p T_0} + 1\right) e^{-T_1/T_p} + 1\right] \qquad (7\text{-}21)$$

Since the maximum value of T_1 is 79 msec,

$$\frac{1}{A_p T_0} e^{-T_1/T_p} > \frac{10000}{79} e^{-79/10000} \gg 1$$

Also,

$$\frac{1}{A_p T_0} = \frac{10000}{79} \gg 1$$

Therefore, (7-21) reduces to

$$i_p(T_b + T_1) = \frac{K_p}{A_p T_0} e^{-T_1/T_p}$$

Thus, K_p in (7-19) and (7-20) is negligible, so that two spikes increase the inhibitory current by a negligible amount compared to the accumulated amount. Since the inhibitory current $i_p(t)$ tends to inhibit the emission of a spike, the interval T_2 is directly related to the value of $i_p(T_b + T_1)$. For the present purpose, let us assume the simple relation,

$$T_2 = \text{constant} \times i_p(T_b + T_1) \qquad (7-22)$$

If the spike is artificially initiated at the instant when a spontaneous spike would have occurred so that $T_1 = T_0$, then the repetitive firing is not disturbed and $T_2 = T_0$. Substituting this condition into (7-22) we have,

$$T_0 = \text{constant} \times \frac{K_p}{A_p T_0} e^{-T_0/T_p} \qquad (7-23)$$

Solving for the constant in (7-23) and substituting in (7-22) we have,

$$T_2 = T_0 e^{-(T_1 - T_0)/T_p} \qquad (7-24)$$

For T_1 in the range of interest $0 < T_1 < T_0$, T_2 is approximately equal to T_0. For example, substituting $T_1 = 20$ msec in (7-25) we have,

$$T_2 = 79 \times \left(1 + \frac{59}{10000}\right) = 79.47 \text{ msec}$$

Similarly, it can be shown mathematically that, in experiment 2, T_2 would be approximately equal to T_0. However, the experimental values of T_2 are significantly larger than T_0 as shown in Figure 7-7. For example, in experiment 1, for $T_1 = 20$ msec, $T_2 = 85$ msec. Consequently, the electrogenic Na pump process cannot cause T_2 to be larger than T_0 as much as experimentally observed.

Next we show mathematically that the experimental results can be accounted for by the negative feedback current due to the potassium conductance

(Δg_K) process. We expect that the Δg_K process is involved because the trajectories of the membrane potential between spikes for the crayfish stretch receptor are similar to those for the motoneuron (11d Figure 14). From the above analysis, we know that a few spikes increase i_p by a negligible amount compared to the accumulated amount. Thus, during the period when the firing is reset, the variable $i_p(t)$ is approximately constant and equal to $i_p(T_b)$. Since the general model is equivalent to the basic model with input $[i(t) - i_p(t)]$, the condition for spike emission becomes, from (5-4) and the statement after (5-10),

$$i(t_{i+1}) - i_p(t_{i+1}) - \Delta i_K(t_{i+1}) = I_{th} \qquad (7\text{-}25)$$

Thus, for the repetitive firing in Figure 7-6(a), the condition for the emission of the spike at $t = T_b + 2 T_0$ is given by,

$$[I - i_p(T_b)] - E_Z \Delta G_{KO} e^{-T_0/T_K} - E_Z \Delta G_{KO} e^{-2T_0/T_K} - \Delta i_K(T_b) e^{-2T_0/T_K} = I_{th}$$

$$(7\text{-}26)$$

where, $[I - i_p(T_b)]$ is the value of $[i(t_{i+1}) - i_p(t_{i+1})]$,

the second term is the component of $\Delta i_K(t_{i+1})$ due to the spike at $t = T_b' + T_0$,

the third term is the component of $\Delta i_K(t_{i+1})$ due to the spike at $t = T_b$,

and, $\Delta i_K(T_b)$ is the value of $\Delta i_K(t)$ at $t = T_b$ due to all the spikes prior to $t = T_b$ and it is given by,

$$\Delta i_K(T_b) = \sum_{n=1}^{N} E_Z \Delta G_{KO}\, e^{-nT_0/T_K} \qquad (7\text{-}27)$$

where, N is a large integer greater than $\dfrac{T_b}{T_0}$. However, the sum

can be found approximately by summing only for the first few values of n.

Similarly, for experiment 1, the condition for the emission of the spike at $t = T_b + T_1 + T_2$ is,

$$[I - i_p(T_b)] - \left[E_Z\Delta G_{K0} + [E_Z\Delta G_{K0} + \Delta i_K(T_b)]e^{-T_1/T_K}\right]e^{-T_2/T_K} = I_{th}$$

(7-28)

Substituting (7-26) and (7-27) into (7-28) and solving for T_2 we have,

$$T_2 = T_K \ln\left[\frac{1 + \left(1 + \sum_{n=1}^{N} e^{-nT_0/T_K}\right)e^{-T_1/T_K}}{e^{-T_0/T_K} + e^{-2T_0/T_K} + \sum_{n=1}^{N} e^{-(n+2)T_0/T_K}}\right]$$

(7-29)

As for experiment 2, the condition for the emission of the spike at $t = (T_b + T_1 + 18 \text{ msec} + T_2)$ is,

$$[I - i_p(T_b)] - \left[E_Z\Delta G_{K0} + E_Z\Delta G_{K0}e^{-18/T_K} + [E_Z\Delta G_{K0} + \Delta i_K(T_b)]e^{-(T_1+18)/T_K}\right]e^{-T_2/T_K} = I_{th}$$

(7-30)

Substituting (7-27) and (7-28) into (7-30) and solving for T_2 we have,

$$T_2 = T_K \ln\left[\frac{1 + e^{-18/T_K} + \left(1 + \sum_{n=1}^{N} e^{-nT_0/T_K}\right)e^{-(T_1+18)/T_K}}{e^{-T_0/T_K} + e^{-2T_0/T_K} + \sum_{n=1}^{N} e^{-(n+2)T_0/T_K}}\right]$$

(7-31)

The plots of T_2 versus T_1 for (7-29) and (7-31) are shown in Figure 7-7. The constants T_0 and T_K were chosen as follows in order to compare the mathematical results with experimental data:

(i) T_0 was set equal to 79 msec as experimentally observed.

(ii) The fact that the neuron studied was firing spontaneously indicates that the input is not much larger than the threshold current and the neuron is firing approximately with the minimum frequency. As a result, T_K was found to be $T_0/3 \approx 25$ msec from (3-3) and (4-3).

There is reasonably good agreement between the experimental curves and the curves predicted by these equations. Consequently, the experimental results can be accounted for by the negative feedback current due to the potassium conductance process.

The experiments were simulated with the general model and the simulation results agree with those of the mathematical analysis. The parameters were chosen equal to those of a MN with $T_K = 25$ msec or $d = 48$ μm, and the applied current was set at $I = 10.5$ nA so that the resultant T_0 was equal to 79 msec. The results are shown in Figure 7-8. The data points denoted by $\triangle$ are the results when the complete general model was simulated. The data points denoted by $\square$ are the results when, in the general model, the inhibitory current Δi_p produced by the artificial spikes was not added to the accumulated $i_p(T_b)$. Thus, the values of T_2 given by the curves $\square$, for which $\Delta i_p = 0$, are due to the increased potassium current Δi_K. The values of T_2 given by the curves $\triangle$, for which Δi_p was added, are slightly larger than the values of T_2 given by the curves $\square$. Consequently, both the simulations and the mathematical

analysis show that the resetting of repetitive firing, is mainly caused by the

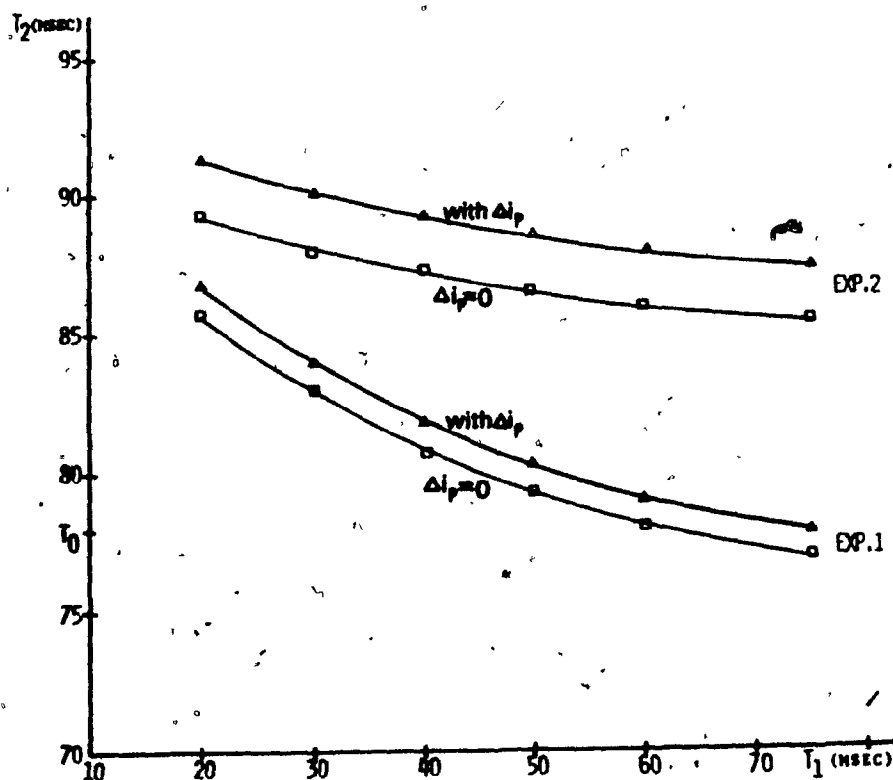potassium conductance process.

FIGURE 7-8   SIMULATION RESULTS OF THE EXPERIMENTS IN WHICH
             REPETITIVE FIRING IS RESET

7.5   Response to stimulation by a tetanic train of pulses

In this section, we shall compare the response of the model to

two related experimental obervations.

Case (i)

Sokolove et al. (45) disturbed the repetitive firing of a crayfish stretch receptor neuron as illustrated in Figure 7-9(a) by inserting a high-frequency train of spikes initiated by applying pulses of current. The interval between the end of the train and the first spike after the train (posttrain interval) was measured. The high-frequency train is called a tetanic train and is described in Figure 7-9(a) by the duration D_T and the spike frequency f_T , much larger than the constant firing frequency f_b . The posttrain interval t_d is dependent on f_b , D_T and f_T . For example, Figure 7-10 shows data obtained by Sokolove et al. (45) from a crayfish stretch receptor by varying f_b and D_T and keeping f_T constant at 100 pps. The posttrain interval t_d was plotted versus the number of spikes in the train, N_T , where N_T is given by,

$$N_T = f_T D_T \qquad (7\text{-}32)$$

Sokolove et al. pointed out that in Figure 7-10:

(i) For a given f_b , the curve relating t_d to N_T is composed of two straight-line segments with a breakpoint at a threshold number of spikes N_{TT} .

(ii) N_{TT} is directly proportional to f_b , and t_d is inversely proportional to f_b .

We have simulated the experiments with the general model. The results from the simulations are shown in Figure 7-11. Although the numerical values in Figure 7-11 are not identical to the experimental data in Figure 7-10, it is evident that the curves in the two figures are similar.

tetanic train with
spike frequency f_T,
duration D_T, and
number of spikes N_T

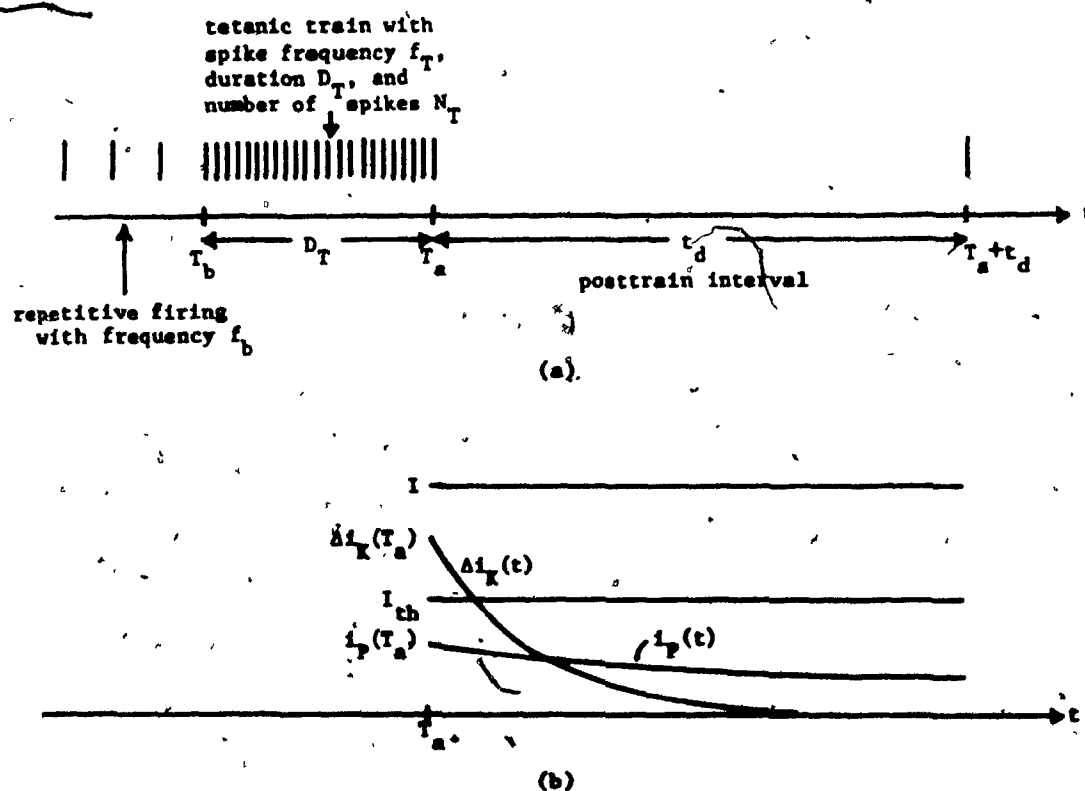repetitive firing
with frequency f_b

(a)

(b)

FIGURE 7-9   DISTURBING REPETITIVE FIRING BY INSERTING A
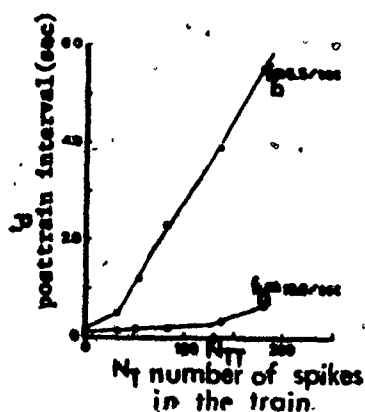TETANIC TRAIN OF SPIKES

FIGURE 7-10 POSTTRAIN INTERVAL OBSERVED FOR THE CRAYFISH
STRETCH RECEPTOR NEURON (45)

The features of the curves can be clarified by analyzing the experiment mathematically with the aid of Figure 7-9(b). In order to find t_d, we must relate $i_P(T_a)$, $\Delta i_K(T_a)$ and $(I - I_{th})$ to f_b, f_T, and D_T. The output $i_P(T_a)$ of $K_P/(s + A_P)$ equals to the output due to the initial condition $i_P(T_b)$ plus the output due to the train as input. Thus,

$$i_P(T_a) = i_P(T_b) \, e^{-D_T/T_P} + \frac{f_T K_P}{A_P} \left(1 - e^{-D_T/T_P} \right) \qquad (7\text{-}33)$$

Since $D_T < 2$ sec and is significantly less than $T_P = 10$ sec, Equation (7-33) can be approximated by,

$$i_P(T_a) = i_P(T_b)\left(1 - \frac{D_T}{T_P}\right) + f_T K_P D_T \qquad (7\text{-}34)$$

By finding the steady-state value in (7-4),

$$i_P(T_b) = \frac{K_P f_b}{A_P} \qquad (7\text{-}35)$$

Substituting (7-35) into (7-34) we have,

$$i_P(T_a) = \frac{K_P f_b}{A_P} \left(1 - \frac{D_T}{T_P} \right) + f_T K_P D_T \qquad (7\text{-}36)$$

The relation for $\Delta i_K(T_a)$ is,

$$\Delta i_K(T_a) = E_Z \Delta G_{KO} + 0.91 E_Z \, \Delta G_{KO} T_K \, (f_T - f_m) \qquad (7\text{-}37)$$

where, the first term is the increment added by the last spike in the tetanic train, and the second term is the steady-state residual from the other spikes in the tetanic train found from (5-24). The residual from spikes prior to the tetanic train, $0.91 E_Z \Delta G_{KO} T_K (f_b - f_m) e^{-D_T/T_K}$ has been neglected because $f_b \ll f_T$ and $D_T \gg T_K$.

By substituting the constant f_b for the adapted firing frequency f_{SP} in (7-8),

$$I - I_{th} = 0.91E_Z \Delta G_{KO} T_K (f_b - f_m) + \frac{K_p f_b}{A_p} \tag{7-38}$$

By using (7-25) we have at the spike emission time $t = T_a + t_d$,

$$I - i_P(T_a + t_d) - \Delta i_K (T_a + t_d) = I_{th} \tag{7-39}$$

Since, during the posttrain interval $i_p(t)$ and $\Delta i_K(t)$ decline with time constant T_p and T_K respectively, (7-39) becomes,

$$I - i_p(T_a) e^{-t_d/T_p} - \Delta i_K(T_a) e^{-t_d/T_K} = I_{th} \tag{7-40}$$

Substituting $i_p(T_a)$, $\Delta i_K(T_a)$, and $(I - I_{th})$ found from (7-36), (7-37), and (7-38) respectively, t_d can be found from (7-40) by using the digital computer. In Figure 7-12 we compare the solution [curves (b)] with the simulation results [curves (a)] for the same conditions. The solutions of (7-40) are similar to the simulation results and thus, we shall analyze this equation in order to clarify the features of the curves.

We shall derive from (7-40) two equations whose solution yield the two line segments of the curves in Figure 7-12. Rearranging (7-40) we have,

$$(I - I_{th}) - i_P(T_a) e^{-t_d/T_p} = \Delta i_K(T_a) e^{-t_d/T_K} \tag{7-41}$$

If $\qquad (I - I_{th}) - i_p(T_a) < 0 \tag{7-42}$

or, by substituting (7-32) and (7-36) into (7-42),

If $\qquad N_T > \frac{(I - I_{th})}{K_p} - \frac{f_b}{A_p}\left(1 - \frac{D_T}{T_p}\right) \tag{7-43}$

Then, as illustrated in Figure 7-13(a), since $T_K \ll T_p$ (7-41) is approxi-
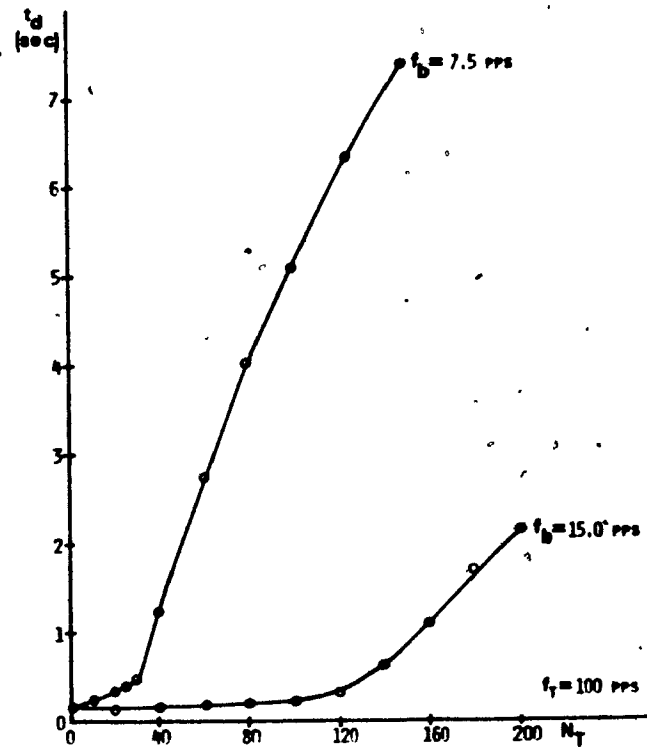
FIGURE 7-11   POSTTRAIN INTERVAL IN SIMULATIONS
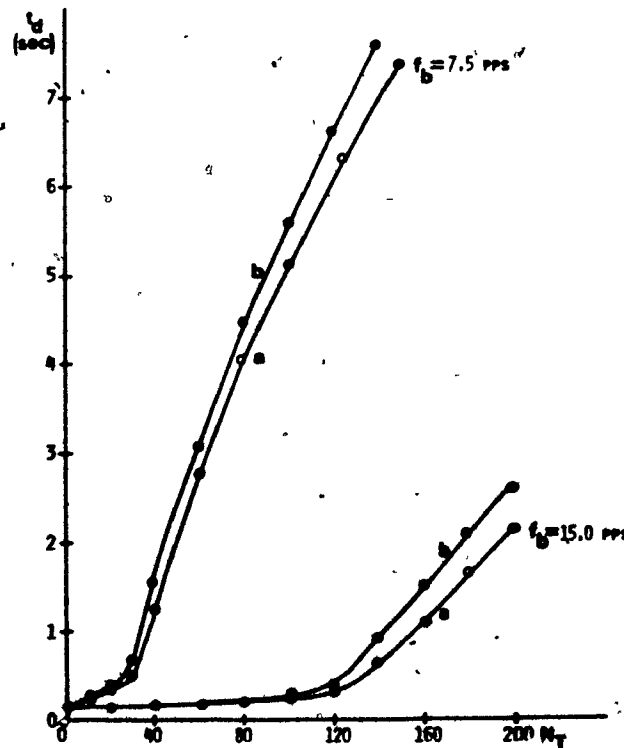OF THE GENERAL MODEL

FIGURE 7-12   COMPARISON OF THE SIMULATION RESULTS (CURVES(a)≡FIG.7-11)
AND THE SOLUTION OF EQUATION 7-40 (CURVES(b))

mately satisfied when the LHS crosses the time axis. Thus t_d can be found from,

$$(I - I_{th}) - i_p(T_a) \, e^{-t_d/T_P} = 0 \tag{7-44}$$

On the other hand,

if $\qquad (I - I_{th}) - i_p(T_a) > 0 \tag{7-45}$

or if, $\qquad N_T < \dfrac{(I - I_{th})}{K_P} - \dfrac{f_b}{A_P}\left(1 - \dfrac{D_T}{T_P}\right) \tag{7-46}$

Then, as illustrated in Figure 7-13(b), since $T_K \ll T_P$ and since

$\Delta i_K(T_a) > I - I_{th} - i_p(T_a)$, (7-41) is approximately satisfied when the RHS is equal to $(I - I_{th}) - i_p(T_a)$. Thus t_d can be found from,

$$(I - I_{th}) - i_p(T_a) = \Delta i_K(T_a) \, e^{-t_d/T_K} \tag{7-47}$$

Let us define the RHS of (7-43) and (7-46) as

$$\dfrac{(I - I_{th})}{K_P} - \dfrac{f_b}{A_P}\left(1 - \dfrac{D_T}{T_P}\right) = N_{TT} \tag{7-48}$$

For $N_T > N_{TT}$, t_d is found from (7-43), whereas for $N_T < N_{TT}$, t_d is found from (7-46). The plot of the solution of these two equations is in fact the same as the plot of the solution of the single equation (7-40).

Case (ii)

When a train of spikes is artificially initiated in a crayfish stretch receptor neuron which is initially at rest, after the train there is a temporary hyperpolarization of the membrane potential (47). A hyperpolarization is also observed in simulations of the general model

as shown in Figure 7-14. The number of spikes in the train N_T was varied, but the spike frequency in the train, f_T, was set at 100 pps, and the parameters of the model are those for the smallest MN ($d=25\mu m$) (Although the cases when the number of spikes is one or a few are not trains of spikes, we also consider these cases). The hyperpolarization declines to zero in two phases: a rapid decline in the first 300 msec, and afterwards, a slow decline with a time constant of 10 sec. The initial rapid decline is due to the fact that $\Delta i_K(t)$ declines with a small time constant, whereas the final gradual decline is due to the fact that $i_P(t)$ declines with a large time constant. These two phases of the after-hyperpolarization have been observed experimentally for the crayfish stretch receptor neuron and for the spinocerebellar tract neuron (46,47).
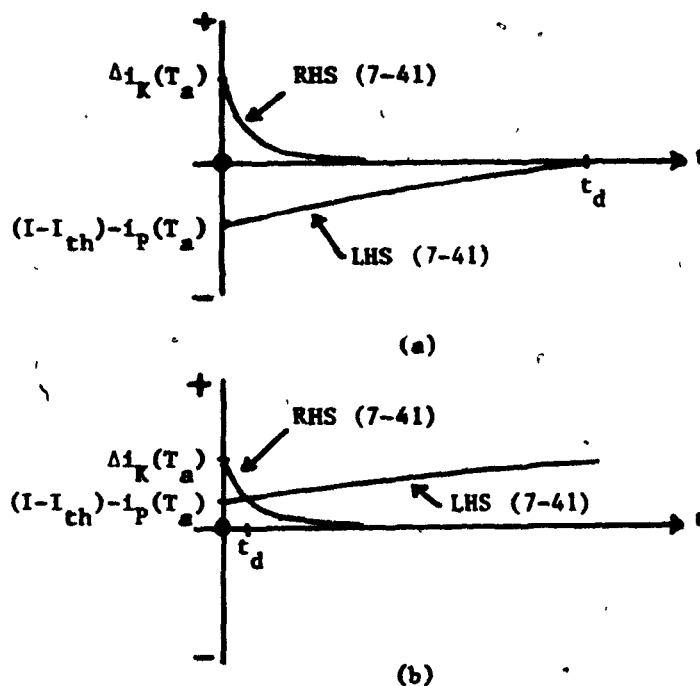
(a)

(b)

FIGURE 7-13   THE TWO CONDITIONS FOR THE SOLUTION OF EQUATION (7-41)

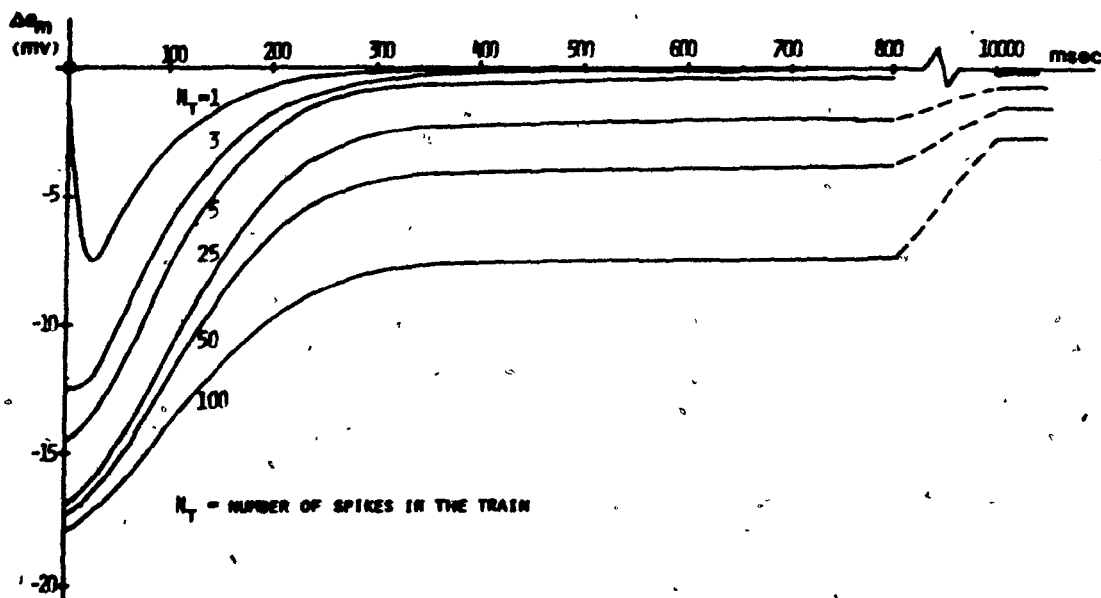N_T = NUMBER OF SPIKES IN THE TRAIN

FIGURE 7-14   HYPERPOLARIZATION AFTER A TETANIC TRAIN OF SPIKES
IS INITIATED IN THE GENERAL MODEL

7.6   Response to stimulation by sinusoids of current

We investigate first the behaviour of the general model when the input amplitude is kept constant but the input frequency is varied. The responses are shown in Figures 7-15 (a) - (j) in order of increasing input frequency from .002 Hz to 15 Hz.   The input $i(t)$ is denoted by *, the inhibitory current $i_p(t)$ is denoted by P, and the instantaneous firing frequency $f(t_1)$ is denoted by + (see Section 4.3 for a detailed description). The responses shown in Figures 7-15 (a) - (j) for $t \geq 25$ sec are the steady-state responses to sinusoidal inputs, since the time constant of the decline of the step response is equal to 5 sec and the transient is over in 25 sec.   The input magnitude is always above the threshold current and it varies from 1.5 to 2.5 times the threshold current.

The responses can be classified into two classes: cases (a) - (e) for which the input frequency is less than or equal to 0.2 Hz, and cases (f) - (j) for which the input frequency is greater than 0.2 Hz. In section 6.1.3 it was shown that for the input frequencies of cases (a) - (e), the response of the basic model was in phase with the input $i(t)$.   Thus, for the general model, the response is in phase with $[i(t) - i_p(t)]$.   As shown in Figures 7-15 (a) - (e), $i_p(t)$ follows $i(t)$ with a phase lag, and therefore the response occurs with a phase lead with respect to $i(t)$.   In section 6.1.3 it was shown that for the input frequencies of cases (f) - (j), the response of the basic model occurred with a phase lead (in the sense defined there) with respect to the input $i(t)$.   Since for cases (f) - (j), $i_p(t)$ is essentially constant with negligible ripple, the response of the general model still occurs with a

phase lead with respect to i(t).

Now we investigate the behaviour of the general model for another input magnitude which reveals a certain feature of the general model. The case is shown in Figure 7-16 for which the input magnitude varies from the threshold current up to 2.5 times the threshold current. We point out that, during the portion of the cycle when the input i(t) is close to the threshold current, $[i(t) - i_p(t)]$ is less than the threshold current and, as a result, no spikes are emitted. This result is to be compared with the result shown in Figure 7-15(c), where the input has the same frequency, but the minimum magnitude of the input is well above the threshold current. In that case, the response f(t) is a sinusoid with no silent period. Thus, the input magnitude affects the behaviour. However, for both cases, the response occurs with a phase lead with respect to the input by the same amount.

The gain and phase versus input frequency characteristics for the general model are shown in Figure 7-17. The data (marked by X) are calculated from the simulation results in Figure 7-15 by using the method described in section 5.3 The curves are the Bode plot of the transfer function $0.91E_Z \Delta G_{KO} T_K (f_{SK}/f_{SP}) H_K(s) H_P(s)$, where $H_K(s)$ and $H_P(s)$ were defined in Figure 7-4 and derived by a mathematical analysis in section 7.3. In order to interpret these results, we can compare them with the Bode plot of only $0.91E_Z \Delta G_{KO} T_K H_K(s)$ which was shown in Figure 6-6. Although the phase curve is the same as before for w >1.0 rad/sec, the phase curve for w <1.0 rad/sec is modified by the effect of the electrogenic Na pump. Thus, the potassium conductance process and the electrogenic Na pump pro-

(A) F = .072 HZ

(B) F = .015 HZ
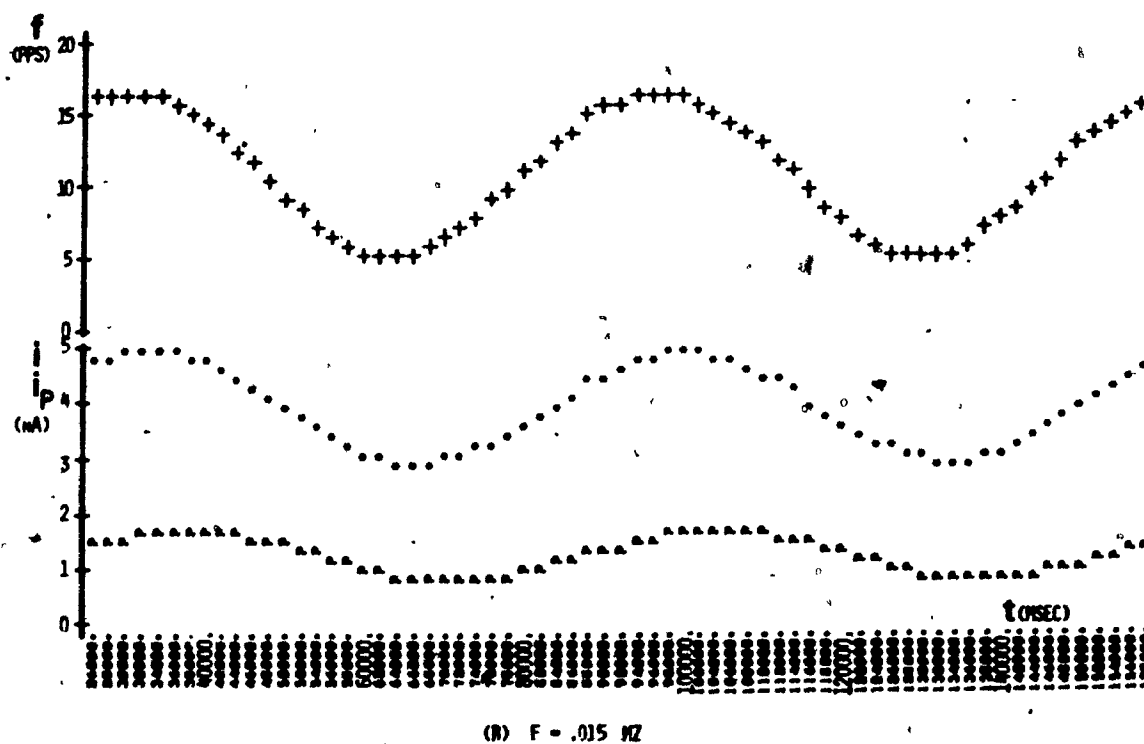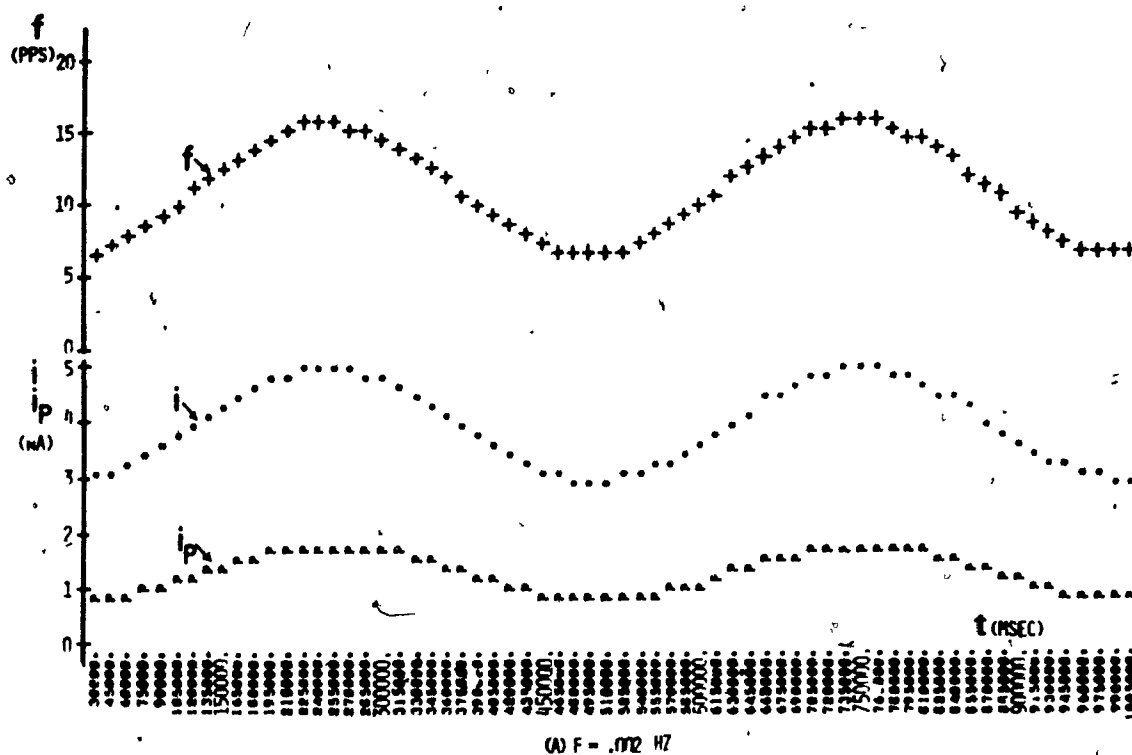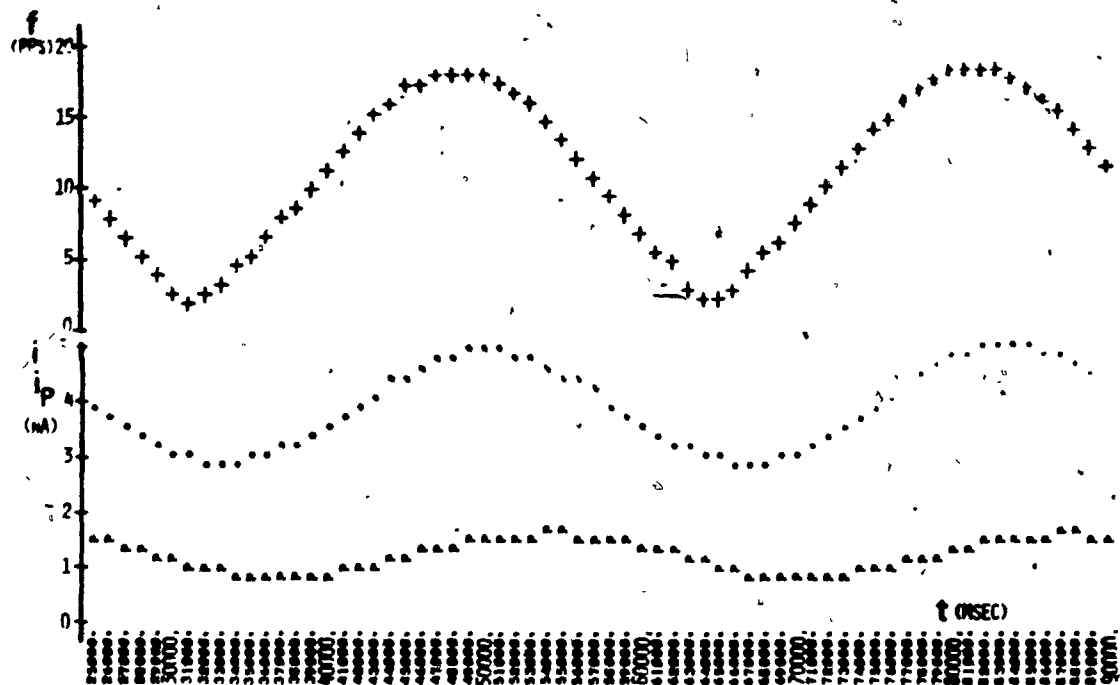
FIGURE 7-15

(C) F = .03 HZ
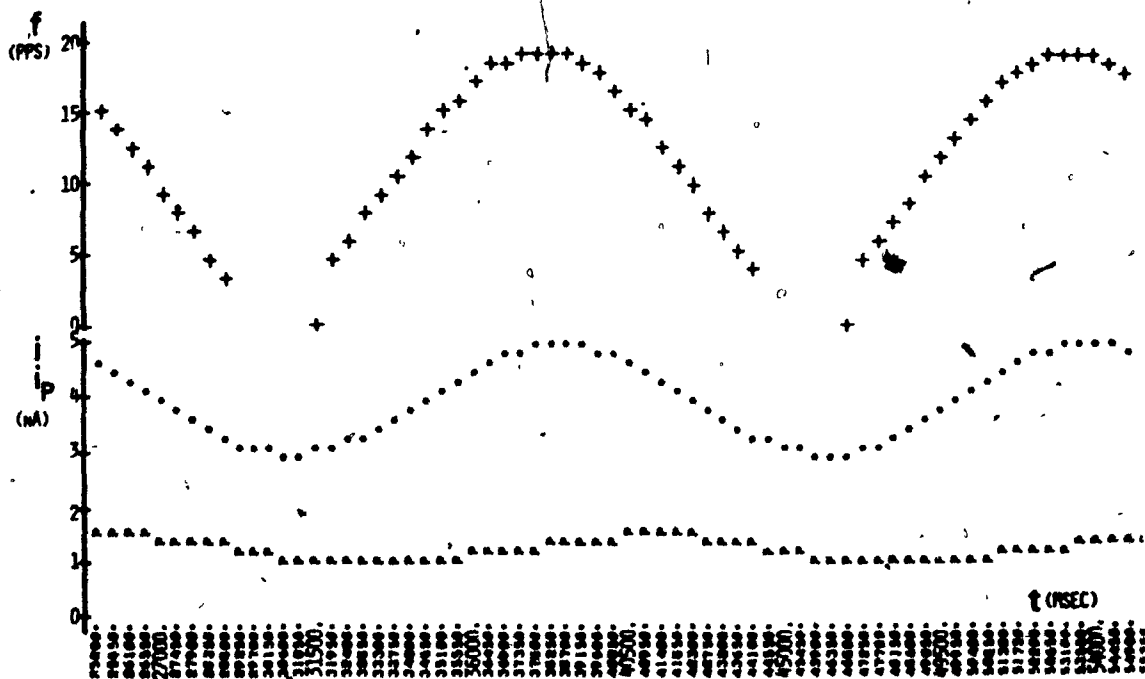
(D) F = .065 HZ

FIGURE 7-15
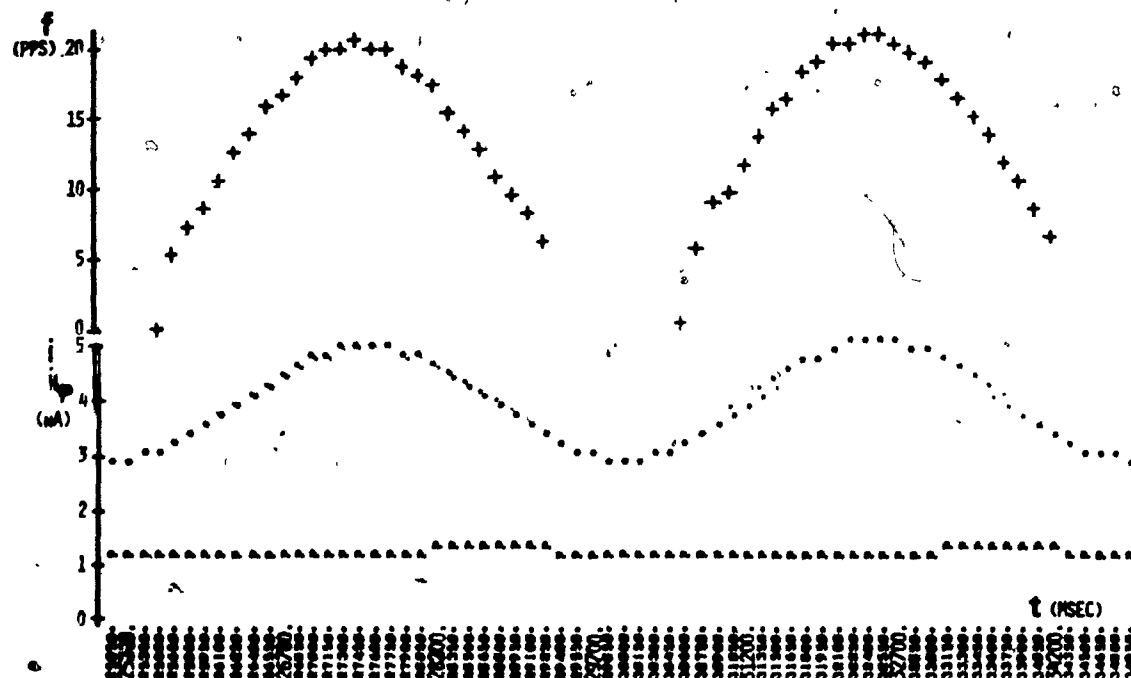
(E) F = .2 HZ
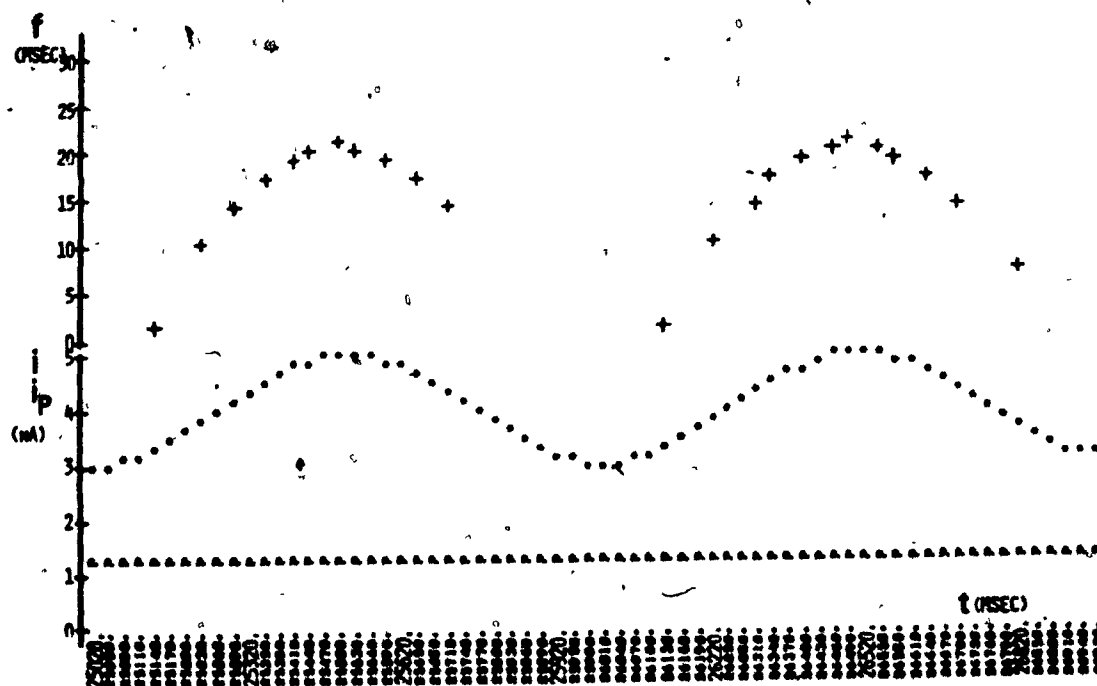
(F) F = 1.0 HZ

FIGURE 7-15
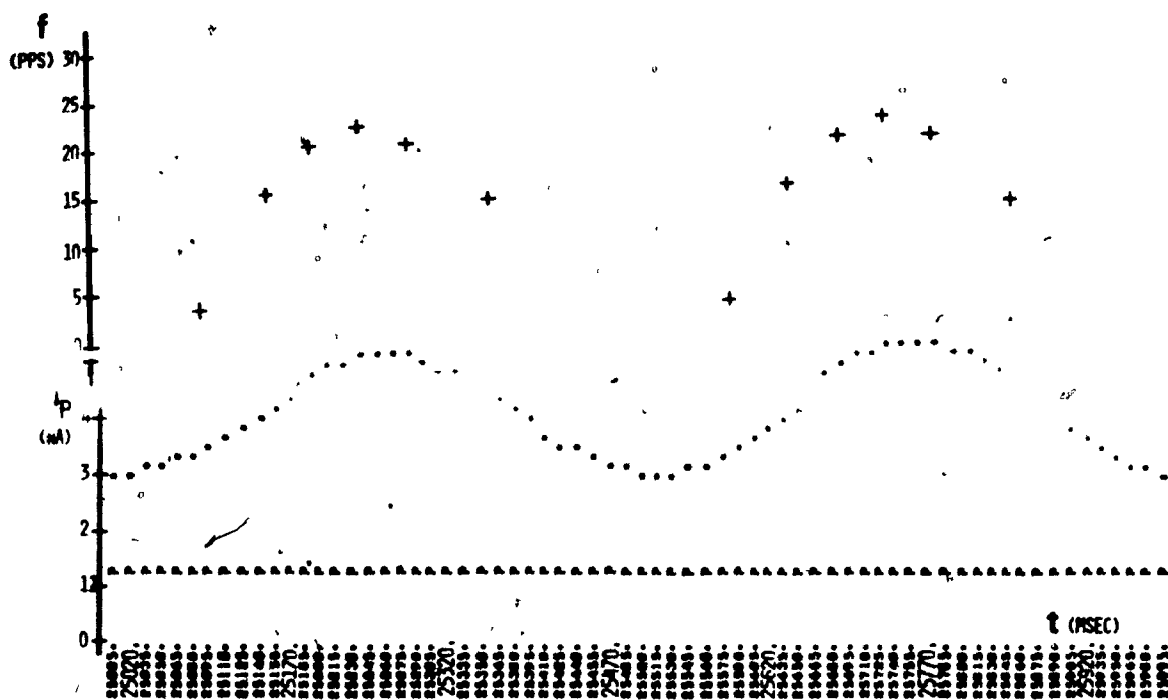
(6) F = 2.0 HZ

(H) F = 4.0 HZ

FIGURE 7-15

(I) F = 8.0 HZ

(J) F = 15.0 HZ
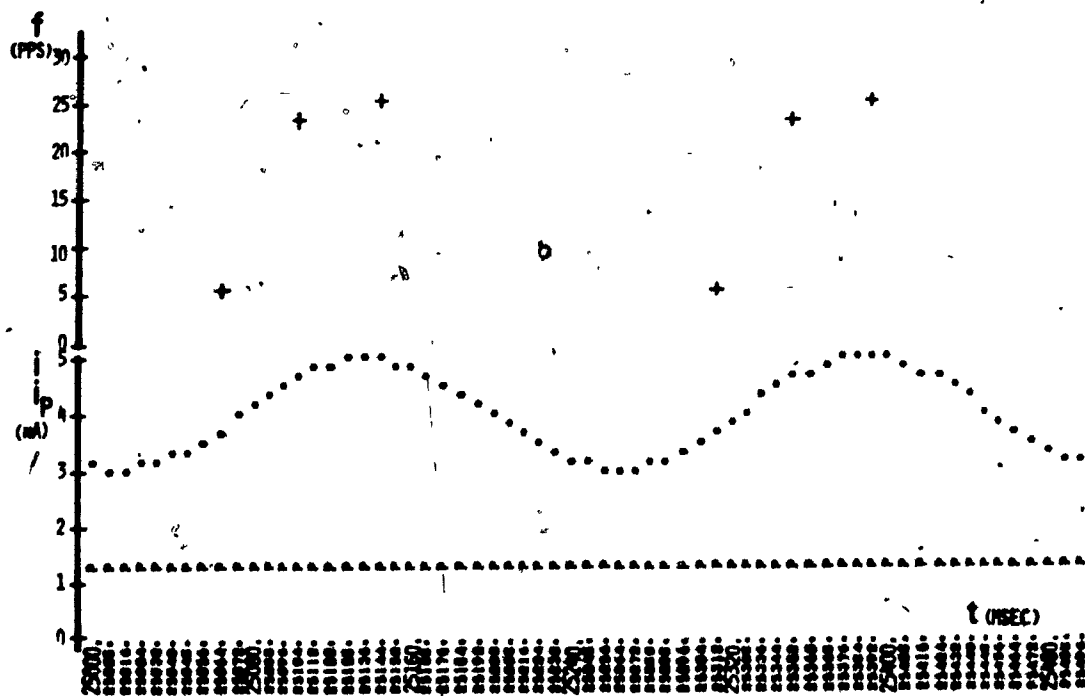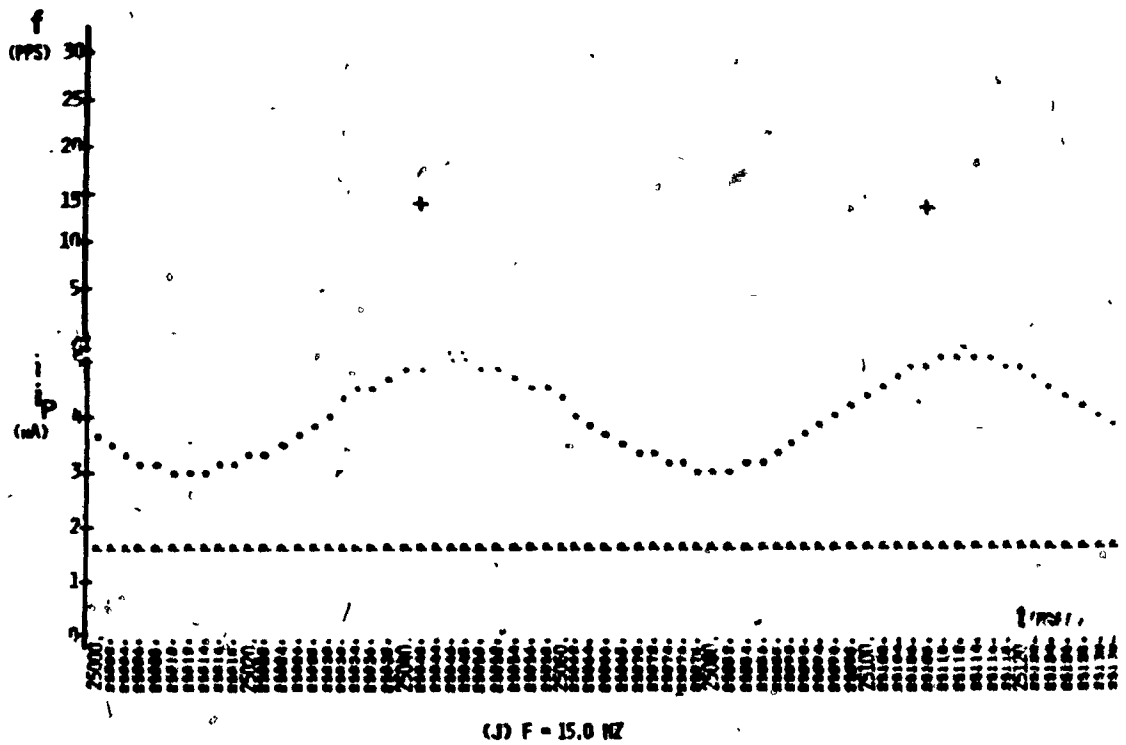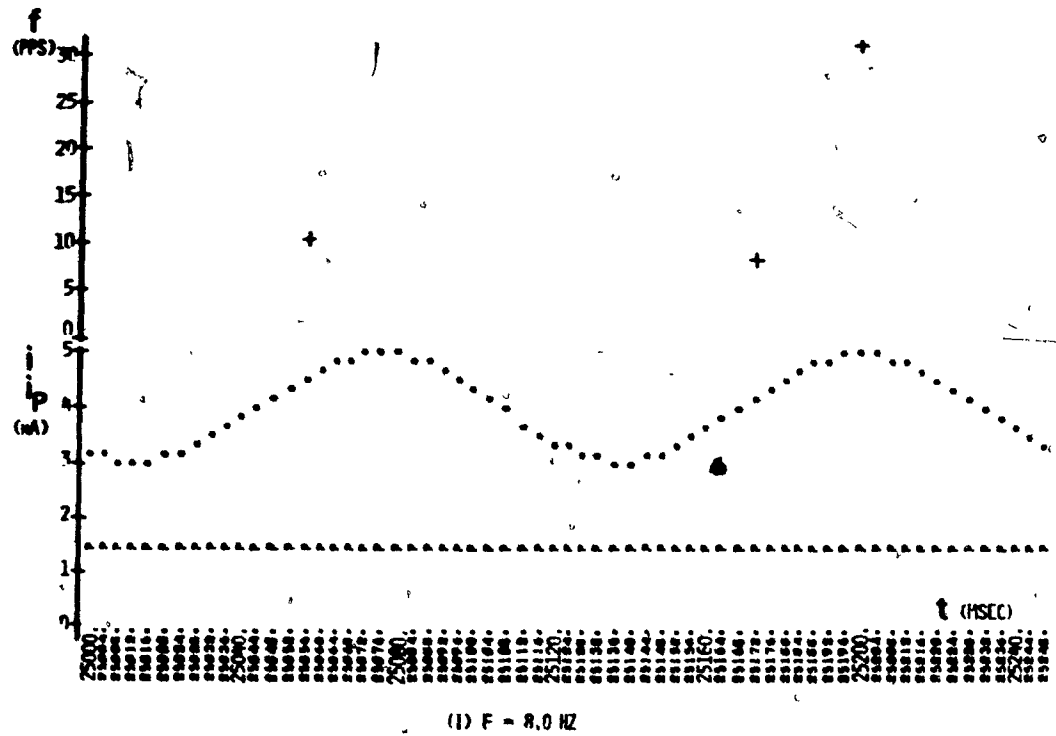
FIGURE 7-15   RESPONSE OF THE GENERAL MODEL TO INPUTS WITH DIFFERENT
FREQUENCY, F, AND CONSTANT AMPLITUDE, i(t)=4-1cos(2Π.F.t/1000)
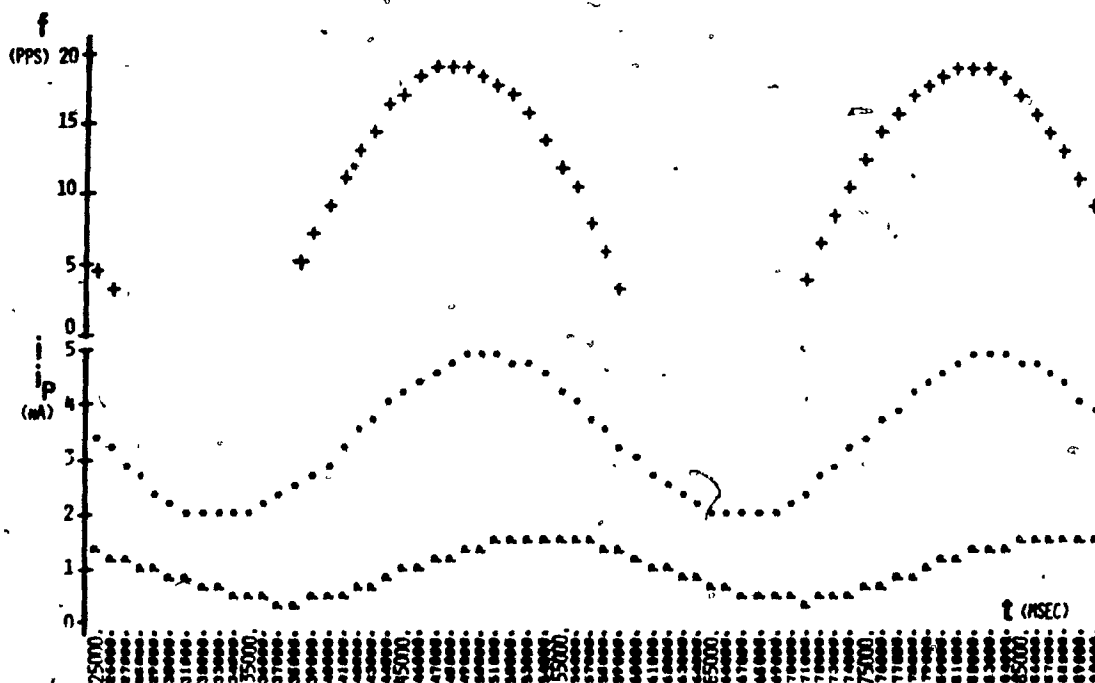
FIGURE 7-16   RESPONSE OF THE GENERAL MODEL TO THE INPUT

$1(t)=3.5-1.5\cos(2\Pi.F.t/1000)$, $F=.03$ Hz
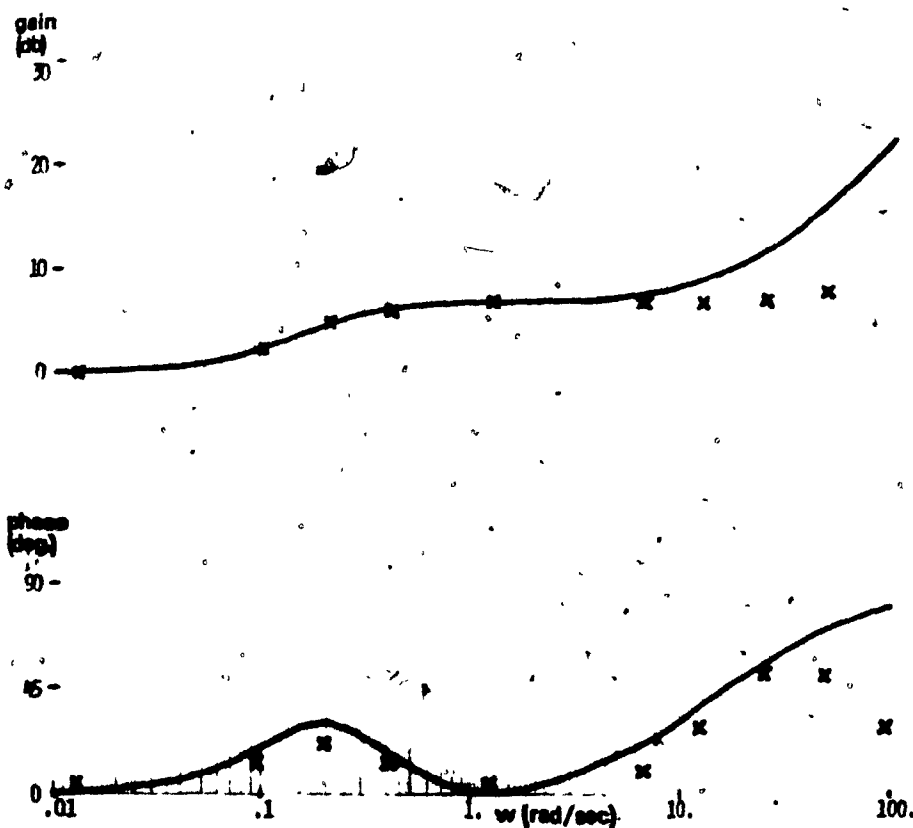
FIGURE 7-17   BODE PLOT OF $0.91E_Z \Delta G_{KO} T_K (f_{SK}/f_{SP}) H_K(s) H_P(s)$

AND DATA(X) FROM SIMULATIONS OF THE GENERAL MODEL

cess introduce a phase lead for different ranges of the input frequency.

It would be desirable to compare the response of the general model for sinusoidal inputs with reported experimental data, but unfortunately we have not found such data.

7.7 Stimulation by stretch

Up to this point, we have compared the response of the model to experimental results obtained by stimulating the crayfish stretch receptor neuron intracellularly. However, in the natural state, this neuron is stimulated by the stretch of the muscle. Thus, we shall now compare the response of the model to observed properties in the natural state.

It is believed (39) that stretch causes a nonselective increase in the ionic permeability of the dendritic endings which creates the so-called generator current. As a result, the membrane potential is depolarized and, if the stretch is sufficiently large, the neuron fires repetitively. The observed trajectories (11d) of the membrane potential between spikes are similar to those reproduced by the model (compare Figures 14 (a) - (c) in 11d to Figure 4-1(c) and Figures 4-4 (b) - (c) in this thesis). Also, the observed firing frequency adapts gradually (11d) as in the model. The former observation indicates that the potassium conductance process is involved in the encoding mechanism and the latter observation indicates that the electrogenic sodium pump process is also involved in the encoding mechanism in the manner described by the general model. However, it should be noted that the input to the model is to be set proportional to the measured generator potential which is the lumped manifestation of the generator current.

7.8 Summary

In this chapter, we have proposed and analyzed a model of the encoding mechanism of the crayfish stretch receptor neuron. The model is composed of the basic model plus a negative feedback path which accounts for a postulated inhibitory current produced by the increased activity of the electrogenic sodium pump activated by the emitted spikes. It was assumed that this inhibitory current is a temporal summation of component currents, each of which is produced by a spike and decays exponentially from a maximum at the time of the spike. The model reproduces the following properties which have been observed by Sokolove et al. when they stimulated the crayfish stretch receptor neuron intracellularly:

(i) There is a gradual adaptation of the firing frequency with a time constant of several seconds when a step input is applied.

(ii) Repetitive firing is reset by inserting one or two spikes.

(iii) If repetitive firing is disturbed by inserting a tetanic train of spikes, the curve relating the posttrain interval to the number of spikes in the tetanic train is composed of two line segments.

(iv) The hyperpolarization, observed after a tetanic train of spikes is applied to a neuron at rest, is composed of an initial rapidly-declining phase and a final gradually-declining phase.

The model predicts that for sinusoidal inputs with low frequencies, the response is in phase with the input. For inputs with intermediate frequencies, the response occurs with a phase lead similar to that of a lead network. For inputs with high frequencies, the response occurs with a phase lead similar to that of a differentiator.

The model was called the general model because in the next

chapter we list other neurons which may be modelled with this model. Furthermore, in the next chapter, we shall classify all the properties of the general model into two groups: those due to the potassium conductance process and those due to the electrogenic sodium pump process.

CHAPTER VIII

CONCLUSION AND DISCUSSION

In this concluding chapter, we discuss various aspects of our model, compare our model with some previous models and suggest areas for further research.

8.1   Properties of the encoding mechanism of the general model

In our general model, we have incorporated two significant physiological processes present in the neuronal membrane: the inner feedback path models the potassium conductance process and the outer feedback path models the electrogenic sodium pump process.   The inner feedback path is based on experimental results reported for the motoneuron. It is believed because of experimental evidence (8, 12, 18, 21, 22) that the hyperpolarization observed after a single spike is produced by a prolonged increase in a potassium conductance.   It has been measured (8, 22) that this increase declines to zero exponentially from an initial value immediately after a spike. This has been considered as the impulse response of this process.   For two or more pulses, summation of the responses has been assumed to be linear, with some experimental support for this assumption (22).

The outer feedback path is based on experimental results reported for the crayfish stretch receptor neuron.   The experimental re-

sults (45, 47) show that the electrogenic sodium pump produces inhibitory effects, since these effects disappeared when the activity of the pump was depressed by several methods. We can consider the pump as a current generator since it actively transports ions across the membrane. Thus, it has been assumed that the inhibitory effects are produced by an inhibitory current which is a linear temporal summation of component currents, each of which is produced by a spike and decays exponentially from a maximum at the time of the spike. However, there is no direct experimental evidence which shows that the impulse response of this process is in fact an exponential decay from an initial value, nor is there any direct evidence which shows that the summation occurs linearly. However, the observed experimental effects were reproduced by the model by assuming only this simple description of the process.

The properties of the encoding mechanism of the general model can be subdivided into two groups corresponding to the two feedback paths. This subdivision is possible because the gain and the time constant of the two feedback paths are considerably different.

1. **Properties produced by the feedback path which models the potassium conductance process**

   1a. The after-hyperpolarization observed after a single spike.

   1b. In part, the initial phase of the hyperpolarization observed after a tetanic train of spikes.

   1c. The characteristic trajectory of the membrane potential between spikes during repetitive firing.

   1d. The adaptation of the firing frequency within the first few

spikes at the onset of stimulation by a step current.

1e. The resetting of repetitive firing by inserting one or two spikes.

1f. The phase lead of the response with respect to the input for sinusoidal inputs with high frequency above about $1/T_K$, where T_K is the time constant in this feedback path.

2. Properties produced by the feedback path which models the electrogenic sodium pump process

2a. In part, the initial phase of the hyperpolarization observed after a tetanic train of spikes and, completely, the long final phase of this hyperpolarization.

2b. The gradual adaptation of the firing frequency with a time constant of several seconds at the onset of stimulation by a step of current.

2c. The phase lead of the response with respect to the input for sinusoidal inputs with intermediate frequency about $1/T_p$, where T_p is the time constant in this feedback path.

2d. The long interval before the first spike is emitted after repetitive firing is disturbed by a tetanic train with many spikes.

8.2 Applicability of the model

In the previous chapter, the general model was shown to be applicable to the crayfish stretch receptor neuron. It should also be applicable to the motoneuron because the potassium conductance process

is present in the MN (see Chapter III), and it is believed that the electrogenic Na pump process is also present in the MN since it is believed to be involved in maintaining the ionic equilibrium (12). Furthermore, Kernell (29) has observed in some MNs a gradual adaptation of the firing frequency, and, in the context of the general model, this gradual adaptation is due to the electrogenic Na pump process. However, the degree of this gradual adaptation is apparently small compared to the initial adaptation in the MN, and compared to the gradual adaptation in the crayfish stretch receptor neuron. Consequently, for the MN, the feedback path which accounts for the electrogenic Na pump process may be removed, and we can use the basic model as a model for the MN (see Chapters III - VI).

In addition to the two types of neurons just discussed, the general model appears to be applicable to other types of neurons. For example, the muscle spindles (48) possess properties 1c, 1e, 2b, and 2d of the list in Section 8.1. Pyramidal tract cells (46) possess properties 1b, and 2a. Sympathetic preganglionic neurons (49) possess property 2d. Interneurons possess property 1c and they fire with large spike frequencies possibly because the repolarization between spikes, or in terms of the model, the gain of the feedback path due to the potassium conductance process is smaller than in MNs (27). Sokolove and Cooke (45) have listed other neurons which possess property 1e, or property 2d. We should point out that one property of each group has to be experimentally observed in order to indicate the presence of the corresponding process in a particular neuron and the corresponding feedback path in the model. Thus, for some of these neurons, the presence of only one of the

two processes has been indicated by a cited property, but we are not familiar with all the information which has been reported.

Some neurons fire repetitively with property lc, apparently in the complete absence of external inputs (3). If a constant input larger than the threshold current is applied to the model, it behaves, in effect, as a neuron with simple spontaneous firing. Nevertheless, the model is not strictly applicable to these neurons.

8.3   Features of the model suited for studying neural systems

Since the model appears to be applicable to various types of neurons, it can be used for studying various neural systems. Furthermore, for this purpose, the model possesses the following features (see discussion in Section 1.1).

(i) The parameters of the model have been expressed as a function of the size of the neuron. The expressions are strictly valid for the motoneuron because they are based on experimental data obtained from the motoneuron. However, it may be expected that similar expressions are valid for other neurons. The variables ΔG_{KO} , K_p , $1/R$, and C are directly proportional to the size simply because these variables are proportional to the surface area of the neuron. The time constant T_K for the MN is inversely proportional to the size, and we suggested the possibility that T_K is inversely related to the dimensions of the structure of the membrane. Although the precise expressions may be different for other neurons, the parameters of the model can be expressed as a function of size as in section 6.1.1 .

(ii) The model consists of four blocks each of which contains only the essentials.   The spike is not reproduced and this avoids considerable complexities.   The model is "simple" enough that it was possible for us to analyze it mathematically.

8.4   Predictions of the model

The model predicts several properties which require experimental verification:

(i) The two distinct groups of properties which are produced by the potassium conductance process and the electrogenic Na pump process were listed in Section 8.1 .   To our knowledge, not all of these properties have been observed in any particular neuron.   We expect that if one property of one group has been observed, then the other properties of the same group will also be present in that neuron.   For example, according to the model, we can infer from the experiment in which repetitive firing is reset by spikes that the potassium conductance process is present in the crayfish stretch receptor neuron.   Consequently, it is fairly certain that there is also an initial adaptation of the firing frequency within the first few spikes at the onset of stimulation by a step of current because this property is also produced by the potassium conductance process.

(ii) The theoretical analysis in Section 3.5 indicated that the prolonged increase in the potassium conductance which produces the after-hyperpolarization occurs in addition to the increase in the potassium

conductance which causes the spike to decline as in the Hodgkin-Huxley model.

(iii) As discussed in Section 6.1.2, the model predicts that the slope of the straight-line relationship between the adapted firing frequency and the current intensity is inversely proportional to the size of the motoneuron. However, Kernell has concluded from some experimental results that the slope is directly proportional to the size. On the other hand, Granit, Kernell, and Lamarre obtained experimental data from which we have inferred (see Section 6.1.2) that the slope is inversely proportional to the size as predicted by the model. Furthermore, the prediction was obtained by varying the parameters as a function of size according to reported experimental data. Consequently, this apparent contradiction between the prediction of the model and Kernell's conclusion remains to be clarified by further experimental work.

(iv) As shown in Sections 4.3 and 7.6, the model predicts that for sinusoidal inputs with low frequencies, the response is in phase with the input. For inputs with intermediate frequencies, the response occurs with a phase lead which is produced by the electrogenic Na pump process. For inputs with high frequencies, the response occurs with a phase lead which is produced by the potassium conductance process. We pointed out in Section 4.3 that, for an input with high frequency, a phase lead has been observed in the motoneuron. Further, for inputs with intermediate frequencies, a phase lead has been observed for the muscle spindle (50). However, in these experiments, the stimulus is a change in the muscle length which is not the same as the input to the neuron because of the synaptic and mechanical transformations. Experiments

should be performed in which neurons are stimulated directly with sinu-
soids of current.

(v) The model reproduces several experimental observations
for step and ramp inputs. Furthermore, the model has been formulated
by considering the significant processes present in the neuronal membrane,
rather than using a "black-box" approach in formulating a model. For
these two reasons, we can expect that the model will reproduce some
observations for inputs of any form.

8.5 Comparison of our model with previous models

Briefly, our model possesses the following two essential
features.

(i) It includes two processes, namely, the potassium conductance
process and the electrogenic sodium pump process. The model shows that
each process produces a distinct group of properties of the encoding.

(ii) The parameters of the model are expressed as a function of
the size of the neuron. The model shows that the size affects the pro-
perties of the encoding.

To the best of the author's knowledge, there is no other model
which possesses these features. It should be pointed out that our model
is not only useful for studying neural systems but, in our opinion, it
also contributes to the understanding of the encoding mechanism of the
individual neuron. In the following, we compare in detail our model
with previous models (see Section 1.2) which were formulated by consider-

ing the processes present in the neuronal membrane which are significantly involved in the encoding mechanism.

Kernell's model did not include the electrogenic sodium pump process. We have modelled the potassium conductance process with the same circuit which was used by Kernell. However, we formulated this circuit in the context of the Hodgkin-Huxley model. Then, we transformed the circuit into a transfer-function representation and we included temporal summation of the potassium conductance process. This summation limits the firing frequency in the high range, so that, in our model, the curve relating the firing frequency to the intensity of the input step is a straight line. The curve does not exhibit a primary and a secondary range as Kernell's work had indicated. We have done a detailed systematic analysis of the consequences of the potassium conductance process. For example, when we varied the parameters as a function of size, the model predicted that the slope of the curve relating the firing frequency to the intensity of the input step is inversely related to the size. As discussed in Section 6.1.2, this prediction contradicts some of Kernell's experimental results.

We have modelled the electrogenic sodium pump process in the same manner as Sokolove. The input current minus the inhibitory current produced by the electrogenic sodium pump process is the effective input. In Sokolove's model, the effective input was applied to an integrator and a spike was emitted when the output of the integrator reached a threshold value. The spikes reset the output of the integrator to zero. The integration was arbitrarily stopped during the time that the effective input was negative. This last assumption permitted his model to repro-

duce the two segments in the curve relating the posttrain interval to the number of spikes in the tetanic train. Furthermore, Sokolove and Cooke (45) attributed to the electrogenic Na pump process the resetting of repetitive firing by inserting spikes. In our model, the effective input is encoded by the basic model which we formulated by considering the potassium conductance process. This process produces the two experimental observations just mentioned.

The models of Lewis, Connor and Stevens, Jenik and Kupfmuller do not include the electrogenic sodium pump process. Furthermore, these models are unnecessarily complex for studying neural systems because, for this purpose, it is not necessary to reproduce the spike. Lewis' model is an electronic analogue of the Hodgkin-Huxley model and we have discussed in Section 3.5 the possibility that the potassium conductance process in our basic model may be different from the potassium conductance process which causes the decline of the spike in the Hodgkin-Huxley model. The theoretical work of Lewis revealed how spontaneous activity can arise in a patch of membrane. In the membranes where this activity is clearly evident, there may be subthreshold oscillations of the membrane potential or spikes may be emitted (3). Our model does not account for spontaneous activity. The model of Connor and Stevens is based on experimental data obtained for the molluscan soma, whereas in Section 3.5 we suggested the possibility that the potassium conductance process for the motoneuron must include the effect of the dendrites.

8.6   Discrepancies between the behaviour of the model and some experimental observations

In formulating the model in Sections 3.3 and 7.2, the following major simplifications have been made: .

    i.   The neuron, which has a distributed structure, was re-presented by a lumped model.

    ii. The time-varying voltage-dependent sodium and potassium conductances for subthreshold operation were replaced with a constant resistance,

    iii.. The postulated inhibitory current produced by the electro-genic Na pump was assumed to be, simply, a linear temporal summation of component currents, each of which is produced by a spike and decays exponentially from a maximum at the time of the spike.

These simplifications may be the cause of the fact that the model reproduces some experimental observations only qualitatively or to a first-order approximation and that some experimental observations are not reproduced at all.   In the following, we list these discrepancies which one should consider when using the model. The seriousness of these discrepancies would depend on the particular application of the model. In spite of these discrepancies, the model has clearly shown in the thesis that many of the observed properties of the encoding mechanism can be classified into two groups, the properties in one group being produced by the potassium conductance process, and the properties of the other group being produced by the electrogenic Na pump process.   Further-more, in the next section we shall propose an improvement for the model

which will remove some of these discrepancies.

In the model the firing frequencies during the initial adaptation within the first few spikes may be as large as 1000 pps whereas, in the experimental case for the motoneuron, they are generally only a few hundred pps (see Section 4.1.2). This quantitative discrepancy arises because the model does not account for the relative refractoriness from 1 to 4 msec after a spike.

For both the theoretical and experimental cases, the threshold current, the minimum firing frequency, and the firing frequencies are directly proportional to the size (see Section 6.1.2). However, the firing frequencies of the model for any particular motoneuron are apparently larger than the experimental values and the slope of the theoretical curve was found to be consistently about 2.3 times larger than the slope of the experimental curve. This quantitative discrepancy may be due, in part, to the first assumption. The lumped model does not take into account the fact that the soma and dendrites are stimulated asymmetrically since the microelectrode is probably inserted into the soma. It may be that a larger stimulating current causes a larger depolarization of the distal dendrites which would permit the spike to invade a larger dendritic area. In such a case ΔG_{KO} would be directly related to the intensity of the stimulating current, since this conductance increase (triggered by the spike) is proportional to the surface area, similar to the fact that the conductance ΔG_{KO} for a large MN is larger than that for a small MN. Thus, in the model, ΔG_{KO} would increase with the input intensity thereby limiting the firing frequency further.

In addition to the quantitative discrepancies just mentioned,

the model does not reproduce the following experimental observations:

(i) In the motoneuron, when a subthreshold depolarizing or hyperpolarizing current step is applied, the resultant change in the membrane potential reaches a maximum at about 15 msec after the onset of the step, and thereafter it declines gradually within 100 msec to a steady level that is about 70% of the maximum value (23). In the model, the overshoot is not reproduced and a steady state is rapidly attained [see Figure 4-1(b)].

(ii) In the motoneuron, there exists a definite threshold current for repetitive firing and this effect is reproduced by the model. However, for input current steps less than this threshold current and greater than a so-called rheobase current, the motoneuron can emit only a few spikes at the onset of the step (29). In the model, for a step input there is either repetitive firing or no firing at all (see Section 4.1.1).

(iii) In the crayfish stretch receptor, if repetitive firing is stopped by applying a hyperpolarizing current, then after removing the hyperpolarizing current, there is a transient increase of the firing rate in proportion to the intensity of the hyperpolarizing current (10). In the model, there is also a transient increase of the firing rate because the inhibition from the electrogenic Na pump process declines during the period that the firing is stopped. However, the inhibition declines by an amount which is dependent only on the fact that the firing is stopped and not on the intensity of the hyperpolarizing current. Thus, in the model, the increase in the firing rate is independent of the intensity of the hyperpolarizing current, contrary to the experimental

observation (these simulation results have not been included in the
thesis).

(iv) In the motoneuron, there is a secondary range of firing
and this range is not reproduced by the model (see Section 4.1.3).

(v) Our model does not account for spontaneous subthreshold
oscillations of the membrane potential or for spontaneous emission of
spikes (3).

8.7 Improvement for the model

In the previous section we have listed several experimental
observations which are not reproduced by the model. During the final
stages in the preparation of this thesis, it became evident to us how the
model could be improved in order to account for three of these experimental
observations. In this section we shall propose this improvement for the
model.

In Section 3.3 we formulated the basic model (see Figure 3-5)
in the context of the Hodgkin-Huxley model (see Figure 2-2). The g_K
branch in the H-H model was subdivided into two branches containing g_{Kb}
and Δg_K as shown in Figure 3-4(a). Then a simplification was made by
lumping the branches containing g_L and the time-varying voltage-dependent
g_{Na} and g_{Kb} into a constant resistance R [see Figure 3-4(b)]. We now
modify this formulation:

In Chapter II, we suggested a simple description for the be-
haviour of the potassium conductance of the squid axon. The transfer

function corresponding to this description is,

$$g_K(s) = \frac{K_S}{s + A_K} \Delta e_m(s) + \frac{G_{Kr}}{s} \qquad (8\text{-}1)$$

where, $g_K(s)$ and $\Delta e_m(s)$ are the Laplace transforms of $g_K(t)$ and $\Delta e_m(t)$, K_S is a constant, A_K is the inverse of the time constant and G_{Kr} is the potassium conductance at the resting potential. We now assume that the same description is valid for the potassium conductance process which pro-duces the after-hyperpolarization observed in the motoneuron, except that that parameters are different. The rationale for this assumption is the following: In the motoneuron, the spike triggers a temporary in-crease $\Delta g_K(t)$ which declines to zero exponentially from an initial value immediately after the spike. This response can be regarded as the im-pulse response of the g_K process and such a response happens to be the impulse response of the transfer function given by Equation (8-1). The input $\Delta e_m(t)$ in Equation (8-1) is composed essentially of two super-imposed inputs, the spikes and the subthreshold change which we also de-note $\Delta e_m(t)$. Consequently, $g_K(t)$ is given by

$$g_K(t) = G_{Kr} + \Delta g_K(t) + g_{KS}(t) \qquad (8\text{-}2)$$

where, G_{Kr} is the potassium conductance at the resting potential, $\Delta g_K(t)$ is the change caused by the spike and is found by applying the spike waveform to $K_S/(s + A_K)$, $g_{KS}(t)$ is the change caused by the subthreshold $\Delta g_K(t)$ and is found by applying $\Delta e_m(t)$ to $K_S/(s + A_K)$. Thus the potassium conductance branch in the Hodgkin-Huxley model can be subdivided into three separate branches containing G_{Kr}, $\Delta g_K(t)$, and $g_{KS}(t)$ as shown in Figure 8-1(a).
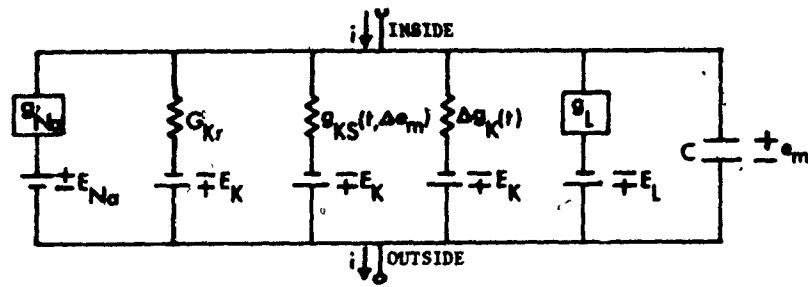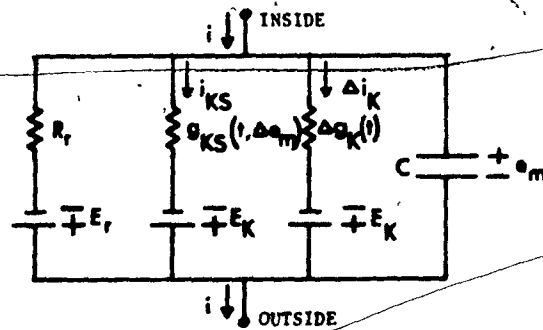
FIGURE 8-1   IMPROVED SIMPLIFICATION OF THE CIRCUIT IN FIG. 2-2
FOR SUBTHRESHOLD OPERATION (cf. FIG. 3-4)

The current pumps have been removed for the moment and they will be con-

sidered below.   We now make a simplification by lumping the branches

containing g_L , g_{Na} and g_{Kr} into a branch containing a constant resistance

R_r is series with the resting potential E_r as shown in Figure 8-1(b).

Again, we are not considering the time-varying voltage-dependent aspects

of the sodium conductance for subthreshold operation.

The circuit shown in Figure 8-1(b) can be represented in terms of transfer functions as shown in Figure 8-2. The spike emitter and the effect of the current pumps have also been included as in Section 3-3 and Chapter VII.
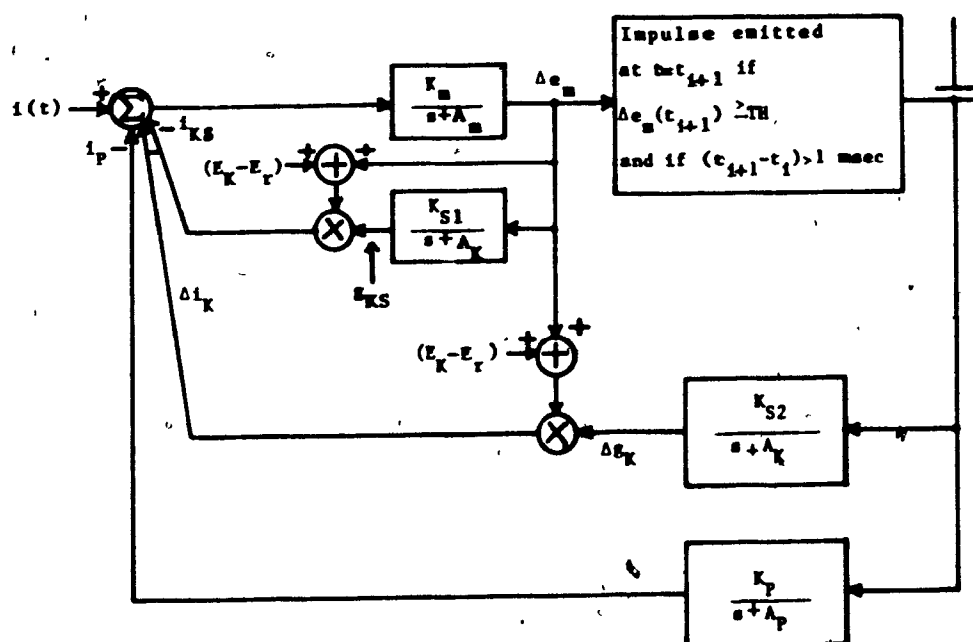
$K_m = 1/C$; $A_m = 1/R_r C$

FIGURE 8-2   IMPROVED GENERAL MODEL OF THE NEURONAL ENCODING
MECHANISM (cf. FIG. 7-1)

Since the spike is represented by an ideal unit impulse whereas Δe_m is not modified, we must use two different gains K_{S1} and K_{S2} instead of K_S

in the feedback paths which produce g_{KS} and Δg_K . As compared to the general model shown in Figure 7-1, an additional feedback path (containing $K_{S1}/(s + A_K)$ is present in this improved model.

We have conducted trial simulations of this improved model and the results show that the additional negative feedback path produces three of the experimental observations which were not accounted for by the general model. The three observations are listed as (i), (ii) and (iii) in Section 8.6. Firstly, the overshoot in the subthreshold step response is due to the slow increase of i_{KS} with a time constant T_K , which gradually counteracts the input step. This subthreshold step response reached a peak at 15 msec and it declined gradually to a steady-state level within 100 msec as experimentally observed. In the simulations, T_K was set as 33 msec, which is equal to one-third of the experimentally observed duration of the AHP and the other parameters were chosen equal to those of a neuron with T_K = 33 msec (for the present purpose K_{S2} was chosen equal to ΔG_{KO}). The parameter K_{S1} was adjusted so that the steady-state level of the step response was equal to 70% of the peak in the overshoot. Secondly, for input steps less than the threshold current and greater than the rheobase current, the model emitted a few spikes at the onset of the step. This property is related to the fact that, for the subthreshold step response, the input current is less effective in depolarizing the membrane during the steady-state than during the overshoot. With the values of the parameters chosen above, the threshold current was 1.5 times larger than the rheobase current, and the peak value of the overshoot was also 1.5 times larger than the steady-state level as observed experimentally. Thirdly, if repetitive

firing by the model was stopped by applying a hyperpolarizing current, then after removing the hyperpolarizing current, there was a transient increase of the firing in proportion to the intensity of the hyper- polarizing current. This property is related to the experimental and simulated observation that, if a hyperpolarizing current is applied to a neuron at rest, on terminating the current there is a rebound de- polarization in proportion to the intensity of the hyperpolarizing cur- rent. In the simulations, the transient increase of the firing was apparent within the first few spikes. We cannot compare quantitatively this result with the experimental observation because it was not re- ported in detail.

This improved model does not account for the two experimental observations which were listed as (iv) and (v) in the previous section. However, the model accounts for thirteen experimentaly observed pro- perties of the neuronal encoding mechanism. According to the model, six properties are produced by the increase in the potassium conductance triggered by the spikes, four properties are produced by the increased activity of the electrogenic sodium pump activated by the spikes, and three properties are produced by the increase in the potassium conductance triggered by the subthreshold change of the membrane potential.

8.8 Areas for further research

As a result of the present work, several problems of an experi- mental and theoretical nature require further research.

Experimental

The properties predicted by the model which are listed in Section 8.4 require experimental verification. One valuable set of experiments would be to stimulate intracellularly many motoneurons of various sizes with steps of current. The results would clarify prediction (iii) and the firing frequencies of the model can be compared to more experimental values. Prediction (iv) can be tested by stimulating motoneurons and crayfish stretch receptor neurons intracellularly with sinusoidal current. For prediction (ii), we suggested in Section 3.5 the possibility that the prolonged increase in the potassium conductance that produces the after-hyperpolarization occurs in the dendrites. It would be of interest to determine the conditions that affect the extent to which the spike invades the dendrites. Prediction (i) can be verified by observing all the properties of the encoding mechanism listed in the two groups in Section 8.1 for any particular neuron. Prediction (v) can be verified by stimulating neurons with inputs of various forms.

Theoretical

It would be desirable to remove the major simplification that we have made in formulating the basic model. We have used a lumped model for the dendrites, soma, and the initial segment. A distributed model would be more appropriate especially when the input is synaptic stimulation or stretch instead of intracellularly applied current. With such a model, one should examine if the spike invades more dendritic area when the stimulating current is increased. If so, then the negative feedback current due to the potassium conductance process would corres-

pondingly increase. In addition, one should examine if synaptic activity modifies the extent that the spike invades the dendrites. Both factors may alter the relationship between firing frequency and current intensity. Kernell has already done some work in this direction (9).

Although the improvement for the model which we have proposed in the previous section can remove some of the discrepancies of the model, this improved model still cannot account for a few experimental observations. Thus it may be possible to improve the model further, as for example, by considering the time-varying voltage-dependent aspects of the sodium conductance, as well as its inactivation. Furthermore, the improved model proposed in the previous section will have to be analyzed in detail.

APPENDIX

MATHEMATICAL EXPRESSION FOR THE EXCITABILITY

OF THE BASIC MODEL AFTER A SPIKE

The basic model is shown in Figure 3-5.

Let, $I_1 \equiv$ intensity of first rectangular stimulating pulse

$I_2 \equiv$ intensity of second rectangular stimulating pulse

$\Delta t_p \equiv$ duration of stimulating pulses which was equal to .25 msec in the experiments (25)

The values of the parameters of the model are given in section 3.3 .

$\therefore \Delta t_p \ll T_m$,

$\therefore$ the minimum value of I_1 necessary to trigger a first spike is given by,

$$I_1 = \frac{TH}{\Delta t_p K_m}$$ (A-1)

Suppose a first spike has been emitted at $t = 0$ and $\Delta e_m(t)$ after this spike is shown in Figure 3-6. If the second stimulating pulse is applied at time t, then the output of the transfer function $K_m/(s + A_m)$ at time $t + \Delta t_p$ is given by

$$\Delta e_m(t + \Delta t_p) = I_2 \Delta t_p K_m - \left[\frac{(\Delta e_m(t) + E_K - E_r) + (\Delta e_m(t + \Delta t_p) + E_K - E_r)}{2} \right] \cdot$$

$$\Delta g_K(t) \Delta t_p K_m + \left[\Delta e_m(t) - A_m \Delta e_m(t) \Delta t_p \right]$$ (A-2)

where, the first term in the RHS of (A-2) is the output due to the second stimulating pulse,

the second term is the output due to the average Δi_K in the

interval from t to $t + \Delta t_p$, and

the third term is the zero-input output of the transfer function.

Substituting in (A-2) $\Delta e_m(t + \Delta t_p) = TH$ which is the condition for a

second spike to be emitted, and solving (A-1) and (A-2) for I_2/I_1 we get,

$$\frac{I_2}{I_1} = \frac{TH - \Delta e_m(t)}{TH} + \frac{\left[\Delta e_m(t) + 2E_K - 2E_r + TH\right]\Delta g_K(t)\Delta t_p K_m}{2TH} + \frac{A_m \Delta e_m(t)\Delta t_p}{TH} \quad (A-3)$$

Substituting in (A-3) $\Delta g_K(t)$ from (3-2) and the values of the parameters

we get,

$$\frac{I_2}{I_1} = \frac{15 - \Delta e_m(t)}{15} + \frac{[\Delta e_m(t) + 55] \cdot 68 \, e^{-t/14.2}}{600} + \frac{\Delta e_m(t)}{300} \quad (A-4)$$

where $\Delta e_m(t)$ is in mv and t is in msec.

The exact values of I_2/I_1 in (A-4) and approximate values of I_2/I_1 found

by neglecting the second and third term in (A-4) for four different times

t are given below,

t	$\Delta e_m(t)$	exact I_2/I_1	approximate I_2/I_1
1.0	5.0	0.75	0.67
2.5	0	1.00	1.06
10.0	-5.0	1.34	1.33
30.0	-2.5	1.17	1.17

Thus I_2/I_1 is given approximately by

$$\frac{I_2}{I_1} = \frac{15 - \Delta e_m(t)}{15} \qquad t \geq 1 \text{ msec} \qquad (A-5)$$

and,

$$\frac{I_2}{I_1} = \infty \qquad\qquad t \geq 1 \text{ msec}$$

because of the condition $(t_{i+1} - t_i) \geq 1$ msec in the spike emitter.

REFERENCES

1. Harmon, L.D., and Lewis, E.R., Neural Modeling, Physiol. Rev., 46:513-591, 1966.

2. Hodgkin, A.L., and Huxley, A.F., A quantitative description of membrane current and its application to condúction and excitation in nerve, J. Physiol. 117:500-544, .1952.

3. Lewis, E.R., Neuroelectric potentials derived from an extended version of the Hodgkin-Huxley Model, J. Theor. Biol. 10: 125-158, 1965.

4. Lewis, E.R., Using electronic circuits to model simple neuro-electric interactions, Proc. of the IEEE, 56:931-949, 1968.

5. Roberge, F.A., A neuron model for the study of small neuron pools, Ph.D. Thesis, McGill University, Montreal, 1964.

6. Hiltz, F.F., Artificial neuron, Kybernetik, 1, No.6, 231-236, 1963.

7. Pertile, G., and Harth, E., A model of adaptation based on relaxation phenomena in the neural membrane, Kybernetik, 9: 189, 1971.

8. Kernell, D., The repetitive impulse discharge of a simple neurone model compared to that of spinal motoneurones, Brain Res. 11:685-687, 1968.

9. Kernell, D., Effects of synapses of dendrites and soma on the repetitive impulse firing of a compartmental neuron model, Brain Res. 35:551-555, 1971.

10. Sokolove, P.G., Computer simulation of after-inhibition in crayfish

slowly adapting stretch receptor neuron, Biophysical J. 12:1429-1451, 1972.

11. Ruch, T.C., and Patton, H.D., "Physiology and Biophysics", 19th edition, W. B. Saunders Co., Philadelphia, 1965.

a) Woodbury, J.W., The cell membrane: Ionic and potential gradients and active transport, Chapter 1.

b) Woodbury, J.W., Action potential: Properties of excitable membranes, Chapter 2.

c) Patton, H.D., Special properties of nerve trunks and tracts, Chapter 3.

d) Patton, H.D., Receptor Mechanism, Chapter 4.

e) Patton, H.D., Spinal reflexes and synaptic transmission, Chapter 6.

12. Eccles, J.C., The excitatory responses of spinal neurones, in, Progress in Brain Research, Eccles, J.C. and Schade, J.P. eds., vol. 12, Elsevier Co., Amsterdam, 1964.

13. Hodgkin, A.L., and Huxley, A.F., Currents carried by sodium and potassium ions through the membrane of the giant axon of Loligo, J. Physiol. 116:449-472, 1952.

14. Katz, B., Nerve, Muscle and Synapse, McGraw Hill, New York, 1966.

15. Hodgkin, A.L., and Huxley, A.F., The dual effect of membrane potential on sodium conductance in the giant axon of Loligo, J. Physiol. 116:497-506, 1952.

16. Eccles, J.C., The Physiology of Nerve Cells, The John Hopkins Press, Baltimore, 1957.

17. Coombs, J.S., Curtis, D.R., and Eccles, J.C., The electrical constants of the motoneurone membrane, J. Physiol. 145:505-

528, 1959.

18.   Coombs, J.S., Eccles, J.C., and Fatt, P., The electrical properties

of the motoneurone membrane, J. Physiol. 130:291-325, 1955.

19.   Frank, K., and Fuortes, M.G.F., Accommodation of spinal moto-

neurones of cats, Arch. Ital. Biol. 98:165-170, 1960.

20.   Rall, W., Distinguishing theoretical synaptic potentials computed

for different soma-dendritic distributions of synaptic input,

J. Neurophysiol. 30:1072-1193, 1967.

21.   Ito, M., and Oshima, T., Temporal summation of after-hyperpolari-

zation following a motoneurone spike, Nature, 195:910-911, 1962.

22.   Baldissera, F., and Gustafsson, B., Regulation of repetitive firing

in motoneurones by the after-hyperpolarization conductance,

Brain Res. 30:431-434, 1971.

23.   Ito, M., and Oshima, T., Electrical behaviour of the motoneurone

membrane during intracellularly applied current steps, J.

Physiol. 180:607-635, 1965.

24.   Burke, R.E., and Bruggencate, G.Ten., Electrotonic characteristics

of alpha motoneurons of varying size, J. Physiol. 212:1-20,

Jan. 1971.

25.   Fuortes, M.G.F., Frank, K., and Becker, M.C., Steps in the pro-

duction of motoneuron spikes, J. Gen. Physiol. 40:735-752, 1957.

26.   Kuno, M., Excitability following antidromic activation in spinal

motoneurones supplying red muscles, J. Physiol. 149:374-393,

1959.

27.   Kolmodin, G.N., and Skoglund, C.R., Slow membrane potential changes

accompanying excitation and inhibition in spinal moto- and interneurons in the cat during natural activation, Acta. Physiol. Scand. 44:11-54, 1958.

28. Connor, J.A., and Stevens, C.F., Prediction of repetitive firing behaviour from voltage clamp data on an isolated neurone soma, J. Physiol. 213:31-53, 1971.

29. Kernell, D., The adaptation and the relation between discharge frequency and current strength of cat lumbosacral motoneurones stimulated by long-lasting injected currents, Acta. Physiol. Scand. 65:65-73, 1965.

30. Kernell, D., The limits of firing frequency in cat lumbosacral motoneurones possessing different time course of after-hyper-polarization, Acta. Physiol. Scand. 65:87-100, 1965.

31. Calvin, W.H., and Schwindt, P.C., Steps in production of motoneuron spikes during rhythmic firing, J. Neurophysiol. 35:297-310, 1972.

32. Kernell, D., The early phase of adaptation in repetitive impulse discharges of cat spinal motoneurones, Brain Res. 41:184-186, 1972.

33. Kernell, D., High-frequency repetitive firing of cat lumbosacral motoneurones stimulated by long-lasting injected currents, Acta. Physiol. Scand. 65:74-86, 1965.

34. Kernell, D., The repetitive discharge of motoneurones, in Nobel Symp. I, R. Granit, Ed. John Wiley and Sons, New York, 1966. pp. 351-362.

35. Rosenthal, N.P., McKean, T.A., Roberts, W.J., and Terzuolo, C.A., Frequency analysis of stretch reflex and its main subsystems in

triceps surae muscles of the cat, J. Neurophysiol. 33:713-749, 1970.

36. Westbury, D.R., The response of α-motoneurones of the cat to sinusoidal movements of the muscles they innervate, Brain Res. 25:75-86, 1971.

37. Roberts, T.D.M., "Neurophysiology of Postural Mechanisms", Butterworths, London, 1967.

38. Kernell, D., Input resistance,electrical excitability, and size of ventral horn cells in cat spinal cord, Science, 152:1637- 1639, 1966.

39. Henneman, E., Peripheral mechanisms involved in the control of muscle, in "Medical Physiology", 12th edition, Mountcastle, V.B. ed., C.V. Mosby Co., St.Louis, 1968.

40. Eccles, J.C., Eccles, R.M., and Lundberg, A., The action potentials of the alpha motoneurones supplying fast and slow muscles, J. Physiol. 142:275-291, 1958.

41. Granit, R., Kernell, D., and Lamarre, Y., Algebraical summation in synaptic activation of motoneurones firing within the 'primary range' to injected currents, J. Physiol. 187:379-399, 1966.

42. Burke, R.E., Composite nature of the monosynaptic excitatory post-synaptic potential, J. Neurophysiol. 30:1114-1137, 1967.

43. Granit, R., Phillips, C.G., Skoglund, S., and Steg, G., Differentiation of tonic from phasic alpha ventral horn cells by stretch, pinna, and crossed extensor reflexes, J. Neurophysiol. 20:470-481, 1957.

44. Granit, R., "The Basis of Motor Control", Academic Press, London, 1970.

45. Sokolove, P.G., and Cooke, I.M., Inhibition of impulse activity in a sensory neuron by an electrogenic pump, J. Gen. Physiol. 57: 125-163, 1971.

46. Koike, H., Mano, N., Okada, Y., and Oshima, T., Activities of the sodium pump in cat pyramidal tract cells investigated with intracellular injection of sodium ions, Exp. Brain Res. 14: 449-462, 1972.

47. Nakajima, S., and Takahashi, K., Post-tetanic hyperpolarization and electrogenic Na pump in stretch receptor neurone of crayfish, J. Physiol. 187:105-127, 1966.

48. Ottoson, D., and Shepherd, G.M., Transducer properties and integrative mechanisms in the frog's muscle spindle, in "Principles of Receptor Physiology", Loewenstein, W.R. ed., Springer-Verlag, New York, 1971, pp.442-499.

49. Polosa, C., The silent period of sympathetic preganglionic neurons, Can. J. Physiol. and Pharm. 45:1033-1045, 1967.

50. Lennerstrand, G., and Thoden, U., Dynamic analysis of muscle spindle endings in the cat using length changes of different length-time relations; Acta. Physiol. Scand. 73:234-250, 1968.

51. Pavlidis, T., A new model for simple neural nets and its application in the design of a neural oscillator, Bull. Math. Biophys. 27:215-229, 1965.

52. Jenik, F., Pulse processing by neuron models, in "Neural Theory and Modeling", Reiss, R.F. ed., Stanford University Press, Stanford, 1964.

53. Harmon, L.D., Studies with artificial neurons, I: Properties and

functions of an artificial neuron, Kybernetik I, No. 3, 89-101, 1961.

54. French, A.S., and Stein, R.B., A flexible neural analog using integrated circuits, IEEE Trans. Biomed. Eng. 17:248-253, 1970.

55. Henneman, E., Organization of the spinal cord, in "Medical Physiology", 12th edition, Mountcastle, V.B. ed., C.V. Mosby Co., St.Louis, 1968.

56. Varano, V., and Lee, H.C., A simulation study of a spinal moto-neuron pool with Renshaw inhibition, 4th CMBEC Conference Digest, pp. 43a-b, Winnipeg, 1972.